INSTRUMENTED IMPACT CONE PENETROMETER

UMESH DAYAL

INSTRUMENTED IMPACT CONE PENETROMETER

by

Umesh Dayal, B.Sc. (Eng.), M.Sc. (Eng.)

A Thesis Submitted in Partial Fulfillment

of the Requirements for the Degree of

Doctor of Philosophy

Faculty of Engineering and Applied Science

Memorial University of Newfoundland

© February 1974

St. John's   Newfoundland

ABSTRACT

This thesis deals with the formulation of an analytical model applicable to low velocity impact penetration problems of soil media and the development of an instrumented impact cone penetrometer for measuring *in situ* strength properties of soil targets.

A penetration theory based on momentum considerations is developed for a cone-tipped right circular cylinder impacting on a C-φ soil target. A relationship is established between the instantaneous velocity, various 'static' and 'dynamic' soil properties, penetrometer characteristics and the instantaneous depth of penetration. It is assumed that impact causes shear failure and the resistance to the motion of penetrometer is provided by the inertial resistance of the accelerated soil mass plus the 'dynamic' soil resistive force distributed over the base and shaft of the penetrometer. The soil resistive force is calculated on the basis of plastic theory modified for 'dynamic' conditions and extending the previous analysis for the 'static' condition. The relationship obtained, in addition to providing the velocity profile and the maximum depth of penetration, can also be used for estimating the 'static' soil strength properties although only under idealized conditions.

The penetrometer utilised, in addition to providing acceleration signatures (as obtained by previous investigators), is capable of recording cone thrust and local side friction simultaneously and continuously. The available test results indicate that with this system the 'dynamic' strength profile, the soil type, location, and

depth of different layers can be directly evaluated up to the penetrated depth. The procedure is outlined for estimating the 'static' *in situ* strength profile from the 'dynamic' strength profile. The experimental results obtained in the laboratory under fully controlled conditions are in good agreement with proposed theoretical model.

Tests conducted on terrestrial soils with a penetrometer developed for shallow depth exploration in marine environment demonstrate the potential value of the proposed instrument for *in situ* testing of marine sediments. Finally, the conceptual description of a marine impact penetrometer suitable for exploring great depths is discussed briefly.

ACKNOWLEDGMENTS

TABLE OF CONTENTS

Page

LIST OF TABLES

LIST OF FIGURES

NOTATION

The symbols used in this report are defined where they first appear. The list will serve as a general reference and a guide for the subsequent appearance of a symbol. In a few instances a given symbol is used to represent two or more entirely different quantities. In general these different quantities do not appear in the same chapter; when this occurs, special subscripts are introduced.

A	=	Cross-Sectional area of penetrometer, maximum projected area of penetrometer, constant
A_o and A_1	=	Constant
a and a_p	=	Acceleration or deceleration of projectile
B	=	Constant, width of foundation
B_1 and B_3	=	Constant
b	=	Constant
C	=	Cohesion, constant
C_o	=	Wave velocity in target material
CRH	=	Calibar radius
C'	=	Apparent Cohesion
D	=	Diameter of Penetrometer
D_f	=	Depth of foundation
E	=	Modulus of elasticity
F	=	External fluid force on the body, soil resistive force
f	=	Constant
F_c	=	'Static' sleeve friction
F_{c_d}	=	'Dynamic' sleeve friction

g	=	Acceleration due to gravity
G.F.	=	Gage factor
H	=	Height of soil mass above original surface
K	=	Constant, soil viscosity coefficient (linear relationship)
K'	=	Hypothetical constant
K_F	=	Adhesion factor
K_L	=	Soil viscosity coefficient (logarithmic relationship)
K_1 and K_2	=	Constant
K_o	=	Coefficient of Earth pressure at rest
L and ℓ	=	Length of penetrometer, constant
L.L.	=	Liquid limit
M and M_1	=	Mass of penetrometer plus soil moving with penetrometer
M_p and m	=	Mass of projectile or penetrometer
N	=	Nose performance coefficient, standard penetration test blow count, constant
N_c, N_q and $N\gamma_r$	=	Bearing capacity factors for cone
N_c, N_q and $N\gamma$	=	Bearing capacity factors
n	=	Constant
P	=	Soil pressure acting on bottom boundary of soil plug
Po	=	Soil pressure at zero penetration, penetration at zero velocity
$\dot{P}$	=	rate of change of distance with time
Q	=	Frontal loading ($\frac{W}{A}$)
Q_c	=	Cone resistance
q_c	=	'Static' cone resistance

q_{c_d}	=	'Dynamic' cone resistance
R	=	Radius of penetrometer, gage resistance
S	=	Soil constant, unconfined compressive strength, sensitivity
s	=	Soil plug height
T	=	Total time of penetration
t	=	time
V	=	Velocity, 'Dynamic' penetration velocity
V_c	=	Critical Velocity
V_i	=	Velocity at any time (t_i)
V_{in}	=	Input voltage
V_o	=	Impact velocity, output voltage
V_s	=	Standard or 'Static' velocity
W	=	Weight of penetrometer
w	=	Moisture content
X	=	Instantaneous penetration depth
X_{max}	=	Maximum depth of penetration
Z	=	Instantaneous penetration depth
Z_m	=	Maximum penetration depth
σ_n	=	Normal stress
σ_h	=	Horizontal effective stress
τ	=	Vane shear strength
α	=	Semi-cone angle, constant, 'dynamic' strain rate
α_s	=	'Static' strain rate
β	=	Constant
γ	=	Shear deformation, constant

γ_d	=	Dry density
γ_t	=	Bulk density
u	=	Constant, Poissons Ratio
ρ	=	Mass density of soils
ρ_p	=	Density of penetrometer
ρ_s	=	Density of solid
ρ_t	=	Density of target
ϵ	=	Strain
ϕ	=	Angle of internal friction
ψ	=	Angle of annular soil cone

CHAPTER I

INTRODUCTION

1.1 General

The ocean floor is one of the last unexplored frontiers on the earth. In recent years a tremendous interest has been generated in the discovery and exploration of this unknown portion of the globe and its exploitation for both military and civilian purposes. Naval strategists are now openly considering the feasibility of deep, fixed, underwater installations--manned and unmanned, fixed underwater monitoring and surveillance stations for naval traffic, marine bench-marks, and navigational aids. In the civilian sector, the last decade has seen an almost unbelievable expansion of ocean floor activities. Offshore drilling, mostly for natural oil and gas, is now carried on in water depths of up to 1000 feet. The feasibility of extracting other raw materials from the bottom of the sea, such as sulphur and nodules of manganese, is seriously being studied. Plans are being made to construct man-made islands both for recreational and meteorological purposes. One fact is clear--increasing demands associated with an increasing population necessitates technology to turn to the ocean for food, energy and other resources.

Depending on the economic feasibility of engineering in the oceans, the list of applications of soil mechanics in marine work is boundless. Some of the past and possible future applications are:

(1) Design and construction aspects:- such as harbour protection

facilities, foundations for off-shore mining and drilling platforms, oil storage reservoirs, recreational facilities, industrial plants, radar towers, naval installations, underwater pipe-lines, cables and tubes, man-made islands, manned and unmanned installations; (2) stability analysis aspects:- such as submarine slopes, erosion, transport of beach sands, silting of harbours, deepening of navigation channels, scour around foundations placed under water; (3) salvage and rescue operations; and (4) mooring and anchoring in ocean sediments.

The design of foundations for sea floor installations as well as most other applications of soil mechanics to marine work requires detailed information on the strength properties of sea floor soils. This information can be obtained either by coring (for subsequent testing) or directly from *in situ* testings. Presently available sampling techniques, however, are known to disturb the soil and provide a very poor engineering sample for laboratory analysis (see Chapter 2.2 for detailed discussion). This suggests the need for an *in situ* method to provide necessary data. A variety of techniques used for terrestrial *in situ* strength measurements is available for adaption to ocean floor work. In addition to the enormous development cost, the complexities involved in deploying and operating any of the modified conventional terrestrial *in situ* testing devices have restricted their use to only very sophisticated projects.

For these reasons, an instrument called 'Impact Cone Penetrometer' has been devised for the rapid *in situ* testing of marine sediments. The term impact cone penetrometer requires some clarification to prevent confusion with other penetrometers or penetration test

instruments used in the normal practice of Geotechnical Engineering, such as static Cone Penetrometer, and Standard/Dynamic Penetration test (SPT). The impact cone penetrometer may be defined as a cone-tipped right circular cylinder which, after impacting, penetrates a target like a soil medium under its own momentum gained during a free or forced drop whereas the other types of instruments mentioned above are driven by some constant force/velocity.

The proposed penetrometer, in addition to recording acceleration/deceleration (as described by previous investigators), is capable of recording cone thrust and local side friction simultaneously and continuously up to the penetrated depth. The working principle of the instrument is very similar to a free falling or triggered corer with velocity on impact being 15 to 30 ft./sec. when triggered approximately 30 ft. above the sea bed. It can be operated from a relatively small ship even in adverse sea conditions and without special handling gear.

1.2 Statement of Problem and Objectives

The problem of impact penetration into terrestrial materials is a classical problem of terminal ballistics. This problem was attempted as early as the 15th century and an immense amount of literature has been published on both the theoretical and experimental aspects. The existing knowledge on impact penetration phenomena and various difficulties encountered in this field has been summarized in Chapter II of this thesis. A short summary of the various existing techniques for *in situ* testing of marine sediment is also given in that chapter.

The major objective of earlier research was to find the depth

of penetration of an impacting projectile to provide passive protection
against bombing or shelling, for personnel and underground installations
(Robertson, 1941).[1] Recent work has highlighted many possible avenues
of engineering applications (McNeill, 1972), among those are obtaining
in situ strength properties of inaccessible terrestrial soils (Sandia
Laboratory, 1968), lunar soils (Anon, 1966), and ocean sediments (Scott,
1967b).

     With the advancement of electronics the present day penetro-
meters are instrumented with accelerometers and are useful tools in
tracing the velocity profile and depth of penetration of the penetro-
meter. Various theoretical relationships, mostly based on Newton's
second law of motion have also been proposed for estimating the velocity
profile, maximum penetration depth, and total force; for example, Wang
(1971); Schmid (1969); Thompson (1966); and Hakala (1965). In these
considerations however, the target material has been assumed to be
homogeneous isotropic half space, either compressible elastic,
incompressible plastic, or viscoplastic. Unfortunately, soil deposits
generally do not satisfy most of the above properties and consequently,
available theoretical relationships have little value from a practical
point of view. To overcome this, attempts have been made to categorize
the soil strength parameters based on the experimental results, but the
limitations of such attempts are legion. In each program the penetro-
meter has been of various dimensions and frequently of different shapes,

---

[1]The citations on the following pages follow the style of the
Canadian Geotechnical Journal published by National Research Council of
Canada.

thus making a comprehensive interpretation very difficult. In very few test programs the soil properties were varied over a sufficiently wide range to identify accurately their effect on the response of an accelerometer monitored impact penetrometer. The results to date indicate that it is not possible to obtain *in situ* strength of the soil from accelerometer signatures alone. Therefore, the existing instrumentation techniques adopted by various investigators are being modified in the current investigation. The present impact penetrometer is capable of recording deceleration, cone thrust, and local side friction. With those recorded values it is possible to predict the 'dynamic' strength of the target continuously at all depths of penetration.

Furthermore, the problem at hand is somewhat different from any of the previous in the sense that:

1. The present investigation is aimed at estimating the soil properties from impact penetration tests whereas most of the previous studies were confined to the mere evaluation of the depth of penetration.

2. Velocity range under which the present impact penetration tests would be performed is low (15 to 30 ft./sec.) in comparison to other investigations (200 to 800 ft./sec.).

3. In the present analysis, the frontal loading ($\frac{W}{A}$) is much higher, and as such, the expected deceleration would be much lower (1 to 10 g.) in comparison to the work carried out by Sandia Laboratory and others, where deceleration was comparatively very high (200 to 1000 g.) because of a relatively

low frontal loading and high impact velocity.

4. By and large, the existing penetrometers are projectile-like in shape and penetrate to a much greater depth than the length of the penetrometer itself. Probably this type of shape and higher impact velocity lead to cavitation phenomena around the penetrometer and in consequence the side or local friction is completely omitted in previous analyses. The proposed penetrometer has been designed for a normal penetration depth not greater than the length of the penetrometer. It is believed that this shape, associated with a low impact velocity, would prevent the cavitation around the penetrometer.

5. In the present investigation, the emphasis is on soils of low to moderate strength simulating those generally found on ocean floor while the existing knowledge is mainly on granular soils or terrestrial soils of high strength.

The objectives of the present study are:

1. To develop the capability of the proposed instrument for laboratory and field usage,

2. To study the response of the instrument under different test conditions,

3. To study the different aspects of low velocity impact penetration mechanism whereby a theoretical model can be developed for the prediction of the target strength, penetration depth, velocity profile, etc.,

4. To attempt a theoretical/experimental approach for obtaining

'static' strength profiles directly from impact penetration test results, and

5. To study the application of impact penetration test results for estimating the soil type on lines similar to friction ratio concepts developed for static cone penetration tests (Schmertmann, 1969).

Chapter III presents the development of the theoretical model based on present experimental investigations and past studies. A theoretical relationship between the instantaneous velocity, various 'static' and 'dynamic' soil properties, penetrometer characteristics, and instantaneous depth of penetration has been obtained from momentum concepts. It is assumed that during impact penetration the shear failure occurs and the shear front is similar to that proposed by Meyerhof (1961) for a deep cone tipped pile. The reasons for adopting the Meyerhof failure criteria, instead of Terzaghi and Peck (1948) which was used by Scott (1962), is that (i) it takes into account the various physical factors (shape, surface roughness, etc.); (ii) the Meyerhof failure patterns have been observed in the two dimensional impact penetration test by Thompson (1966); and (iii) the experimental values agree better with the analytical values obtained from the Meyerhof pattern than those of other failure criteria. In addition, the dynamic effects on soil strength which was completely ignored by Scott, have been incorporated in the present analysis.

Chapter IV deals with the experimental program and instrumentation techniques adopted in this investigation. The test program included mainly laboratory testings conducted under fully controlled

conditions in order to study the response of the proposed instrument to different test conditions and to evaluate the validity of the proposed theoretical model. The tests included constant velocity penetration tests performed at different penetration velocities on two and three dimensional targets, and impact penetration tests. The obtained experimental results have been analysed in Chapter V. Some examples have been presented for estimating the 'static' target strength from 'dynamic' results and also from theoretical considerations.

In Chapter VI the design and development of a field penetrometer for 8 ft. penetration is outlined. The experimental results obtained with this penetrometer on terrestrial soils have been presented. The possibility of developing the impact penetrometer for greater depth exploration work has also been discussed briefly. Finally, the conclusions and recommendations for future extension of the work have been presented in Chapter VII.

The project, besides contributing to the knowledge of low velocity impact penetration mechanism, would provide a means for measuring most needed information for off-shore structural designers and would make a significant contribution to the knowledge of marine geotechnique. The work can be applied to other areas of *in situ* strength testing where the site is not easily accessible (e.g. swamps, lunar soil exploration program, snow, glacier and sea ice).

CHAPTER II

THE STATE OF THE ART AND LITERATURE REVIEW

Previous research in the field of "Impact Penetrometer and its application for *In situ* testing of Marine Sediments" may broadly be divided in two independent research areas:

1. Impact penetration of Terrestrial Materials,
2. *In situ* testing of Marine Sediments.

2.1 Impact Penetration of Terrestrial Materials

The problem of an object penetrating into a terrestrial material is a classical problem of terminal ballistics. An immense amount of literature both theoretical as well as experimental exists on the subject and most of these investigations are concerned with projectiles striking a relatively hard target at considerably high velocities. In this thesis, the term high velocity will be used to describe events for which impact velocity is greater than perhaps 50 ft./sec. The term low velocity will be used to describe events for which impact velocity is lower than 50 ft./sec. Leonardo da Vinci (McNeill, 1972) in the late 1400's was possibly one of the first to attempt a scientific appraisal of penetration; even before Newton's time, Da Vinci considered the "power of the bombard" (-ing projectile) and "the resistance of the object (stone wall) struck" in designing fortification walls for Count Sforza of Milan. In 1742, in one of the earliest serious studies of penetration, Robins observed in his report

"Principles of Gunnery" that the depth of penetration of a ball into a body was proportional only to the square of its striking velocity and concluded that the resistance of a given target was always constant. The great mathematician Euler (1745), used Robins' work to derive the Robins-Euler Prediction equation which states that penetration is solely dependent on the target property. Poncelet (1892) published a study which concluded that penetration was proportional both to target strength and penetration velocity. Petry's analysis was made in 1910. From 1910 to 1943, Peres, Probert, Morin and Didion, H. P. Robertson, Nobile de Giorgi and others reported work which evaluated the constants in the formula previously developed.

Recently the impact penetration problem has been attacked from many directions to achieve some meaningful relationships. The bulk of the literature available to date can be classified in the following three categories:

(i)   Theoretical Studies,

(ii) Empirical Studies,

(iii) Experimental Investigations.

2.1.1. Theoretical Studies

Theoretical and quasi-theoretical expressions relating the dependent and independent variables of the impact penetration problem have been developed by many researchers. All have assumed the soil target to be homogeneous, isotropic and half-space and the projectile or missile impacts normal to the half space and that its axis is a tangent to the trajectory. The penetration path is considered to be vertical.

Basic Theory of Earlier Research

Newton's equation of Motion is the starting point for most of these theories:

$$Mg - F = M.a_p \qquad \text{II-1}$$

which must hold when the projectile is at any depth and moving with any velocity, where

M = Mass of projectile plus soil moving with projectile

g = Acceleration due to gravity

F = Soil resistance to movement

a_p = Acceleration or deceleration of projectile.

Gravity force on the projectile is small compared to the soil resistance force and the soil mass moving with the projectile is relatively very small and hence may also be neglected. Thus equation II-1 may be rewritten as:

$$- F = M_p \frac{dV}{dt} \qquad \text{II-2}$$

where

M_p = Mass of projectile.

In general, the resisting force F is a function of projectile velocity (V) or

$$F = f(V) \qquad \text{II-3}$$

$f(V)$ is a combined result of three components viz., $f_1(V^0)$, $f_2(V^1)$ and $f_3(V^2)$ respectively.

Substituting in the value of F, equation II-2 may be written as

$$- M_p \frac{dV}{dt} = f(V) = f_1(V^0) + f_2(V^1) + f_3(V^2) \qquad \text{II-4}$$

Equation II-4 essentially postulates that during the first phase of penetration, at high velocity, the motion is governed by the resistive force proportional to the square of velocity. This force would be analogous to the drag resistance in fluid flow. Subsequently at moderate velocities, the resistance is proportional to the first power of velocity and, hence, during this phase the resistance is analogous to the viscous resistance in fluid phase. In the last phase the resistance is primarily caused by static forces.

If the functions in equation II-4 are assumed to be constant coefficients, the statement is simplified to

$$- M_p \frac{dV}{dt} = \alpha + \beta V + \gamma V^2 \qquad \text{II-5}$$

Equations II-4 or II-5 are the starting point of most of the past and present theoreticians. Equation II-5 is the general form of various well known penetration formulae. If for example one takes $\beta = \gamma = 0$, one obtains the Robins-Euler Formula. For the case of $\beta = 0$, we obtain Poncelet's equation. The following is a list of formulae proposed by various investigators based on the general solution of equation II-5.

Robins (1742) and Euler (1745)

$$- M_p \frac{dV}{dt} = \alpha \qquad \text{II-6}$$

Giving the maximum penetration,

$$X_{max} = \frac{M_p V_o^2}{2\alpha} \qquad \text{II-7}$$

where V_o = Impact velocity

Poncelet (1829)

$$-M_p \frac{dV}{dt} = \gamma V^2 + \alpha \qquad\qquad \text{II-8}$$

giving

$$X_{max} = \frac{M_p}{2\gamma} \ell n \left[1 + \frac{\gamma V_o^2}{\alpha} \right] \qquad\qquad \text{II-9}$$

Resal (1895)

$$-M_p \frac{dV}{dt} = \gamma V^2 + \beta V \qquad\qquad \text{II-10}$$

giving

$$X_{max} = \frac{M_p}{\gamma} \ell n \left[1 + \frac{\gamma V_o}{\beta} \right] \qquad\qquad \text{II-11}$$

Allen et al. (1957)

$$-M_p \frac{dV}{dt} = \gamma V^2 \text{ for } V_o > V > Vc \qquad\qquad \text{II-12}$$

$$-M_p \frac{dV}{dt} = \beta V^2 + \gamma \text{ for } Vc > V > o \qquad\qquad \text{II-13}$$

Where Vc = critical velocity.

Based on experimental results Allen et al. proposed the
critical velocity as 200 ft./sec. They characterized that impact at
a velocity greater than Vc is largely inelastic and at a velocity
less than Vc the projectile simply pushes the sand aside more or less
elastically.

Chisholm et al. (1962)

$$-M_p \frac{dV}{dt} = \beta V + \gamma \qquad\qquad \text{II-14}$$

Hakala (1965)

$$- M_p \frac{dV}{dt} = \gamma V^2 + \alpha X + \mu \text{ for } V_o > V > V_c \qquad \text{II-15}$$

$$- M_p \frac{dV}{dt} = \beta V + \alpha X + \mu \text{ for } V_c > V > o \qquad \text{II-16}$$

Schmid (1969), Grasshoff (1953)

$$- M_p \frac{dV}{dt} = \alpha + \beta V + \gamma V^2 \qquad \text{II-17}$$

The solution of equation II-5 or II-17 depends on the magnitude of the coefficient α, β, and γ, and has been presented by Schmid (1969) in the following forms:

(I) for the case where $\beta^2 < 4\alpha\gamma$;

$$X = \frac{M_p}{2\gamma} \ell n \frac{\gamma V_o^2 + \beta V_o + \alpha}{\gamma V^2 + \beta V + \alpha} - \frac{M_p}{\gamma} A (4\alpha\gamma - \beta^2)^{-\frac{1}{2}} \qquad \text{II-18}$$

$$t = 2A \ M_p \ (4\alpha\gamma - \beta^2)^{-\frac{1}{2}} \qquad \text{II-19}$$

where X is the instantaneous penetration at time t and velocity V and V_o is the velocity of impact.

$$A = \tan^{-1} (2\gamma V + \beta)(4\alpha\gamma - \beta^2)^{-\frac{1}{2}} - \tan^{-1}$$
$$(2\gamma V + \beta)(4\alpha\gamma - \beta^2)^{-\frac{1}{2}} \qquad \text{II-20}$$

(II) for the case where $\beta^2 > 4\alpha\gamma$;

$$X = \frac{M_p}{2\gamma} \ell n \frac{\gamma V_o^2 + \beta V_o + \alpha}{\gamma V^2 + \beta V + \alpha} - \frac{M_p}{\gamma} B (\beta^2 - 4\alpha\gamma)^{-\frac{1}{2}} \qquad \text{II-21}$$

and $t = \frac{2M_p}{} (\beta^2 - 4\alpha\gamma)^{-\frac{1}{2}} \qquad \text{II-22}$

$$B = \frac{1}{4} \ln \frac{\{2\gamma \, V + \beta + (\beta^2 - 4\alpha\gamma)^{\frac{1}{2}}\}\{2\gamma \, V_o + \beta - (\beta^2 - 4\alpha\gamma)^{\frac{1}{2}}\}}{\{2\gamma \, V + \beta - (\beta^2 - 4\alpha\gamma)^{\frac{1}{2}}\}\{2\gamma \, V_o + \beta + (\beta^2 - 4\alpha\gamma)^{\frac{1}{2}}\}} \quad \text{II-23}$$

(III) for the special case where $\beta^2 = 4\alpha\gamma$;

$$X = \frac{M_p}{2\gamma} \ln \frac{\beta + 2\gamma \, V}{\beta + 2\gamma V_o} - \frac{\beta}{\gamma} \frac{CM_p}{\gamma} \quad \text{II-24}$$

$$t = 2 \, CM_p \quad \text{II-25}$$

where $C = (2\gamma \, V + \beta)^{-1} - (2\gamma V_o + \beta)^{-1}$. II-26

(IV) for this same case ($\beta^2 = 4\alpha\gamma$) β can also be expressed as $\beta = 2\alpha^{\frac{1}{2}} \gamma^{\frac{1}{2}}$ and the integration of equation II-5 will lead to:

$$X = \frac{M_p}{\gamma} \ln \frac{\alpha^{\frac{1}{2}} + \gamma^{\frac{1}{2}} \, V_o}{\alpha^{\frac{1}{2}} + \gamma^{\frac{1}{2}} \, V} - \alpha^{\frac{1}{2}} \gamma^{\frac{1}{2}} \frac{V_o - V}{(\alpha^{\frac{1}{2}} + \gamma^{\frac{1}{2}} \, V_o)(\alpha^{\frac{1}{2}} + \gamma^{\frac{1}{2}} \, V)} \quad \text{II-27}$$

and

$$t = M_p \frac{V_o - V}{(\alpha^{\frac{1}{2}} + \gamma^{\frac{1}{2}} \, V_o)(\alpha^{\frac{1}{2}} + \gamma^{\frac{1}{2}} \, V)} \quad \text{II-28}$$

Wang (1971)

$$- M_p \, V \frac{dV}{dX} = \alpha + \beta \, V^2 + \gamma \, X \quad \text{II-29}$$

This is similar to the equation II-15 proposed by Hakala. The solution of this equation is given in the following form:

$$V = \left[\left\{ V_o^2 - \frac{M_p}{2\beta} \left(\frac{\gamma}{\beta} - \frac{2\alpha}{M_p} \right) \right\} \exp \left\{ - \left(\frac{2\beta}{M_p} \right) X \right\} - \left(\frac{\gamma}{\beta} \right) X \right.$$
$$\left. + \frac{M_p}{2\beta} \left(\frac{\gamma}{\beta} - \frac{2\alpha}{M_p} \right) \right]^{\frac{1}{2}} \quad \text{II-30}$$

and deceleration versus penetration is given as

$$- a = \left\{ \frac{\beta V_o^2}{M_p} - \frac{1}{2} \left(\frac{\gamma}{\beta} - \frac{2\alpha}{M_p} \right) \right\} \exp \left\{ - \frac{2\beta}{M_p} X \right\} + \frac{\gamma}{2\beta} \qquad \text{II-31}$$

The use of above mentioned formulae for general purposes is restricted by the fact that the material constant values α, β, and γ have to be determined for each material and the impacting object. While these formulae have been used in expressing the wide variety of the test results, their validity has been tested only with a limited range of impact velocities. Besides, the values of the constants proposed by different authors are on the basis of impact velocity and depth of penetration. Most of the previous works failed to record or recognize the properties of the target material such as density, angle of internal friction, cohesion, etc. For those reasons, correlation between those constants and *in situ* soil properties is not well developed.

In recent developments of the penetration theory, the behaviour and the failure mechanism of the target material have also been incorporated. The problem has been attempted from different angles in which the failure mechanism of target material has been assumed in the form of simplified mathematical models. In the subsequent paragraphs, the work of a few of the principal authors has been briefly discussed.

Scott (1962) developed theoretical solutions, assuming the target material both (a) compressible – elastic, and (b) incompressible–plastic. For compressible soil, the penetration resistance is assumed to be a function of the instantaneous depth of penetration instead of

the instantaneous velocity of penetrometer and the weight of the soil
moving with the penetrometer is considered through a simple model.
Scott assumed that a soil plug of height(s), width 2R (2R = Diameter
of penetrometer), and density ρ_2 moves with penetrometer and is acted
on by a pressure of

$$P = Po + bZ^f$$

in which P is the soil pressure acting on the bottom horizontal boundary
of the soil plug, Po is the soil pressure at zero penetration, Z is the
instantaneous depth of penetration, and b and f are constants.

In the case of incompressible-plastic target materials, Scott
developed the theoretical relationship by adopting a classical solution
for the bearing capacity of soils. To calculate soil resistance, he
assumed the general shear failure mechanism as suggested by Terzaghi
and Peck (1948) for the soil target and added inertial resistance of
the accelerated soil mass to the static bearing resistance of the soil.
Similar treatment may be found in other reports (for example, Shipley
(1967), Schmid (1969)). Though Scott's later approach is a realistic
one, his assumption of the failure pattern is very conservative. Besides
this, no consideration is given to the dynamic effects on the soil
resistive force. However, the validity of those formulae could not be
established in the absence of experimental results.

Thompson (1966) made a most comprehensive theoretical study
of penetration problems. He has considered the equation of motion,
the continuity equation, the equation of state, and constitutive
soil relationships to obtain a set of partial differential equations
for the impact penetration problem. Unfortunately, those equations

can not be solved in closed form, and it appears that they are too highly non-linear to be solved numerically.

Moore (1967) developed an equation for total impact penetration based on the principle of conservation of energy under the following assumptions:

1. Soil penetration resistance is proportional to the soil density, the acceleration of gravity, and to the instantaneous depth of penetration.

2. The energy available for penetration is proportional to the kinetic energy of the penetrometer immediately before impact.

The equation derived by Moore is:

$$\frac{Z}{L} = K \left(\frac{\rho_p}{\rho_t} \right)^{\frac{1}{2}} - \frac{V_0}{g^{\frac{1}{4}} L^{\frac{1}{2}}} \qquad \text{..II-32}$$

in which Z is the depth of penetration, L is the length of penetrometer, ρ_p and ρ_t are the densities of the penetrometer and the target respectively, and K is a constant. Again the value of K has to be determined experimentally for different target materials and penetrometer's size and shape.

Tsai and Schmid (1969), Schmid (1966), and Anon (1966) studied the penetration phenomena for a projectile having an increasing area of cross-section. Anon carried out his research for the development of the Lunar Penetrometer of spherical shape. The resulting equation of motion--a non-linear differential equation, has been expanded by utilizing the Taylor series expansion. A relationship between the instantaneous velocity and the density and compressive strength of the target material, mass and diameter and impact velocity of the penetrometer

has been obtained. A very good agreement is claimed for the velocity range from 500 to 6000 ft./sec. and for target materials ranging from soft polyethylene to glass fibre reinforced epoxy resins. However, for the impact velocity range of interest in ocean bottom penetration, no experimental confirmation of the validity of the equation is available.

Schmid (1969, 1966), Tsai (1967), Tsai and Schmid (1969) have considered the problem assuming target material either (a) ideal plastic, or (b) viscous. Further, the target material (soil) is represented by rheological model consisting of springs and dashpots. Unfortunately a functional relationship between the soil resistance and time must be assumed in order to predict the response of impact penetrometers from those equations. In general, soil resistance versus time plots: (1) assume a fixed functional shape within only limited ranges of the independent variables, and (2) are complex curves which would be difficult to represent mathematically. Thus, those solutions may be valid only in special cases.

Based on the assumption that during impact penetration the displacement field can be obtained to describe the motion of soil media at all times during penetration, Reeves (1969) employed finite element to model a soil half space by the generation of an axisymmetric body of revolution. The calculation of strain and inertial energies is done on a time increment basis and at the end of each increment, the sum of energy put into soil medium is subtracted from the kinetic energy of the projectile until the projectile is stopped. The result of this operation is an ensemble of depth, velocity, force, and

transfer of energy relations each obtained as a function of time. A comparison of his analysis with experimental results shows the variation of 15 to 50% at impact velocities ranging from 183 ft./sec. to 200 ft./sec.

2.1.2. Empirical Studies

Because of the complexity in developing the analytical formula of impact penetration, quite a large number of empirical relationships can be found in the literature. These are designed to develop empirical, analytical relationships from the test results of experimental programs and are mostly concerned with high impact velocities.

Tolch and Bushkovitch (1947) recommend for small projectiles striking soft rock:

$$X_{max} = 4.6 \frac{W}{D^{1.83}} 0.001 \, V_o \qquad \text{II-33}$$

and for large projectiles:

$$X_{max} = 1.4 \frac{W}{D^{1.53}} (0.001 \, V_o)^{1.8} \qquad \text{II-34}$$

Lang (1956) on the other hand reports:

$$X_{max} = \frac{KW}{D^2} V_o \, 1.96/S^{0.065} \qquad \text{II-35}$$

where W = weight of projectile

  D = diameter of projectile

  S = unconfined compressive strength of the target-rock or soil

  K = constant

For penetration into rock, Maurer and Rinehart (1960) find:

$$X_{max} = K_1 \frac{W}{D^2} (V_o - K_2)$$

II-36

where for softer material such as soil, Rinehart (1960) and Palmore (1961) suggest:

$$X_{max} = \frac{K_1 W}{D^2} \ln (1 + K_2 V_o^2)$$

II-37

Where X_{max} is total penetration in inches, W is the weight of the impacting object in pounds, D is the diameter in inches, and V_o is the impact velocity in ft./sec. The coefficients K_1 and K_2 are material parameters.

Goldsmith (1960) reports the following equations:

$$X_{max} = \frac{1}{2} \frac{Mp}{B_1} \ln \left(\frac{B_1}{B_3} V_o^2 + 1 \right)$$

II-38

and

$$X_{max} = BD \left(\frac{V_o}{Co} \right)^n \quad \text{for } 0.1 < \frac{V_o}{Co} < 1.0$$

II-39

Where D is the diameter of a projectile and Co is the wave velocity in target material. The values B_1, B_3 and B are determined from test data.

McCarty and Carden (1962) report the following results from the low velocity (V_o = 5 to 30 ft./sec.) tests in which cylindrical penetrometers tipped with hemispherical noses were impacted onto dry sand.

$$X_{max} = 2.6 Mp^{\frac{1}{2}} V_o^{2/3} /D$$

II-40

Where X_{max} is maximum penetration in inches, Mp is the
penetrometer mass in pounds sec.^{2}/in, V_o is the penetrometer impact
velocity in in./sec. and D is diameter in inches.

From the series of high velocity (V_o = 190 to 900 ft./sec.)
test in which 3 inch diameter cylindrical penetrometer tipped with
hemispherical and conical noses was impacted onto a layered soil
profile consisting of silty sand, sandy clay, and clayey sand, McCarty
and Carden found that

$$X_{max} = 0.005 \, MpV_o^{3/2} \qquad\qquad II-41$$

It should be noted that in formulae II-40 and II-41 a single
value for the coefficient has been given covering a wide variety of soils.

Hechtl (1964) made an experimental study on the medium velocity
projectile penetration problem and established a correlation with the
impact test values and C.B.R. (California Bearing Ratio) test. Hechtl's
correlation may be useful in assessing the soil trafficability problem.

Utilizing experimental data derived from tests conducted by the
Sandia Laboratories in which a wide range of impact velocities and soil
types were investigated, Woodward, Clyde, Sherard and Associates
(1962-1967) developed two empirical expressions for the total depth of
penetration:

$$X_{max} = \frac{1}{a} \ell n \, (1 + \beta V_o) \qquad\qquad II-42$$

$$X_{max} = \frac{1}{d} \ell n \, (1 + bV_o^2) \qquad\qquad II-43$$

in which:

$$\alpha = \frac{(80 + N)\,\rho_t C g}{625,000\,\,\ell Q}$$ II-44

$$\beta = 1.26A \times 10^{-6}$$ II-45

$$d = \frac{(85 + N)(1.29 - 3.5V_o \times 10^{-4})\,\rho_t R C}{14,000\,\,\ell Q}$$ II-46

$$b = 0.431A \times 10^{-6}$$ II-47

$$C = 1.0 + 1.5 \,\text{sech}\left(\frac{N}{10}\right) - 2.5 \exp\left(-\frac{N^2}{52}\right)$$ II-48

$$\ell = 0.042 \,(CRH) + 0.942$$ II-49

and N is the standard penetration test blow count, ρ_t is the soil target density in lbs. - sec.^{2}/ft.^{4}, g is the local acceleration of gravity in ft./sec.^{2}, Q is the penetrometer frontal loading in psi, A is the frontal area of penetrometer in in.^{2} and CRH is caliber radius head of the penetrometer nose. These equations were based on the test results obtained from long slender penetrometers tipped with blunt to very sharp noses.

Young (1969) assumed a functional relationship to describe the penetration event in the form

$$X = f_1(N)\,\,f_2(A)\,\,f_3(W)\,\,f_4(V)\,\,f_5(S)$$ II-50

where W = weight of penetrometer in lbs.

A = cross-sectional area of the penetrometer in in.^{2}

N = a vehicle nose performance constant

S = a constant which lumps together all pertinent soil properties over the total penetration depth

By judicious interpretation of numerous field tests, Young evaluated the functions in the following equations:

$$X_{max} = 530 \, SN \sqrt{Q} \times 10^{-3} \, \ln (1 + 20 \times 10^{-6} \, V_o^2) \text{ for}$$

$V_o < 200 \text{ ft./sec.}$ \hfill II-51

$$X_{max} = 3100 \, SN \sqrt{Q} \times 10^{-6} \cdot (V_o - 100) \text{ for } V_o > 200 \text{ ft./sec.}$$ \hfill II-52

where the terms are as previously defined and

Q = frontal loading or W/A.

Young's equation is amenable to graphic solution, and requires some approximate value of S for tested material. Values of S (measured) lie within a wide range from less than 1 to 50 or perhaps more. Thus, the investigator has a wide choice of S values available to characterize a given deposit. It is necessary to assume that S is constant for a given target. Thus, for a penetration in layered media of widely different properties, the correct equivalent uniform value of S will depend on the total depth penetrated. For this reason, application of Young's or other empirical approaches require a great deal of experience and judgement for estimating the values of the soil constant.

Mitchell *et al*. (1969) conducted a statistical evaluation of several equations for total penetration utilizing available test results. Out of the seven equations evaluated, the following equation gave the best fit to experimental data.

$$X_{max} = KNQ^{\frac{1}{2}} V_o + Po$$ \hfill II-53

where K = Soil constant

N = Penetrometer nose shape and dimension constant

Q = Penetrometer frontal loading (W/A)

V_o = Impact velocity

Po = Penetration at zero impact velocity

Mitchell *et al.* also experimentally investigated oblique impact penetration of soil target. Those studies indicate that the above equation will adequately predict total penetration if the term (V_o) is taken to be equal to the component of the impact velocity normal to the target surface.

Dunlap (1972) performed impact penetration tests on several selected sites to encompass a representative distribution of soil types, ranging from sands through silts to clay. Based on *in situ* measurements of soil parameters and penetration depth, two relationships have been proposed, one for sand and the other for silts and clays.

Murff and Coyle (1973B) tried different polynomials in velocity and depth to fit the experimental data obtained under fully controlled conditions and found that a linear function of velocity and depth gave an excellent fit both for clay (correlation coefficient 0.98) and sand (correlation coefficient 0.93). The value of different coefficients was established in terms of unconfined compressive strength and relative density for clay and sand respectively.

2.1.3. Experimental Investigations

Numerous experimental investigations have been conducted to

develop a qualitative understanding of the impact penetration problem. In those studies a wide range of dependent and independent parameters have been studied. Independent parameters investigated have included penetrometer's weight, shape and size, penetrometer impact velocity and angular orientation at impact, properties of soil target and the ambient environmental conditions. Among the quantities which have been recorded in these studies are the acceleration time history of the penetrometer, the total depth of penetration, the dimension of the post-impact target surface, and the deformation pattern produced within the soil target during penetration. The effects of changes in various independent parameters on the output of an accelerometer-monitored impact penetrometer are summarized below.

2.1.3.1 Penetrometer characteristics

The independent variables like weight and diameter of impact penetrometer have been studied by McCarty and Carden (1962, 1968); Clark and McCarty (1963); Hanks and McCarty (1966); Anon (1966), Carden (1967); Caudle et al. (1967); Moore (1967); Mitchell et al. (1969); Young (1969), and Murff and Coyle (1972, 1973A). It has been indicated that an increase in penetrometer weight yields an increase in total penetration, an increase in the characteristic times (e.g. the time to reach maximum deceleration and the total time of the penetration event) and a decrease in measured decelerations, whereas the increase in the diameter of the penetrometer produces a decrease in total penetration, a decrease in characteristic time, and an increase in measured decelerations.

Thompson (1966), Woodward, Clyde, Sherard, and Associates (1962-1967), Young (1969), and Murff and Coyle (1972, 1973A), have made the experimental study of the nose sharpness and shape of the impact penetrometer and found that an increase in nose sharpness yields an increase in total penetration. Murff and Coyle indicate that Penetrometer geometry and the ratio of weight to cross-sectional area profoundly influence the performance of penetrometers.

2.1.3.2. Impact Velocity and Impact Angle

Grasshoff (1953), McCarty and Carden (1962, 1968), Hanks and McCarty (1966), Anon (1966), Caudle, et al., (1967), Carden (1967) and Murff and Coyle (1972) have studied the performance of penetrometers with varying impact velocity. It is concluded from their studies that an increase in penetrometer impact velocity yields an increase in measured decelerations, decrease in characteristic times and an increase in total penetration. Murff and Coyle further indicate that depth of penetration is a linear function of the impact velocity.

Anon (1966), McCarty and Carden (1968), and Mitchell et al., (1969) have carried the experimental investigation to study the effects of impact angle (the angle between the path of the penetrometer and normal to the soil target surface). It is concluded from their study that an increase in the impact angle produces a decrease in total penetration, a decrease in measured decelerations, and an increase in the characteristic times.

2.1.3.3. Soil Characteristics

Field and laboratory investigations have been conducted to

study the response of different types of soils and rock on impact penetration. It has been recognized that the penetration depth, as well as the shape of the deceleration versus time records, is highly dependent on soil properties. In addition, the deceleration signatures are quite sensitive to soil type. For example, clay generally exhibits a low deceleration and a smooth acceleration time-signature (Woodward, Clyde, Sherard and Associates (1962-1967), Caudle et al. (1967)). In gravel, larger decelerations are recorded than in sand, and the acceleration time signatures are also rougher than in sand.

Hakala (1965), Thompson (1966), and Awoshika and Cox (1968) have mentioned that sand and gravel may be comminuted during penetration. Wang (1971) has given a theoretical expression for the energy expended on pulverization, though very little change in the gradation has been observed in his experiments (velocity range, $V_o = 25$ ft./sec.). Womack and Cox (1967) have also observed air blast effects such as the ejection of material during impact on sand.

Vey and Nelson (1965, 1967), Hanks and McCarty (1966), Anon (1966), Moore (1967), Carden (1967), McCarty and Carden (1968), and Orrje and Broms (1970) have investigated the soil density effects on the penetration event. It is inferred from their investigations that increase in soil density yields a decrease in total penetration, an increase in measured deceleration, and decrease in characteristic times. The effects of moisture content and degree of saturation on penetration event have also been studied by various workers (see for example Reichmuth 1967). It is stated that impact penetration forces will decrease considerably as the percentage by weight of solids is

increased and will increase to a lesser extent as the water content is increased.

2.2. *In situ* Testing of Marine Sediment

The growing interest in placing engineering structures or equipment on the ocean floor or carrying out certain operations on it generally requires a knowledge of the mechanical properties of the material. Only relatively recently have attempts been made to measure the relevant properties of ocean floor sediments as obtained in core samples (McLelland (1956), Hamilton (1963, 1965), Richards (1962, 1964, 1967), Lee (1973) and others). The present sampling techniques, however, are known to disturb the soil and provide a poor engineering sample for a sophisticated laboratory analysis (U.S. Navy Hydrographic Office (1965), Richards and Keller (1961), Anderson *et al.* (1965), Richards and Parker (1967) and others). Based on vane shear tests conducted *in situ* and on collected cores, Lee (1973) has reported disturbances of even up to 50 percent. To minimize the sample disturbance in cores, Richards and Parker recommend a design criteria of a corer which may minimize the physical disturbance of the type mentioned by Hovorslev (1949), Calhoon (1956) and Noorany and Seed (1965). There are other difficulties associated with obtaining and bringing to the surface the soil sample from deep ocean bottom. A few of these problems are: (a) Core deformation (Richards and Parker 1967), (b) Piston movement (Anderson *et al.* 1965), (c) Change in the geochemical properties (Jerbo 1967), (d) Change in the moisture content (Richard 1967), and (e) Environmental change (Vey and Nelson 1967). The environmental change may cause the expansion of pore water

volume by 0.14 percent for every 1000 ft. of water. This expansion may occur laterally and/or longitudinally, depending on the inside clearance ratio of the sampling tube. Even this expansion in volume may cause sufficient disturbance in the structural arrangement of the soil mass thereby changing the strength properties considerably.

Since it is not practical to eliminate all these problems, one obvious alternative is to examine the strength of the soil in its natural location on the ocean floor. The present description deals with some of the possible techniques of accomplishing such strength measurements which have been attempted in recent years.

2.2.1 Direct Methods

A variety of techniques used for terrestrial, in situ measurements is available for adoption to ocean floor work. However, not all are directly applicable because of the environmental hindrance. The following techniques have been tried, but are still in the stage of development.

2.2.1.1. Vane Shear Test

Fenske (1957) has reported the use of vane-shearing tests in the Gulf of Mexico. Taylor and Demars (1970) have developed an instrument "The Deep Ocean Test in Place and Observation System" (DOTIPOS) for measuring in situ shear strength with the help of vane shear and a static cone penetrometer. The DOTIPOS is pyramidal shaped with an 18 feet square base and a height of 17.5 feet supported on three 4 x 4 feet bearing pads and weighs approximately 6000 lbs. in air. This instrument is capable of measuring shear strength to a

sediment depth of 10 ft. at water depth to 600 ft. McNary and Frolich (1970), and Inderbitzen *et al.* (1971) have reported vane shear devices which can be operated by divers, for testing superficial sediment deposits. Doyle *et al.* (1971) have developed a remote controlled wire line vane probe for shear strength measurements of sediment which can be operated from either a fixed or floating base. The instrument has successfully been tested up to sediment depth of 75 ft. and water depth up to 185 ft. The wire line vane probe can be used only in bore holes and, as such, this system may be quite useful in conjunction with drilling and borings for obtaining *in situ* strength properties of marine sediments. Richards *et al.* (1971) have reported an *in situ* vane shear testing equipment capable of testing up to 10 ft. depth at one foot intervals under water depths of up to 15,000 ft. The dimensions and weight of this rig are of the same order as those described for DOTIPOS.

2.2.1.2. Static Cone Penetration Test

Static cone penetration test, in terrestrial use, is described as driving a cone tipped cylindrical rod at constant low speed whereby the cone thrust or both cone thrust and local side friction are measured either mechanically or electrically. Although this test has not been standardized formally a generally accepted practice has been developed. The cone always has a base area of 10 sq. cm. and an apex of 60°. The friction sleeve has generally a surface area of 150 sq. cm. The adopted rate of penetration is of the order of 1½ cm./sec. to 2 cm./sec. For advancing the cone, hollow rods are used with an outside diameter of 36 mm. usually in sections of 1 meter.

The development of static cone penetration tests for *in situ* measurement of ocean floor sediment has been reported by Ruiter (1971) and Hirst, *et al.* (1971) in addition to Taylor and Demars (1970). Ruiter's probe has been successfully tested for 13 meter penetration in up to 50 meters of water depth whereas Hirst's probe is operable up to an ocean depth of 1200 meters and penetration depth of two to three meters. The weight of Ruiter's probe is approximately 12 tons whereas other probes are of the same order as those mentioned for DOTIPOS. These probes take up to 4 hours for one deployment.

2.2.1.3. Plate Bearing Test

Harrison and Richardson (1967) have performed the Plate Bearing Test in shallow water (16 to 20 feet deep) in the conventional manner. The plate was loaded with a hydraulic jack and the balancing reactions were provided with the help of massive concrete blocks. However, this system is not suitable for deep water testing unless some modifications are made. Kretschmer and Lee (1969) have reported a device, developed by N.C.E.L. for performing *in situ* plate bearing tests on sea floor sediments. It is a very compact, and electronically operated remote control device and is capable of performing the test to a water depth of 14,000 feet. The equipment has an approximately 12 feet square base with a height of approximately 7 feet and weighs 4 tons in air. It can accommodate bearing plates ranging in size from 9 inches to 1.5 feet diameter and can apply a maximum load of 6000 lbs. From the analysis of the test results obtained with it, it has been established that the traditional soil mechanics concept involving elastic and bearing capacity theories appears to be applicable to analysis of weak upper strata of

sea floor soils.

2.2.1.4. Impact Penetration Test

In recent years, several studies of the penetration of the projectile at low and high velocities into soils and other granular materials have been made (refer to detailed description under the heading "Impact Penetration of Terrestrial Materials"). Based on this principle, Scott (1967A, 1967B) built an accelerometer monitored corer which collects the soil sample and records the deceleration of corer simultaneously. With the recorded acceleration, the velocity and displacement of the corer can also be computed by integration and double integration w.r.t. time respectively. This technique has been tried for both gravity and free fall types of corers. In the gravity type of corer, a simple mathematical relationship has been proposed (neglecting the drag, inertial, and other forces) for calculation of shearing resistance of soil from accelerometer records.

Korties (1969), in addition to the parameters considered by Scott, has taken into account a soil viscosity coefficient in deriving a theoretical relationship based on the force law, thereby showing a significant contribution to total force from viscous effects. Preslan (1969) has made use of accelerometer records in calculating the drag force and added mass of a free falling corer. Smith (1969), Migliore and Lee (1971), and Wilkes (1972) made use of accelerometer monitored rods for predicting the depth of penetration of sunken objects. Based on the experimental results, Smith and Migliore, and Lee have performed a regression analysis and a correlation has been proposed relating total force to the power of velocity and depth of

penetration.

2.2.1.5. Other Methods

The following are a few of the techniques which have been used
for the determination of material properties of terrestrial and extra-
terrestrial materials and can be tried for the *in situ* testing of ocean
floor also. However, it should be noted that these techniques will not
provide a direct measurement of shear strength but from observed values
the qualitative strength properties of materials can be estimated.

Pressuremeter: A technique devised by Menard (1960) to measure
the soil properties involves the expansion of a cylindrical membrane
in a prepared cavity in the soil. The membrane forces the walls of the
hole to expand as a result of internal fluid pressure. Both the
pressure and corresponding volume changes are measured and plotted.
Comparison of the experimental pressure-volume relationship with that
of the theoretical enables the values of material parameters such as
elastic modulus and yield strength. However, the application of this
method requires the preparation of a bore hole.

"Surveyor" surface sampler (Le Croissette, 1965), "Mole" (Scott
1966) or similar types of devices which have been used for determination
of material properties of the moon, Mars and Venus may be adoptive to
the ocean bottom work. "Surveyor", initially designed for obtaining
samples of surface material of the moon has been instrumented for
static and dynamic penetration measurements. In a dynamic mode of
operation it is raised and dropped onto surface, whereupon the history
of deceleration during the impact is recorded. "Mole" is a vehicle
capable of propelling itself through soft soil by means of two

counter-rotating augers driven by an internal electric motor. The power requirements of the motor, if monitored, supply an indication of the strength of the soil through which the mole is driven.

2.2.2. Indirect Methods

2.2.2.1. Acoustic

It has been found that the velocity of sound in saturated sediments is closely related to the porosity, density and mean grain size of the material (Hamilton, 1963, 1965; Lewis et al., 1969). For unconsolidated ocean sediments measured velocities range from 1.5 km/sec. to 1.8 km./sec. while the porosities range from 35 to 85 percent. However, to date no method is available to estimate the strength characteristics of marine sediments by knowing their acoustical properties.

2.2.2.2. Nuclear

The in situ bulk density and water content of sediments have been measured by Gamma radiations and neutron radiations respectively. (Meigh and Skipp, 1960; Keller, 1963; Preiss, 1968; Lai et al., 1961). In Gamma ray method the number of electrons present in each cubic centimeter of sediment is measured and related in a simple way to bulk density of sediment. Whereas, in neutron radiation the number of hydrogen nuclei present in each cubic centimeter of sediment is measured and can be expressed in grams of water per cubic centimeter. In the nuclear method, the accuracy required from an instrument is an important design criterion. If readings accurate to 5% are required, design, construction and calibration are simple, if, however, an accuracy of 1 percent or better is required, design of the system and choice of the

calibration specimens require much time and effort.

In summary, the present state of the art of *in situ* shear strength testing of marine sediment has been developed for obtaining the soil profile up to 10 ft. in deep water and up to 41 ft. in shallow water by means of either a vane shear test or a static penetration test. However the economical use of those instruments in the routine ocean sediment *in situ* tests are prevented from a combination of facts:

1. Development costs are very high, which again depends on the requirements and sophistication of the system. For example, the overall development cost of DOTIPOS is more than a million dollars.

2. Rig is extremely heavy (3 to 12 tons weight in air).

3. Handling and installations require a considerable amount of money and ship time in addition to suitable weather conditions.

4. Use of those instruments in obtaining greater depth profile in deep water is extremely difficult because of the complication of the system.

5. The overall dimensions of the instrument are limited by the characteristics of the boom on board the ship and this in turn limits the depth of penetration of either a vane or a static cone penetrometer.

CHAPTER III

THEORETICAL INVESTIGATION

This part of the thesis deals with the theoretical relationship established from the momentum considerations between the instantaneous velocity, various 'static' and 'dynamic' soil properties, penetrometer characteristics and the instantaneous depth of penetration for, a cone-tipped right circular cylinder impacting vertically at a low velocity on the target material consisting of $C - \phi$ soils. It is assumed that during the impact penetration shear failure occurs and the failure mode is similar to that proposed by Meyerhof (1961) for deep cone-tipped pile foundation. Meyerhof's failure criterion is used instead of the physical model proposed by Scott (1962) because: (i) it takes into account the physical characteristics of the projectile (shape and surface roughness); (ii) the failure patterns observed in plane-strain model impact penetration tests by Thompson (1966) and in present investigation (discussed in Chapter V) can be approximated to that of Meyerhof's failure pattern; and (iii) the experimental results agree better with the analytical values based on the Meyerhof patterns. In addition to assuming a very conservative failure pattern, Scott completely omitted the dynamic effect on soil resistive force.

Analysis

Upon impact on the soil mass, a penetrometer pushes against soil particles thus causing rupture in the soil structure. As mentioned

earlier, these rupture planes are assumed to be similar to that
proposed by Meyerhof (1961) and shown in Figure 1. Figure 1 indicates
that upon impact the conical end of cylindrical prism pushes aside the
soil below the tip via zone b, into a curvilinear shear failure zone c.
The zone b is of triangular shape for a smooth base whereas it is a
continuous curved path for a rough base.

Figure 2 shows the generalised path of soil movement during
penetration. It should be noted that annular cylindrical movement (region
4) of adjacent soil has been assumed to simplify the numerical cal-
culations. The volume occupied by the annular cylindrical region (4)
above the original surface is equal to the volume of hole made by the
penetrometer under the no volume-change condition. The shape of zone
(2) depends on the surface roughness (or the adhesion between the
surface and soil) of the penetrometer, and the soil properties. For a
smooth base, the angle ψ depends on the angle of internal friction of
the soil. The angle ψ increases as the angle of internal friction
increases whereas it is a minimum for cohesive soils and equal to the
semi-angle a of cone. In the case of a rough base, region (2) dis-
appears and forms a continuous curved flow path. Thus, the volumes of
the different regions depend on the soil properties and the surface
roughness of penetrometer and are, in general, tedious to compute.
However, numerically, the values will not differ greatly and as such it
is assumed, to simplify the calculation of the volume of different
regions, that the soil possesses only cohesion and the penetrometer is
smooth. Figure 3 shows the flow path as adopted in calculating the
volume of different regions required in generating the equation of motion.
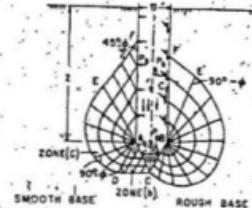
FIG 1 FAILURE ZONE NEAR CONE SHAPED FOUNDATIONS (MEYERHOF 1961)
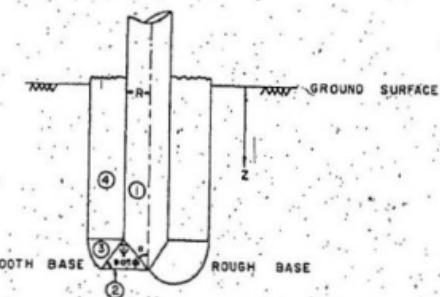
FIG 2 GENERALIZED PATH OF SOIL MOVEMENT
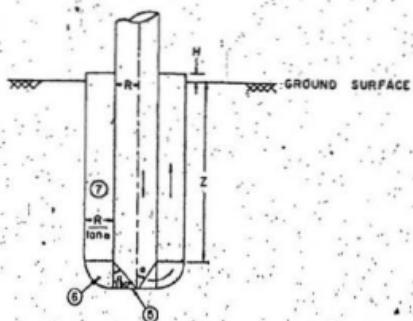
FIG 3 ASSUMED PATH OF SOIL MOVEMENT

The full arrow in Figure 3 show the relative movements of the penetrometer and the different soil masses.

3.1 Equation of Motion

The equation of motion is determined from momentum considerations. At any time t ,after impact, let the depth of penetration and velocity of penetrometer be Z and V respectively. The momentum contributions are from the penetrometer at velocity V, the annular region (5) of triangular cross-section (refer to Figure 3), the annular curved region (6) at velocities compatible with the condition of no volume change and the annular cylindrical volume (7) whose velocity is again determined from the displacement condition.

In the present investigation the adopted cone angle of the penetrometer is $60°$, and as such the masses of different regions calculated below are for the semi cone angle (α) of $30°$.

Region (1) = penetrometer mass = m

Region (5) = mass of annular triangular region = $\frac{2}{3} \pi \rho R^3$

Region (6) = mass of annular curved region = $2\sqrt{3} \pi \rho R^3 + \frac{3}{2} \pi^2 \rho R^3$

Region (7) = equivalent mass of annular cylinder (calculated

from displacement considerations) = $\frac{4 + 2\sqrt{3}}{3 + 2\sqrt{3}} \pi \rho R^2 Z$

$$= \frac{7.464}{6.464} \pi \rho R^2 Z$$

Where ρ = mass density of soil and R = radius of penetrometer.

Equivalent Mass

Referring to Figure 3, the height of heave (H) is calculated under the assumption that the volume of soil displaced by the penetrometer

is equal to the increase in volume above the original surface.

$$\pi R^2 Z = \pi [(\sqrt{3}R + R)^2 - R^2]H$$

$$H = \frac{Z}{3 + 2\sqrt{3}}$$

The volume of region (7) moving upward $= \pi [(\sqrt{3} \cdot R + R)^2 - R^2] \cdot X$

$$\left(Z + \frac{Z}{3 + 2\sqrt{3}}\right)$$

$$= (4 + 2\sqrt{3}) \pi R^2 Z$$

When the system moves a distance Z this mass moves only

$$\frac{Z}{3 + 2\sqrt{3}}$$

and consequently the velocity of this mass is also reduced in the same

proportion. To maintain a uniform momenta expression in terms of Z,

this mass has been reduced by

$$\frac{1}{3 + 2\sqrt{3}}$$

and given the term "equivalent mass" which is equal to:

$$\left(\frac{4 + 2\sqrt{3}}{3 + 2\sqrt{3}}\right) \rho \pi R^2 Z$$

Let $M_1 = M + AZ$

where $M = m + \frac{2}{3} \pi \rho R^3 + 2\sqrt{3} \pi \rho R^3 + \frac{3}{2} \pi^2 \rho R^3$

and $A = \frac{7.464}{6.464} \pi \rho R^2$

The rate of change of momentum w.r.t. time:

$$\frac{d(M_1 V)}{dt} = \frac{dM_1}{dt} V + M_1 \frac{dV}{dt} = \frac{d(M + AZ)}{dt} V + (M + AZ) \frac{dV}{dt}$$

Thus
$$\frac{d(M_1 V)}{dt} = AV^2 + 1/2 (M + AZ) \frac{d(V^2)}{dZ} \qquad (1)$$

Expression 1 must be equated to the resistance of motion to obtain the complete equation of motion. The motion is aided by the weight of the penetrometer and resisted by the weights of regions (5), (6) and (7). In addition, the motion is resisted by the resistive force offered by the soil. The magnitude of different forces can be calculated as follows:

(i) Contributions from the weight of the penetrometer and different soil masses:

$$= mg - \left(\frac{2}{3} \pi \rho g R^3 + 2\sqrt{3} \pi \rho g R^3 + \frac{3}{2} \pi^2 \rho g R^3 + 7.464 \pi \rho g R^2 Z\right) \quad (2)$$

(ii) Soil Resistance:

During the impact penetration, the penetrometer is subjected to a resistance due to 'dynamic' soil bearing capacity all the way from entry until the conclusion of penetration. Well established formulae are available for estimating the bearing capacity for 'static' loading, however, no formula is known to the writer to be adequate for 'dynamic' loading. Furthermore, the behaviour of soil under 'dynamic' loading is still not well understood. It is believed that the 'dynamic' case at low velocity is similar to the 'static' case. It is, therefore, desirable to examine all possible factors which could cause difference between

the 'static' and 'dynamic' bearing capacities of soils at these low penetration velocities. The present discussion is confined to the following two factors which are believed to be the major cause for the difference in 'dynamic' bearing capacity over 'static' bearing capacity.

(1) Strain rate effect, and

(2) Modes of failure.

3.2 Strain Rate Effect

For 'dynamic' loading conditions to and beyond failure, as in the case for impact penetration, not only will yielding occur but also viscous flow will be present. Recent tests have indicated that the angle of internal friction may not be influenced much by the rate of deformation, but the cohesion term appears to be highly influenced by the deformation rate (Casagrande and Wilson (1951), Healy (1963), Whitman and Healy (1962)). Taylor (1948), Casagrande and Shannon (1949) and Whitman (1957) have found that the strength of clay increases somewhat under 'dynamic' loading while only a slight increase in sand has been reported. Hampton and Yoder (1958) have also demonstrated a significant increase in the strength of clay soil in rapid test and it is as much as 160% in loosely compacted samples. The experiments on sand by Whitman and Healy (1962) have shown that the value of ϕ changes by 2 to 3% over a loading speed of up to 100 inches per second. Schimming et al. (1966) have also reported similar observations. Mitchell (1964) from the theory of rate process, and Peck (1962) from the results of Casagrande and Wilson (1951), Crawford (1959), Osterberg and Perloff (1962), and also from his own results, have concluded that the shear strength of clay soils is directly proportional to the logarithm of strain rate.

These results indicate that the strain rate effect on the angle of internal friction ϕ is insignificant for the low velocity penetration. On the other hand in fine grained soils, the strength is influenced by the rate of straining, and as such, its strength governing parameters should be modified for the dynamic loading condition. If the increase in apparent cohesion is assumed to be directly proportional to the logarithm of the penetration rate, the following flow condition would be obtained for the Mohr-Coulomb envelope:

$$\tau = C + K_L C \log_{10} \frac{V}{V_S} + \sigma_n \tan \phi \tag{3}$$

where

τ = Shear resistance on flow surface

C = Cohesion as defined for so called 'static' yielding case

σ_n = Normal stress

ϕ = Ultimate angle of internal friction

K_L = Apparent soil viscosity coefficient (assuming Logarithmic Variation)

V = 'Dynamic' penetration velocity

V_S = Standard or 'static' penetration velocity

If C' is called the apparent cohesion then

$$C' = C + K_L C \log_{10} \frac{V}{V_S} \tag{4}$$

3.3 Modes of Failure

Based on two and three dimensional impact penetration tests, Thompson (1966) concluded that the phenomena of impact penetration is primarily one of shear deformation. There appears to be a shear front,

defined as the line bounding the zone in which no shearing of medium
has occurred, travelling with the penetrometer. The shape of the
leading edge of the front seems to be a log spiral in the case of a
blunt-nosed projectile penetrating a half space. Furthermore,
Thompson has indicated that at any time, the displacement of the
particle is very similar to the displacement initially approximated
by Prandtl for the indentation of an infinitely long footing or a punch
into a half space of rigid-plastic weightless materials. Though his
study indicates that the shear front is similar to the log spiral
surface observed in 'static' penetration, it is not known if the shape
is related to target materials and penetrometer shape and velocity.

Colp (1965), Thompson (1966), Caudle *et al.* (1967) and
McNeill (1972) believe that mounds or craters are formed during high
velocity impact penetration and consequently no side wall resistance
is offered to the penetrometer. Whereas, based on a simple mathematical
model, Murff and Coyle (1972, 1973A) indicate that side wall resistance
is a significant portion of the total resistance in clay. For sand and
sand-clay mixture, this effect is present but is less significant. It
is believed that a critical velocity exists for all soils and for
impact velocity above this critical value, cavitation occurs. Where
cavitation, defined as encapsulation of the penetrometer by a cavity,
does occur, resistance is developed only by penetrometer nose. The
critical velocity is a function of both soil and penetrometer properties.

Based on the preceding discussion and present investigation
(explained in Chapter V) it is presumed that under the low velocity
impact the failure mode is basically of a 'static' nature (the soil

resistance is distributed over the base and shaft of the penetrometer) and the effect of the strain rate on the angle of internal friction is insignificant whereas for cohesive soils it is accounted by considering Equation (4).

3.4 Base or Cone Resistance

The cone resistance for static condition can be estimated from the following equation given by Meyerhof (1961) for the bearing capacity of cone-tipped pile foundation:

$$Q_c = \pi R^2 \{(CN_c + K_o \rho g Z N q_r + \rho g R N \gamma_r)\} \quad (5)$$

Where N_c, Nq_r and $N\gamma_r$ are bearing capacity factors for cone, and K_o is the earth pressure coefficient on shaft over the base, which is about 0.5 for sand and 1.0 for clay. Figures 4(a), 4(b), and 4(c) show the bearing capacity factors for different angles of internal friction, semi-cone angles and for the limiting conditions of perfectly smooth and perfectly rough cone surfaces. The bearing capacity factors for the intermediate degree of roughness can be found by linear interpolation between the above.

For the 'dynamic' condition, C' (equal to $C + K_s C \log_{10} \frac{V}{V_s}$) is substituted instead of C in Equation (5) and thus is modified in following form:

$$Q_{cd} = \pi R^2 \{(C + K_s C \log_{10} \frac{V}{V_s}) N_c + K_o \rho g Z N q_r + \rho g R N \gamma_r\} \quad (6)$$

3.5 Skin or Local Side Friction

Expression (6) gives only base or cone resistance to which must e added any skin friction on the shaft to obtain total resistive force
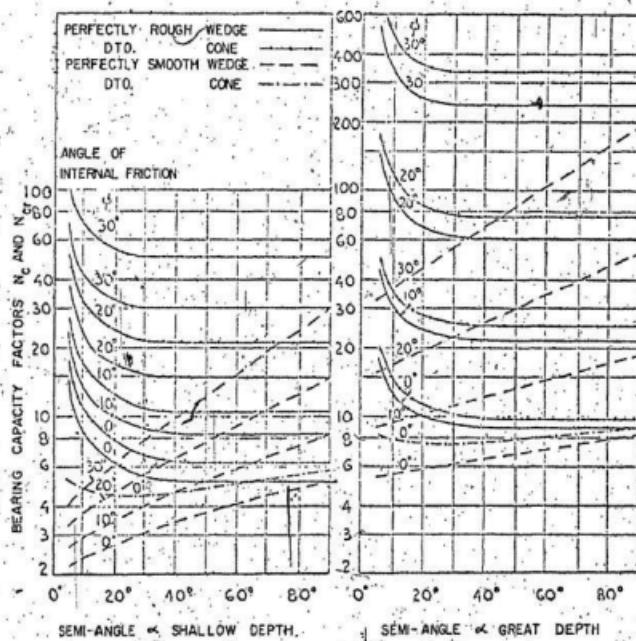
FIG.4(a) BEARING CAPACITY FACTOR N_r (MEYERHOF 1961)

SEMI-ANGLE ∝ SHALLOW DEPTH   SEMI-ANGLE ∝ GREAT DEPTH
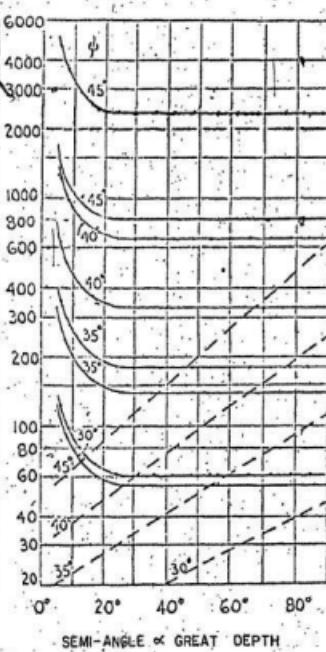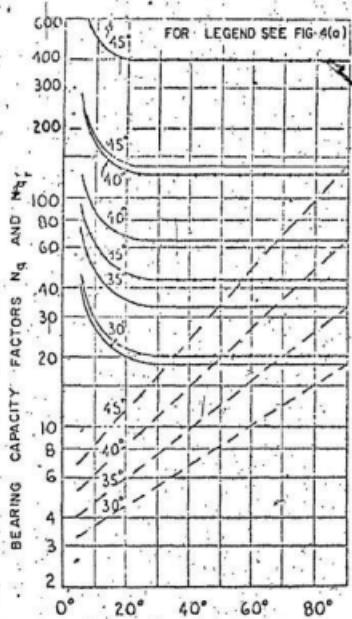
FIG-4(b) BEARING CAPACITY FACTOR N_q (MEYERHOF 1961)
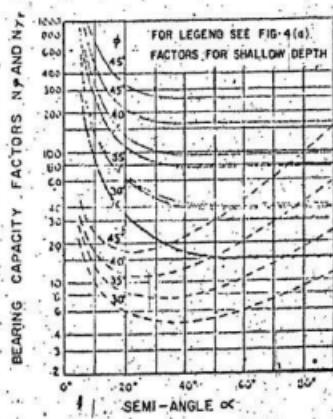
FIG-4(c) BEARING CAPACITY FACTOR N_γ (MEYERHOF 1961)

48

offered by the soil. The choice of the proper value of skin friction is rather difficult. However, it can be calculated under the simplifying assumption proposed by Scott (1962) that unit skin friction is equal to shearing resistance of soils.

The shearing resistance of a $C - \phi$ soil for the 'dynamic' condition is given by the Eqn. (3). The effective vertical stress $\bar{\sigma}_n$ on a horizontal plane in a soil mass is equal to $\rho g Z$ (neglecting the ambient pore pressure effects), but the horizontal effective stress $\bar{\sigma}_h$ on a vertical plane is variable depending on the stress history of the material. It is usually expressed by (Wu, 1966):

$$\bar{\sigma}_h = K_o \rho g Z \tag{7}$$

Thus, Equation (3) can be rewritten by putting the value of effective stress from Equation (7) to obtain 'dynamic' unit skin friction on the shaft:

$$\tau = C + K_L C \log_{10} \frac{V}{V_s} + K_o \rho g Z \tan \phi \tag{8}$$

and the total skin friction on the cylindrical surface area of the penetrometer at depth Z can be calculated and given as:

$$2\pi R Z (C + K_L C \log_{10} \frac{V}{V_s}) + \pi K_o \rho g R Z^2 \tan \phi \tag{9}$$

The net resistance to the motion at any depth can be calculated by subtracting expressions (6) and (9) from expression (2) viz.

$$mg - (\frac{2}{3} \pi \rho g R^3 + 2\sqrt{3} \pi \rho g R^3 + \frac{3}{2} \pi^2 \rho g R^3 + 7.464 \pi \rho g R^2 Z)$$

$$- \pi R^2 ((C + K_L C \log_{10} \frac{V}{V_s}) N_c + K_o \rho g Z N_q + \rho g R N_\gamma)$$

$$- 2\pi R Z (C + K_L C \log_{10} \frac{V}{V_s}) - \pi K_o \rho g R Z^2 \tan \phi \tag{10}$$

Equating the expression (10) with expression (1) and after rearranging the different terms the following equation is obtained:

$$\frac{d(V^2)}{dZ} + \frac{2AV^2}{M+AZ} = \frac{2(\alpha - \beta Z - \gamma Z^2)}{M + AZ} - \frac{K_L C(2\pi N c_r R^2 + 4\pi RZ)}{M + AZ} \log_{10} \frac{V}{V_s}$$

(11)

where $\alpha = mg - \left\{ \frac{2}{3} \pi \rho g R^3 + 2\sqrt{3}\pi \rho g R^3 + \frac{3}{2} \pi^2 \rho g R^3 + CN c_r \pi R^2 + \pi \rho g N \gamma_r R^3 \right\}$

$\beta = 7.464\pi \rho g R^2 + \pi K_o g N q_r R^2 + 2\pi RC$

$\gamma = \pi K_o \rho g R \cdot \tan \phi$

The Equation (11) is a non-linear differential equation of which neither an exact nor an approximate solution could be found. However, it is soluble numerically by using a fourth order Runge-Kutta integration process (Carnahan *et al.* 1969). The process is a single step method in which the value of V at $Z = Z_n$ is used to compute $V_{n+1} = V(Z_{n+1})$. A computer program has been developed whereby the penetration velocity *vs.* depth relationship is obtained both in tabular and graphical forms at different depth increments, up to the maximum depth of penetration. This method provides a quick computation of a theoretical penetration velocity profile and the maximum depth of penetration for known physical properties of soils, penetrometer characteristics and impact velocity. The use of this method for a direct evaluation of the characteristic shear strength properties such as C and φ of the target material from impact penetration test is possible only by comparing the experimental velocity profile with a family of theoretical velocity profiles obtained by encompassing a wide

range of soil strength properties for a known penetrometer charac-
teristic and impact velocity.

Obviously this method, in addition to high computation cost,
is time consuming as any variations in target material, impact velocity
or penetrometer properties would require a new set of curves. To
overcome these difficulties it is assumed that the increase in apparent
cohesion due to dynamic loading is directly proportional to the rate of
penetration, as a first approximation, the following flow condition
would be obtained for the Mohr-Coulomb envelope:

$$\tau = C + KV + \sigma_n \tan \phi \tag{12}$$

Where K = soil viscosity coefficient (assuming linear variation)

It is interesting to note that the results (discussed in
Chapter 5.3.2.) obtained by using either logarithmic variation
(Equation 3) or straight line variation (Equation 12) do not produce
any significant difference.

Thus using the apparent Cohesion value as $C' = C + KV$ and
proceeding in the same manner as those described for the development
of relationship 11, the following equation is obtained:

$$\frac{d(V^2)}{dZ} + \frac{2AV^2}{M+AZ} - \frac{2(a - BZ - \gamma Z^2)}{M + AZ} - \frac{K(2\pi N_c R^2 V + 4\pi R VZ)}{M + AZ} \tag{13}$$

Where all the terms are previously defined.

Equation (13) is a non-linear differential equation of which an exact
analytical solution could not be found. However, its approximate
solution is obtained analytically and numerically. The approximate
analytical solution is obtained by applying one degree perturbation

(Bellman 1966) as explained in Appendix A. Putting $2\pi N c_r R^2 K = L$, $4\pi R K = N$, and impact velocity $= V_o$, we get,

$$V^2 = \frac{-1}{(M+AZ)^2}\left[\left\{2\alpha M - LMV_o\right\}Z + \left\{A\alpha - \beta M - \frac{L\alpha}{2V_o} - \frac{NMV_o}{2}\right\}Z^2\right.$$

$$- \frac{1}{3}\left\{2\gamma M + 2A\beta + \frac{LA\alpha}{2MV_o} - \frac{L\beta}{2V_o} + \frac{N\alpha}{V_o}\right\}Z^3$$

$$- \frac{1}{2}\left\{A\gamma - \frac{L}{6}\frac{(\gamma M + A\beta)}{MV_o} + \frac{N(A\alpha - \beta M)}{4MV_o}\right\}Z^4$$

$$\left. + \left\{\frac{LA\gamma}{2QMV_o} + \frac{N(\gamma M + A\beta)}{15MV_o}\right\}Z^5 + \frac{NA\gamma Z^6}{24MV_o} + M^2 V_o^2\right]\qquad (14)$$

The equation (14) is the general solution by which the solutions for various special applications can be obtained.

For example:

(1) Maximum depth of penetration (Z_m)

$$V_o^2 = \frac{-1}{M^2}\left[\left\{2\alpha M - LMV_o\right\}Z_m + \left\{A\alpha - \beta M - \frac{L\alpha}{2V_o} - \frac{NMV_o}{2}\right\}Z_m^2\right.$$

$$- \frac{1}{3}\left\{2\gamma M + 2A\beta + \frac{LA\alpha}{2MV_o} - \frac{L\beta}{2V_o} + \frac{N\alpha}{V_o}\right\}Z_m^3$$

$$- \frac{1}{2}\left\{A\gamma - \frac{L}{6}\frac{(\gamma M + A\beta)}{MV_o} + \frac{N(A\alpha - \beta M)}{4MV_o}\right\}Z_m^4$$

$$\left. + \left\{\frac{LA\gamma}{2QMV_o} + \frac{N(\gamma M + A\beta)}{15MV_o}\right\}Z_m^5 + \frac{NA\gamma Z_m^6}{24MV_o}\right]\qquad (15)$$

Equation (15) provides the relationship between impacting velocity and maximum depth of penetration. As it is not obtainable in closed form, the maximum depth of penetration may be estimated by interpolation.

(2) For the pure cohesive soils ($\phi = 0$):

$$V^2 = \frac{1}{(M+AZ)^2} \left[\left\{ 2\alpha M - LMV_0 \right\} \cdot Z + \left\{ A\alpha - \beta M - \frac{L\alpha}{2V_0} - \frac{NMV_0}{2} \right\} Z^2 \right.$$

$$- \frac{1}{3} \left\{ 2A\beta + \frac{LA\alpha}{2MV_0} - \frac{L\beta}{2V_0} + \frac{N\alpha}{V_0} \right\} Z^3 + \frac{1}{2} \left\{ \frac{LA\beta}{6MV_0} - \frac{N(A\alpha - \beta M)}{4MV_0} \right\} Z^4$$

$$\left. + \frac{NA\beta}{15MV_0} Z^5 + M^2V_0{}^2 \right]$$

(16)

(3) For the condition K (soil viscosity coefficient) = 0:

$$V^2 = \frac{1}{(M+AZ)^2} \left[2\alpha MZ + (A\alpha - \beta M) Z^2 - \frac{2}{3} (\gamma M + A\beta) Z^3 \right.$$

$$\left. - \frac{A\gamma Z^4}{2} + M^2V_0{}^2 \right]$$

(17)

(4) For pure sand (C = 0):

The equation (17) is valid for pure sandy soils also because here again the strain rate effect on angle of internal friction (ϕ) is insignificant.

The analytical solution, in addition to providing the velocity profile and maximum depth of penetration, can be used for estimating the conventional shear strength parameters such as C and ϕ of the target materials for a known impact velocity and maximum depth of penetration. It is seen from these relationships that in a case of pure cohesive soils the determination of cohesive strength is a straight forward task whereas in case of sandy soils at least three tests with different initial conditions are required. However, since

the penetrometer is instrumented with an accelerometer, the experi-
mental velocity vs. depth profile is obtainable by the integration of
an accelerometer record. The angle of internal friction can be
calculated from this profile by choosing any three velocities and the
corresponding depths of penetration.

CHAPTER IV

EXPERIMENTAL PROGRAM

The objective of the experimental program was (1) to develop the capability of the proposed instrument to measure directly the *in situ* shear strength properties from an impact penetration test; (2) to study the mechanism of how soil is displaced during penetration so that realistic assumptions concerning the velocity and stress field can be made; (3) to obtain evidence of the validity of the theoretical work; (4) to study the influence on penetration mechanism of selected parameters such as: impact velocity, weight of penetrometer, nose shape and physical and engineering properties of soils; (5) to study the application of impact penetrometer test results for estimation of soil type on lines similar to what has been in practice for static cone penetration test; and (6) to study the performance of the penetrometer in layered soils.

Types of Experiments

The laboratory test programs adopted in the present investigation were of the following three types,

(i) Impact Penetration Tests,

(ii) Constant Velocity Penetration Tests,

(iii) Two Dimensional Constant Velocity Penetration Tests.

The first two types of experiments were performed under fully controlled conditions in which the penetrometer was either dropped or

penetrated at constant velocity into a tank filled with target material, whereas, in the last type of experiment the constant velocity penetration tests were performed into a target material confined between two clear plexiglas plates so that the whole event of penetration could be recorded using high speed photography.

4.1 Impact Penetration Tests

The laboratory impact penetration tests were performed on different types of target materials under varying initial conditions. The main emphasis was to perform low velocity impact penetration tests on fine soil target material which generally occur on the continental shelf and slope. Under this test program 29 test results will be discussed in this thesis.

4.1.1 Impact Penetrometer Design

The criteria for selection of the penetrometer used in this investigation are based on the considerations of:

(i) The ease with which the penetrometer could be handled and adapted to different environments,

(ii) The sensitivity of the penetrometer's response to variation in *in situ* soil properties with depth,

(iii) The ability to analytically evaluate the penetrometer output.

The basic dimensions of the penetrometer selected for this experimental program are the same as those generally adopted for the static cone penetration test so that the available knowledge on static penetration tests could be utilized in analysing the test results. The impact penetrometer is a cone-tipped right-circular cylinder having

the following nominal dimensions and characteristics:

Diameter: outer   = 1.405 in. (35.6 mm.)

Height: Below the weight carriage = 2 ft.

          Overall height   = 3.25 ft.

Cone Angle   = 60°

Weight of Penetrometer: Variable weight adjustment system

                        providing 15 lbs. to 65 lbs. range

Area of Cone base   = 1.55 in.^{2}(10 cm.^{2})

Area of Friction sleeve   = 23.25 in.^{2}(150 cm.^{2})

Material: Cold drawn round seamless steel tube

The resulting instrument is shown in Fig. 5 and Fig. 6.

4.1.2. Instrumentation

The impact penetrometer has been instrumented with three sensors: accelerometer, cone load cell, and friction sleeve load cell.

Accelerometer

The accelerometer is housed inside the penetrometer and mounted in the direction of the penetrometer axis at approximately weight carriage height to facilitate the load cell wiring connecting to the recorder. The accelerometer used in this investigation is of the following specifications:

Endevco Model 2262 - 25 Serial No. AA47

Type: Piezoresistive Accelerometer

Rated Range: $\pm$ 25 g

Frequency Response: DC to 750 Hz

Sensitivity: 19.87 mv/g (at 10V DC excitation)

GROOVE FOR HOLDING THE PROBE

TO RECORDING SYSTEM

ACCELEROMETER

LEAD WEIGHT (UP TO 4 OF APPROXIMATELY 10 LBS. EACH)

WEIGHT CARRIAGE

PENETRATION ROD (36 MM. O.D. AND 1.27 MM. I.D.)

STRAIN GAGES

LOAD CELL

FRICTION SLEEVE (150 CM²)

60° CONE WITH 10 SQ. CM. BASE.

NOT TO SCALE
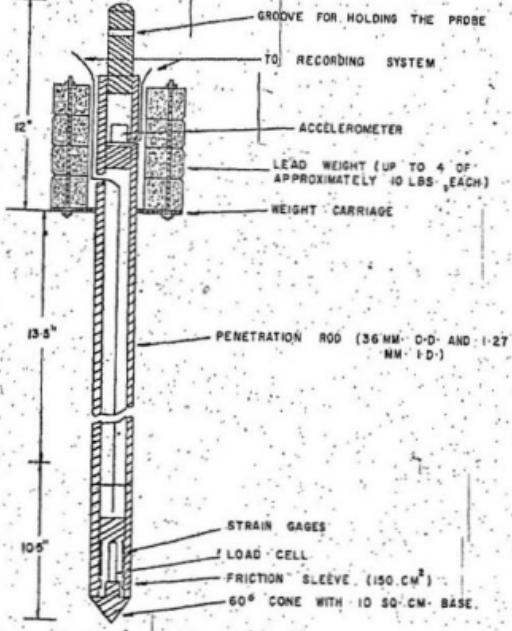
FIG-5 DETAILS OF LABORATORY IMPACT PENETROMETER

FIG 6 PHOTOGRAPH OF LABORATORY IMPACT PENETROMETER

Load Cells

In the initial stage of this investigation the load cells used for the impact penetrometer were the ones developed by 'Fugro' for the Static Cone penetrometer and a detailed description of which has been given by Ruiter (1971). However, frequent breaking of internal connections and pick up of electrical noise was interrupting the progress of the work. This led to the development of a new penetrometer which was designed with the following objectives:

(i)   To provide high sensitivity and minimum electrical noise,

(ii) Rugged enough to withstand any accidental high impact force,

(iii) To prevent the breaking of internal connections and wiring system,

(iv) To protect the strain gauges from damage from moisture and soil water,

(v)   To compensate for bending stresses in the cone and friction sleeve tube.

The cross-sectional view of the cone and sleeve friction measuring devices are shown in Figure 7 which has the same outer dimensions as those of the 'Fugro' penetrometer. The detailed designing procedure is given in Appendix B. The developed penetrometer has given excellent service even after sustaining a number of high impact forces. The following are the specifications of Cone and Friction Sleeve load cells.

Cone

Diameter of Cone: 1.405 in. (35.6 mm.)

Base area of Cone: 1.55 in.^{2} (10 cm.^{2})

CABLE

CONNECTION WITH ROD

WATERPROOF BUSHING

O-RING

FRICTION SLEEVE (150 cm²)

FRICTION-STRAIN GAGES

CONE-STRAIN GAGES

O-RING

CONICAL POINT (10 cm²)

NOT TO SCALE
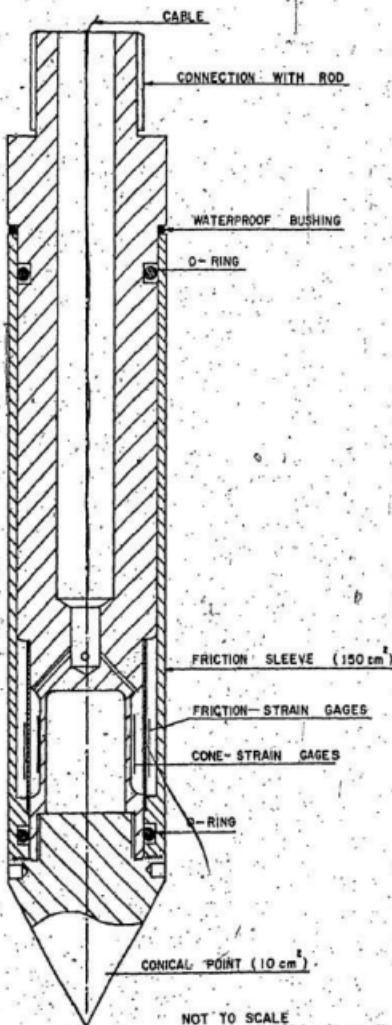
FIG. 7   DETAILS OF LOAD CELL ARRANGEMENTS

Cone Angle: adaptable to any end shape; in present investi-
gation 30°, 60°, 90° and blunt end tips were used.

Rated Range: 2000 lbs.

Sensitivity: 378 lbs./mv (at 8VDC excitation).

Friction Sleeve:

Outer diameter: 1.405 in. (35.6 mm.).

Area of sleeve: 23.25 in.^{2} (150 cm.^{2}).

Rated Range: 1000 lbs.

Sensitivity: 237.5 lbs./mv (at 8VDC excitation).

Recording System:

The output signals of the accelerometer, cone load cell, and
friction sleeve load cell were initially recorded by means of a two
channel 'Tektronix' oscilloscope and a single channel storage scope
equipped with a polaroid camera. This recording system was modified
by using a 'Hewlett Packard' four channel high speed instrumentation
tape recorder to provide better flexibility and reproduction facility.
In addition, the recorded tape can directly be fed into computer for
data reduction and processing. The signals were amplified by selecting
suitable gain on the amplifiers before feeding into the recorder. The
recording was generally done at a tape speed of 15 in./sec. and was
reproduced at a tape speed of $\frac{15}{16}$ in./sec. on a 'Brush' U-V recorder.

Before starting each test the following calibration checks
were made:

(i) The actual gain of all the amplifiers including that of the
tape recorder,

(ii) Balancing of the amplifiers,

(iii) The imput voltage of each sensor,

(iv) The calibration of accelerometer by the turnover method. In this method first the accelerometer was oriented with its sensitive axis in vertical direction and then turning over 180° resulting in a change of 2g.

(v) Balancing the bridge of cone and friction load cells.

After completion of each test series the calibration of cone and friction load cells were rechecked.

4.1.3. Triggering System

In this investigation both electrical and mechanical systems are used for releasing the penetrometer. In the electrical system the penetrometer is triggered with the help of remotely controlled relay system which include a 28V relay Solenoid working at 5A current. A switch has been provided to energize the relay for giving instantaneous free fall and simultaneously starting the recording system. This system is designed for a maximum load of 50 lbs. For a penetrometer having more than 50 lbs. weight the mechanical system is used. In the mechanical system a horizontal pin is pushed and kept in position by means of high tension spring. The rear end of the pin is connected with a cord passing over a pulley; thereby pulling of the cord causes the instantaneous free fall of the penetrometer. Figure 8 shows the schematic diagram of the experimental set up being used in laboratory impact penetration test. Figure 9 shows the complete view of the experimental set up.

MECHANICAL SYSTEM
(ALTERNATE ARRANGEMENT)

SWITCH TO
ENERGIZE RELAY
(TO DROP PENETROMETER)

28 VDC
5 A
POWER SUPPLY

26V RELAY
SOLENOID

MOVEABLE
SCAFFOLDING

PENETROMETER

ACCELEROMETER

SIDE FRICTION STRAIN GAGES

CONE LOAD CELL

DROP
HEIGHT

D-C POWER SUPPLY

TEST
CONTAINER

DIFFERENTIAL
AMPLIFIERS

INSTRUMENTATION
TAPE RECORDER

CHART
RECORDER
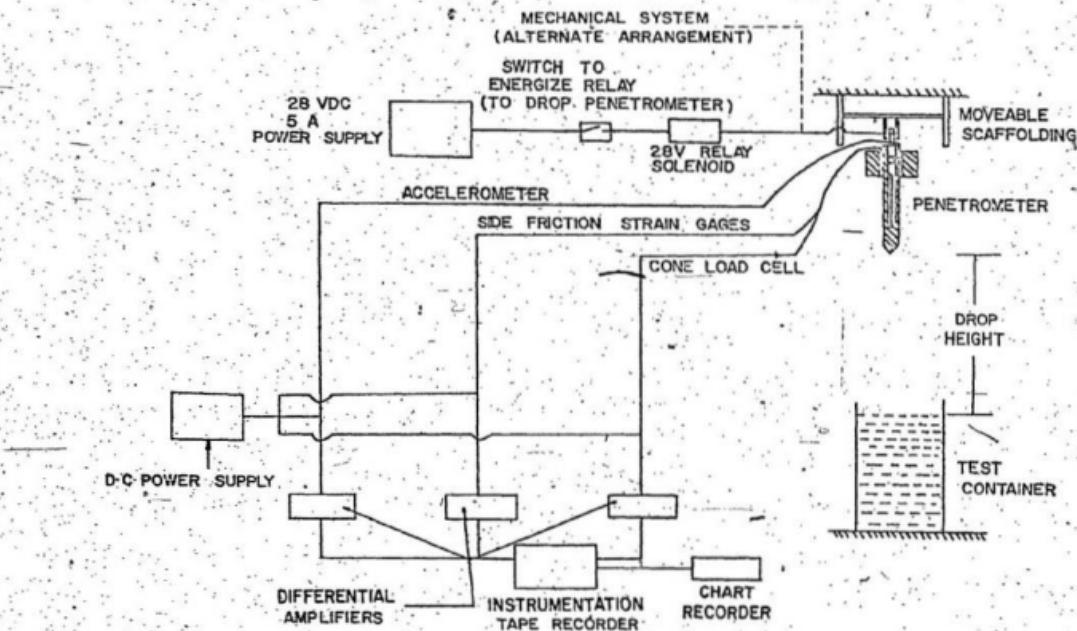
FIG-8 EXPERIMENTAL SET-UP FOR LABORATORY IMPACT TEST
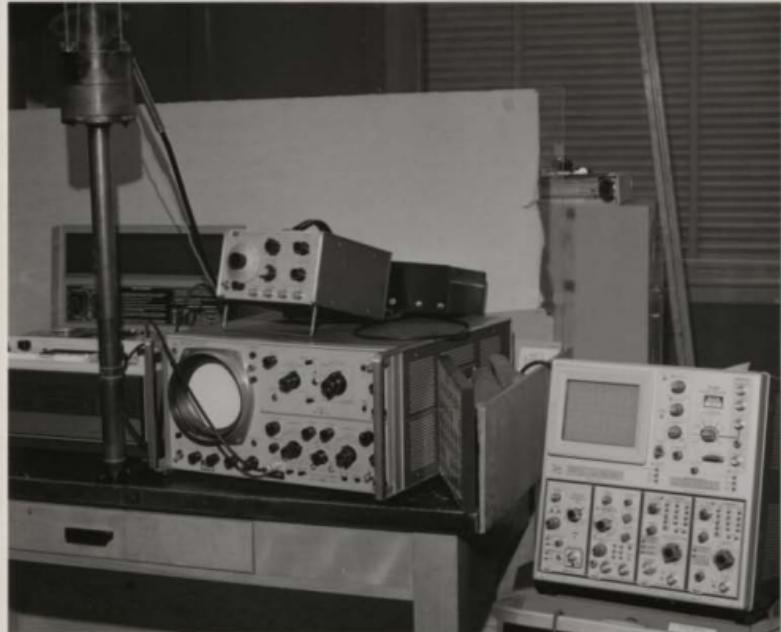
FIG·9 PHOTOGRAPH OF LABORATORY SET-UP FOR IMPACT
TESTING

4.1.4. Independent Variables

As mentioned earlier, the final form of the instrument would be used for measuring the *in situ* strength properties of marine sediment where the impact velocity will range from 15 to 30 ft./sec. for normal free fall height. Therefore the scope of the present laboratory investigation was limited to low velocity impact penetration. The impact velocity was controlled by the free fall height of the penetrometer.

For supporting the penetrometer a movable scaffolding was constructed which could be positioned to any pre-selected height. The dropping mechanism was attached to the scaffolding. At every position, the perfect levelling of the scaffolding was obtained from the use of a spirit level and the vertical alignment of the penetrometer was checked from the plumb bob.

Weight

The laboratory penetrometer was designed to provide a varying weight system ranging from 15 to 65 lbs. so that a pre-selected weight could be used in particular tests.

4.1.5. Target Construction

Cohesive Soils

The material selected for testing was thoroughly dried and pulverized. It was placed in a large concrete mixer and mixed with a metered amount of water to obtain a specific moisture content. The material was recycled until the mixture was homogenous and was then

removed from the mixer.

Targets were constructed in cylindrical steel molds of 18 in.
diameter and 24 to 36 in. high. For soft mud targets the upper
range of mold height was used. The soil mixture was placed in the
mold in layers (normally 4 to 8 in. layer) and compacted with modified
AASHO hand hammer. The desired density was controlled by the number
of blows per layer of soil.

During target construction the samples were collected at 6 in.
intervals for moisture content determination. After construction of
the target up to approximately mid height the *in situ* vane shear tests
were performed at 6 in. intervals. The vane test for the remaining
upper half was performed either before or immediately after the impact
tests at 6 in. intervals. The vane shear tests were performed near the
target boundaries by motorised vane apparatus. For *in situ* vane shear
testing, the available 'Wykeham Farrance' laboratory vane apparatus was
modified so that it could be used up to depth of 18 in. without causing
many disturbance in the target. Depending upon the strength of the
target either 1 in. by 1 in. or ½ in. by ½ in. vanes were used.
Figure 10 shows the modified vane apparatus. Since the empty weight
and volume of the mold were known, the average densities were determined
by weighing the target with the mold.

In addition to the program described above, several tests were
conducted to determine the physical properties of the soil. These
included specific gravity, grain size analysis, Atterberg limits, and
mineral composition. The tests were performed immediately after
preparation of the target. Results indicated that as many as 5 tests

FIG. 10 MODIFIED VANE SHEAR APPARATUS

could be performed in one 18 in. diameter target without adversely influencing the results. The capability of performing multiple tests allowed several tests with varying penetrometer parameters without varying the soil properties.

Cohesionless Soils

The difficulty of constructing homogenous samples of cohesionless soil is well known. The greatest control of properties can be obtained by the construction of a very dense or a very loose sample. However, in a loose sample no matter how carefully it is handled and transported some disturbance will take place. For this reason the majority of tests were conducted for dense sand.

The dense targets were constructed by placing sand in 6 in. layers and compacted with modified AASHO hand hammer. The desired density was obtained by controlling the number of blows per layer for the soil. For construction of the loose target, the raining technique was used in which the dry material was poured through a sieve held at a fixed height (9 in.) above the existing target surface. Only one test was performed on each target because of the excessive disturbances caused from a single test.

For saturated targets, the same procedure was adopted as previously explained for dry samples. After the target was constructed water was added at a slow rate through a connection at the bottom of soil sample which was resting on a rigid support of fine mesh.

The density determination was done in the same way as explained for cohesive soils. The moisture content of saturated soil was determined after completion of the test by taking samples at random locations.

The strength characteristics of the target material were determined by preparing the sample with the same density and moisture content as that of the target material and testing in the direct shear test. Other tests such as grain size analysis and specific gravity tests were also performed.

Sand-Clay Mixture and Layered Soils

In the case of Sand-Clay mixture target, the procedure described for cohesionless soils was followed for 8% fine soils and 92% sand mixture and for 50% sand, 50% fine soils the procedure described for cohesive soil was adopted. Similarly, depending on the types of layered material either of the procedures was adopted.

4.2 Constant Velocity Penetration Tests

The constant velocity penetration test is a continuous vertical penetration test at a constant speed obtained by means of some external driving system. The main objective of this test was to study the influence of rate of penetration on the shear strength of soils and to establish the experimental/empirical relationship between dynamic and static shear strength of soils applicable to low velocity impact tests. In addition, this test in conjunction with impact penetration test provided a qualitative and quantitative comparison of the dynamic cone thrust and local side friction values with static values. Under this test program, 43 tests were performed on different types of material ranging from sandy gravel to clay, with different penetration velocity ranging from 0.004 ft./sec. to 2.662 ft./sec.

The equipment used for this investigation consisted of an

instrumented penetrator, a hydraulic linear actuator, and different soil targets.

Instrumented Penetrator

The instrumented penetrator used in this investigation is of the same dimensions as those described for the impact penetrometer. It was coupled with a hydraulic actuator which in turn was connected to a heavy duty pump. The complete rig as shown in Figure 11 was mounted on a loading frame capable of withstanding the penetration reaction.

The same instrumentation and recording system as that of impact penetrometer was used for recording cone thrust and local side friction. For measuring the velocity of the penetrator, a system has been developed which consists of a fixed pointer and a resistance wire. The wire is connected to the moving shaft so that any movement in the shaft causes the change in the length of the resistance wire with respect to fixed pointer. This results in a change in voltage and when connected with the U.V. recorder, with a proper calibration, a direct plot in time v_a. displacement is obtained. The displacement record was also stored in instrumented tape recorder.

Hydraulic Actuator

The hydraulic actuator used in this investigation was capable of providing different speed system ranging from 0.004 ft./sec. to 2.662 ft./sec. and stroke up to 1.83 ft. To obtain such a high velocity and stroke the hydraulic actuator of the following specifications was designed:
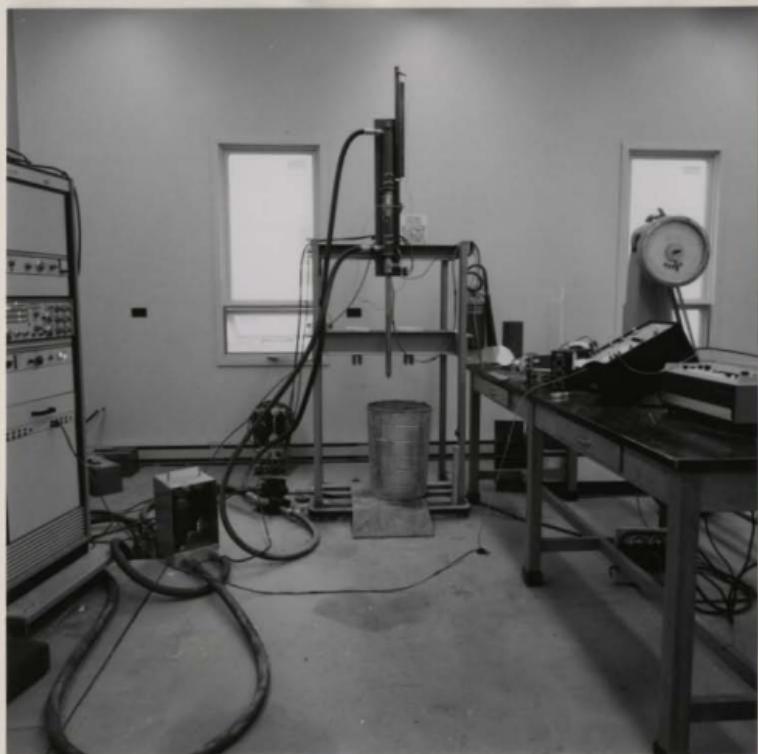
FIG·II PHOTOGRAPH OF CONSTANT VELOCITY PENETRATION
TEST SET-UP

Specifications of hydraulic actuator:

       Type: Double acting

       Stroke: 22 in.

       Internal Diameter of Cylinder: 2 in.

       Diameter of Shaft: 1.5 in.

       Pressure Rating: 3,000 p.s.i.

     The actuator of above specifications when connected with heavy duty pump (40 H.P. and 20 G.P.M.) available with M.T.S. provided the required velocity and penetration. The velocity and penetration depth for any particular test could be adjusted from M.T.S. speed and stroke console.

Target Construction

     For the construction of target, same procedures were adopted as those explained for impact penetration tests.

4.3 Two Dimensional Constant Velocity Penetration Tests

     The solution to 'static' bearing capacity problems involves the assumption of a failure mode. The strength parameters (ϕ, C) are then assumed to be developed along the failure surface. These assumptions permit the calculation of the ultimate bearing capacity. The solution to 'dynamic' bearing capacity problems also requires that the type of failure mode be known. To study if the failure mode resulting from 'dynamic' loading is similar to that resulting from 'static' loading, a series of continuous vertical penetration tests were performed using half and full sectional penetrators at various constant velocities into both cohesive and granular soils.

The equipment used for this investigation consisted of a hydraulic linear actuator, a target tank with a front transparent face, penetrators, different soils, and a sequence camera for recording the failure patterns.

Penetrator

Initially both full and half sectional penetrators were tried. Both the penetrators were of 1.4 inch diameter with 60° cone angle and 18 inches in length. In the latter part of the studies only half sectional penetrators were used because a more distinct distortion of the grids were obtained from them.

Target Tank

The target tank was 12 inches wide by 24 inches high and 1.525 inches thick so that either half sectional or full sectional penetrator of 1.4 in. diameter could enter with minimum friction on its front or back. By this system, a true two-dimensional (x-y) test had been achieved. The front face of the target tank was removable type 3/4 in. thick plexiglas to permit observation of the movement of the target material during penetration.

Gridding Procedure

To facilitate the visual observation of the movement of the soil, a reference grid was marked on one side of the sample. Following the required compaction, the cover of the container was firmly clamped against the top surface of the soil. The container was then placed on one side, levelled, and the exposed plexiglas side removed. Two

methods of marking the grid were tried. In the first method, as suggested by Peck (1962) two similar frames of thin angle iron section, the same size as the plexiglas plates, were constructed. Series of cords, spaced 1 inch apart, were stretched between the opposite sides of the frame. In one frame the cords were stretched horizontally and in the other frame they were stretched vertically. The frames are shown in Figure 12. To make the grid, the cords were dusted with colored marking powder and the frame was placed in position on the exposed surface of the soil, the cords being just clear of the soil surface. Each cord was then flicked, leaving a thin colored line on the surface. The procedure was repeated with the other frame to draw the lines at 90° to the previous ones and thus, the grid of 1 inch was obtained on the exposed surface. The second method was that used by Selig (1961), the grid lines being formed by colored sand sprinkled on a slotted plexiglas frame. There again, two frames were used of the same dimensions as that of the removable plexiglas plate, with horizontal and vertical slots. The frames are shown in Figure 13.

After drawing the grid the removable plexiglas plate was again replaced and tightened in position. The container was placed upright, ready for testing. Both the gridding procedures mentioned above were tried and it was found that in case of dry sand and mud samples the second method was more satisfactory, whereas, for compacted and moist soils the first method gave good results. In spite of all the precautions the second method did not give even lines but as it caused the least disturbance in sample this method was preferred for the loose samples since they were susceptible to disturbances. In the case

FIG·12 PHOTOGRAPH OF GRID FORMER OF CHORD TYPE

FIG 13 PHOTOGRAPH OF GRID FORMER OF PLEXIGLAS TYPE

of mud samples on optically visible grid could not be obtained by the first method, as on flicking, the colored dust left by the cords were absorbed by the excess water squeezed from the sample. Figure 14 and Figure 15 show the positions of the grids before and after the penetration test for the mud sample.

Photographic Arrangement

The optical observations of the operation of each test were made with a Bolex Model H-16 millimeter movie camera equipped with both battery/electrical motor and clock work. In case of low speed steady penetration tests the camera was operated by means of electric motor, whereby, the speed of 24 frames/sec. was selected. In high speed tests, the camera was operated by clock work whereby the fastest frame rates (64 frames/sec.) was obtained. The films were projected on the screen for sequential studies of the failure pattern at every stage of penetration.

Test Variables

The tests were conducted on coarse sand, fine sand, and on clay soils, at different moisture contents ranging from room dry to saturated conditions. For those soils the tests were performed for most loose, most dense, and intermediate densities. For each test series at least two similar targets were prepared so that the failure patterns could be studied individually in both low and high velocity steady penetration tests. The low velocity tests were performed mostly at 0.042 ft./sec., whereas, the high velocity tests were conducted at 2.662 ft./sec. Some tests were also performed at a velocity of 0.0044 ft./sec.
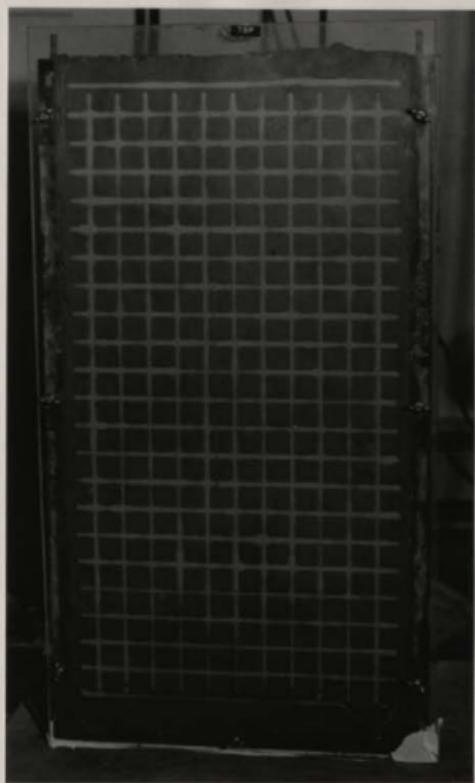
FIG 14 FORMATION OF I IN· GRID ON MUD SAMPLE
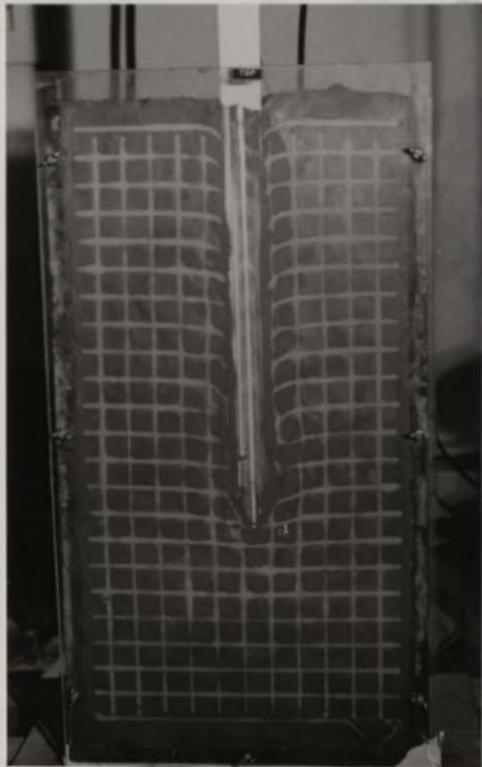
FIG· 15 DISTORTED GRID AFTER HIGH VELOCITY (2·662 FT/SEC)
PENETRATION

4.4 Processing of Test Output Records

Impact Penetration Test

The penetrometer provides the following time dependent parameters of target material at the moment of impact right down to full penetration depth:

(1) Acceleration/deceleration,

(2) Cone thrust, and

(3) Sleeve friction.

From the recorded acceleration/deceleration time history, penetration velocities and depth are calculated by numerical integration at suitable time intervals (explained in Appendix C). At the instant of impact the time and penetration depth are assigned zero values whereas the velocity assigned is that of the impact velocity calculated from the measured free-fall height neglecting air resistance. This can be verified from the acclerometer record. Using the calculated time vs. penetration depth relationship, the depth vs. cone thrust and depth vs. sleeve friction profiles are obtained from recorded time vs. cone thrust and time vs. sleeve friction relationships by cross calculation. Similarly depth vs. deceleration, and depth vs. velocity profiles are also obtained from the time vs. deceleration and time vs. velocity relationships, respectively. The obtained depth vs. sleeve friction profile is modified by subtracting 0.22 ft. (7 cm.) for each calculated depth because of the geometry separating the cone and sleeve. The present penetrometer therefore enables the following target characteristics to be computed. (1) Depth of penetration. (2) Provides depth vs. sleeve-friction profile, depth

vs. cone thrust profile, depth *vs.* penetration velocity profile, and depth *vs.* acceleration profile.

Constant Velocity Penetration Tests

In this test the following time dependent parameters are obtained:

(i) Displacement,

(ii) Cone thrust, and

(iii) Sleeve Friction.

The actuator provides a constant velocity throughout the penetration. This could be verified from voltage variation *vs.* time relationship giving a straight line. The penetration velocity is calculated by knowing the total time of voltage variation (calculated from U.V recorder's chart speed) and the throw of the actuator. With suitable calculation the displacement of the penetrometer is calculated for each time division on chart, and for different penetration velocity. Thus, the recorded time *vs.* cone thrust and sleeve friction relationships is directly convertible to depth *vs.* cone thrust and sleeve friction profiles. Again, the correction of 0.22 ft. is applied to the calculated depth for sleeve friction profile.

CHAPTER V

TEST RESULTS AND DISCUSSION

5.1 Test Materials

A series of impact penetration and constant velocity penetration tests were performed on the following materials.

(1) Modelling clay,

(2) Silica-70 sand,

(3) Mixtures of 1 and 2,

(4) Gravelly sand,

(5) Marine clay.

To standardise the experimental technique, modelling clay, and silica-70 sand were selected because these were readily available in large quantities and provided uniform target materials. Those materials were used to simulate the clay and sand targets. The main emphasis of this study was on fine soils as these are generally found in continental shelf and slope.

The test results are quoted in three series.

Series I—Clay

The grain size distribution of the material used is shown in Figure 16. According to M.I.T. System of soil classifications it is classified as clayey silt size. It has the following properties:

Liquid Limit = 37 %

Plastic Limit = 21 %

Plasticity Index = 16 %

SERIES I SILT 58 %, CLAY 42 %, CLAYEY SILT SIZE
SERIES II MEDIUM SAND 37 %, FINE SAND 63 %, MED TO FINE SAND SIZE
SERIES III A SAND 48 %, SILT 27 %, CLAY 25 %, CLAYEY SILTY SAND SIZE
SERIES III B SAND 92 %, CLAYEY SILT 8 %, SILTY SAND SIZE
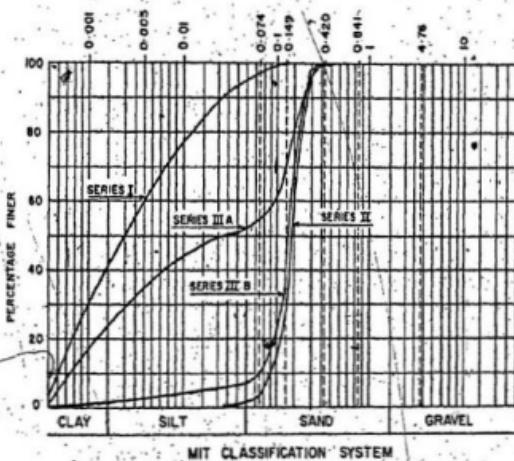
FIG-16 GRAIN SIZE DISTRIBUTION CURVE

Specific Gravity = 2.615

It consists mainly of Illite and Chlorite minerals with some percentage of Quartz, Feldspar, and Kaolinite.

Series II--Sand

The grain size distribution of the material used is shown in Figure 16 and is classified as medium to fine sand size. The photograph of this sand is shown in Fig. 16A. It is very uniformly graded. The specific gravity of the material is 2.668.

Series III--Sand-Clay Mixtures

In this test series, two different percentages of the mixtures were used. In one mixture approximately 50% sand was mixed with 50% clay. This mixture is designated by Series IIIA. The grain size distribution of Series IIIA is shown in Fig. 16 and is classified as clayey silt sand size. In other mixture approximately 8% clay was mixed with 92% sand. This mixture is designated by Series IIIB. The grain size distribution is shown in Fig. 16 and is classified as silty sand size.

5.2. Two Dimensional Test Results

Figure 14 and Figure 15 show the photographs taken before and after the test on a mud target using half-sectional penetrator at a constant penetration velocity of 2.662 ft./sec. It can be seen that the particles at a distance greater than approximately 2 times the penetrator diameter away from the penetrator centre line are not affected during the penetration. The distortion of the horizontal and vertical grid lines indicate that within the disturbed zone the particles moved downward and away from the penetrator. A uniform soil
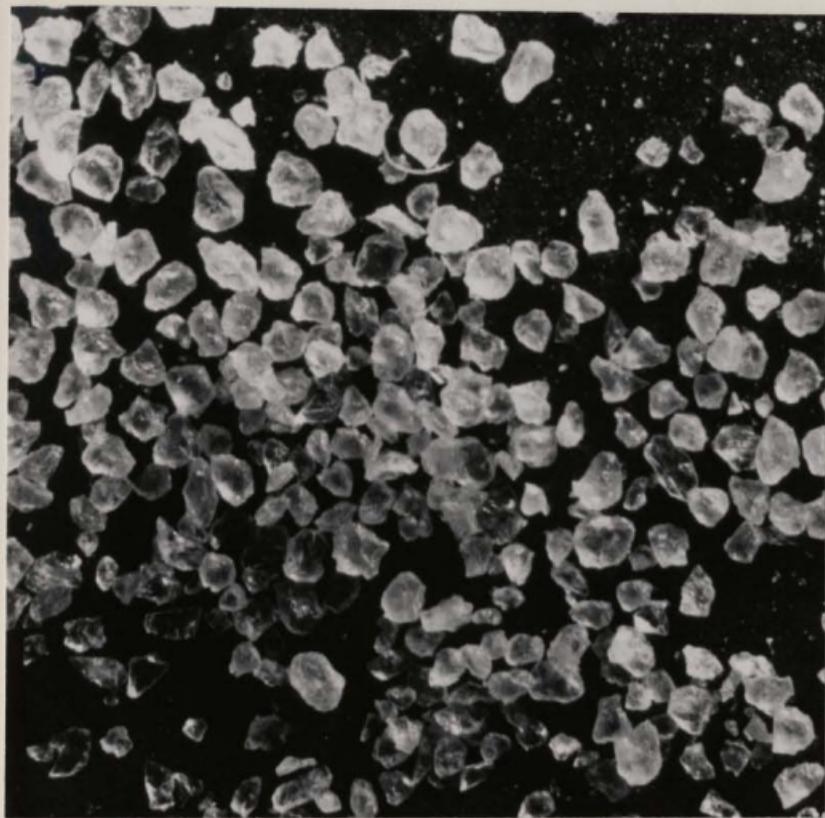
FIG I6A PHOTOGRAPHIC VIEW OF SILICA-70 SAND
(MAGNIFICATION APPROX 40)

nose is formed on and around the tip of penetrator which pushes down-
ward and outward the soil mass. Furthermore, the distortions of grid
lines indicate that the failure mode is a combination of both shear
and punching with latter one predominating.

A sequential study of the failure patterns at different depths
of penetration was made by projecting the film over a paper board
marked with square grids. Furthermore, attempts were made to study
the failure pattern at different velocities. From the data obtained
from these studies, the following conclusions could be drawn:

(1) There is no significant difference in failure patterns obtained
by either high velocity (2.662 ft./sec.) or low velocity
(0.0044 to 0.042 ft./sec.) penetration tests. The ratio of
'dynamic' to 'static' velocity was ranging between 60 to 630.

(2) In high velocity tests the formation of craters were generally
observed up to a depth of 0.1 to 0.21 in. below the target surface.

(3) From the failure patterns, observed for different types of
soils at different densities and at different moisture contents,
it may be inferred that the failure apparently occurred
principally through two mechanisms: shearing and punching.
In dense, well-packed, or tightly bound soils, penetration
occurred primarily by shearing. This is substantiated, from
the study of the distortions of the grids, and the fact that
the radial cracks extending to the surface and the upheaval
of the materials around the penetrator were generally seen in
the case of the penetration of the densely packed sandy soils.
In loose or inefficiently packed soils and in saturated clay

penetration was accomplished chiefly by punching as seen in Figure 15.

(4) The movement of the soils beneath the penetrator was predominantly downward and outward.

(5) The soil nose formed on and around the conical-tip of penetrator was clearly visible in all the cases. Both for low and high velocity penetration the size and shape of the soil nose, for any particular target, was more or less constant for all depths of penetration. There appears to be a shear front, defined as the line bounding the zone in which no shearing of the medium has occurred, travelling with the penetrator at a constant depth from the tip of the penetrator.

Various investigators have studied the modes of failure during dynamic loading and the findings of several are briefly discussed here. Selig and McKee (1961) found that failure modes are different in dynamic loading than in the static loading for sand. The dynamic test resulted in a punching type of shear, rather than the classical general shear type-failure. Cunny and Sloan (1962) have also observed punching shear modes of failure, while Shenkman and McKee (1961) observed general shear failure for dynamically loaded footings.

Jackson and Hadala (1964) performed some static and dynamic load tests on footings resting on clay. Visual observations indicated that the static and dynamic failure modes were significantly different. In the dynamic tests there appeared to be a slight heave of the soil surface around the footing where the soil surface around the statically loaded footing experienced upward movements and cracks developed from

the four corners of the footing and extended outward. The slight heave around the dynamically loaded footing was characteristic of punching modes of failure. Based on the model tests performed on the clay sample for 'static' loading conditions, Peck (1962) indicated that at about one-half of the failure load, the footing commenced to punch in vertically. A 'plastic' or 'sheared' zone formed near the edges of the footings, causing the punching effects.

Thompson (1966) performed two dimensional constant velocity penetration tests on needle bearing rollers for velocities ranging from 0.15 to 0.367 ft./sec. and also two dimensional impact penetration tests on Ottawa sand for impact velocity ranging 106 to 478 ft./sec. Based on the distortions of the grids, obtained by a high speed movie camera, he concluded that the deformation patterns observed for impact penetration tests were quite similar to those seen in constant velocity penetration tests and the displacement of the particles was very similar to the displacement initially approximated by Prandtl for the inden-tation of an infinitely long footing or punch into a half space of rigid plastic weightless material. Similar observations have been reported by Colp (1965) and Chou (1972) from steady penetration tests performed on simulated cohesionless and cohesive soils respectively.

The overall results of the various investigators are somewhat confusing in that some observed the general shear type of failure and the others found punching shear type of failure for dynamically loaded footings. The reasons for discrepancies in the results are legion. Besides the variations in soil types, the shape and size of the footings, the various investigators used different testing systems, such as

controlled stress device, controlled displacement device, and the dropping of weights, to achieve dynamic conditions.

In fact, it is difficult to conceive a unique failure pattern applicable to all problems pertaining to dynamic loadings because each problem is constrained by a different boundary condition. However, based on the previous studies and present experimental investigations, it is implied as a first approximation that in the case of densely packed target the general shear failure criterion can be adopted, while in loosely packed sandy samples and in mud the local shear failure criterion can be adopted in developing the theoretical model for the impact penetration of targets like soil media.

5.3 Test Results of Series I

The test results reported in Series I is on clay soils and include both constant velocity penetration and impact penetration tests. In conjunction with these tests the *in situ* vane shear tests were performed for each target and the average vane shear strength obtained is referred to as (τ). Moisture content and bulk density were also determined for each target.

5.3.1. Constant Velocity Penetration Tests

The constant velocity penetration tests were performed on clay targets of varying strength ranging from $\tau = 64$ lbs./ft.^{2} to 1671 lbs./ft.^{2}. The tests were generally performed at four different velocities, 0.0044 ft./sec., 0.042 ft./sec., 0.456 ft./sec. and 2.662 ft./sec. In some tests two additional penetration velocities, 0.0244 ft./sec., and 0.247 ft./sec. were used.

Figures 17, 18, 19 and 20 show the constant velocity penetration test results for fine soil targets having shear strength 64 lbs./ft.², 962 lbs./ft.², 1066 lbs./ft.², and 1671 lbs./ft.², respectively. Figure 21 shows the test results for a layered system of two different strengths 198 lbs./ft.² and 1354 lbs./ft.² of top and bottom layers respectively. In each test unit cone thrust and unit sleeve friction profiles are plotted up to penetration depth of 15 in. for four to six different penetration velocities.

As reported by previous investigators (summarized by Sanglerat, 1972) both cone and sleeve friction resistance increases continuously up to penetration depth of approximately 4D (D = diameter of penetrator) and beyond this depth a constant value of these resistances are obtained. The interpretation of the results appearing in subsequent paragraphs is based on the cone and friction resistance values of beyond the penetration depth of 4D.

As mentioned previously, the main aim of the constant velocity penetration tests is to study the influence of rate of penetration on shear strength of cohesive soils. The results presented here clearly demonstrate that the increase in the penetration velocity causes an increase of cone and sleeve friction resistance. The increase in resistance could be represented mathematically by logarithmic variation of velocity. Figure 22 shows the plot of experimental results between

Unit dynamic cone resistance (q_{cd})

Unit cone resistance at lowest penetration velocity (q_c)

versus

FIG 17: CONSTANT VELOCITY PENETRATION TEST RESULTS

TEST NO CC1
NDP CONE - 1.40" DIA PENETRATION
TARGET: VERY SOFT CLAY
$\gamma_b = 79.2$ LBS/CU FT
$W = 43.5\%$
$P = 64.1$ LBS/FT^3

92

FIG. 18 - CONSTANT VELOCITY PENETRATION TEST RESULTS

Left graph axes:
UNIT CONE FRICTION (LBS/FT²)
PENETRATION DEPTH (IN)

Curve labels:
0.0044 FT/SEC
0.043 FT/SEC
0.459 FT/SEC
2.082 FT/SEC

Right graph axes:
UNIT CONE PRESSURE (LBS/FT²)
PENETRATION DEPTH (IN)

Curve labels:
0.0044 FT/SEC
0.043 FT/SEC
0.459 FT/SEC
2.082 FT/SEC

PENETRATOR
W = 25.5 %
Y = 102 LBS/FT³

94

TEST NO. C-23
CRISP 3016 4125 TON PENETRATOR
TARGET MEDIUM STIFF CLAY
θ = 73.9 lbs
V = 25.5 %w
γ = 0.046 LBS/FT³

Unit Nozzle Friction (LBS/FT²)

0.0044 FT/SEC
0.0548 FT/SEC
0.242 FT/SEC
0.217 FT/SEC
0.694 FT/SEC
2.682 FT/SEC

Unit Cone Pressure (LBS/FT²)

Penetration Depth (IN)

0.0044 FT/SEC
0.048 FT/SEC
0.458 FT/SEC
0.647 FT/SEC
2.682 FT/SEC

FIG-9 CONSTANT VELOCITY PENETRATION TEST RESULTS

FIG. 20 CONSTANT VELOCITY PENETRATION TEST RESULTS

FIG 21 CONSTANT VELOCITY PENETRATION TEST RESULTS FOR TWO LAYERS SYSTEM

TEST NO. C.C.3
60° CONE 1.405" DIA PENETRATOR
TARGET: TWO LAYERS OF CLAY
TOP LAYER:
  γ_t = 49.2 LBS/CU.FT
  W = 55 %
  τ = 98 LBS/FT²
BOTTOM LAYER:
  γ_t = 69.5 LBS/CU.FT
  W = 23 %
  τ = 1254 LBS/FT²

0.0044 FT/SEC
0.042 FT/SEC
0.247 FT/SEC
0.456 FT/SEC
2.962 FT/SEC

0.0044 FT/SEC
0.042 FT/SEC
0.247 FT/SEC
0.456 FT/SEC
2.962 FT/SEC

FIG. 22 $\frac{P_{cd}}{q_f}$ V$_h$ $\log_{10} \frac{V}{V_h}$ RELATIONSHIP

LOWEST VELOCITY OF PENETRATION USED (V$_h$)

DYNAMIC UNIT CONE PRESSURE AT LOWEST PENETRATION VELOCITY (P_{cd})

UNIT CONE PRESSURE (q_d)
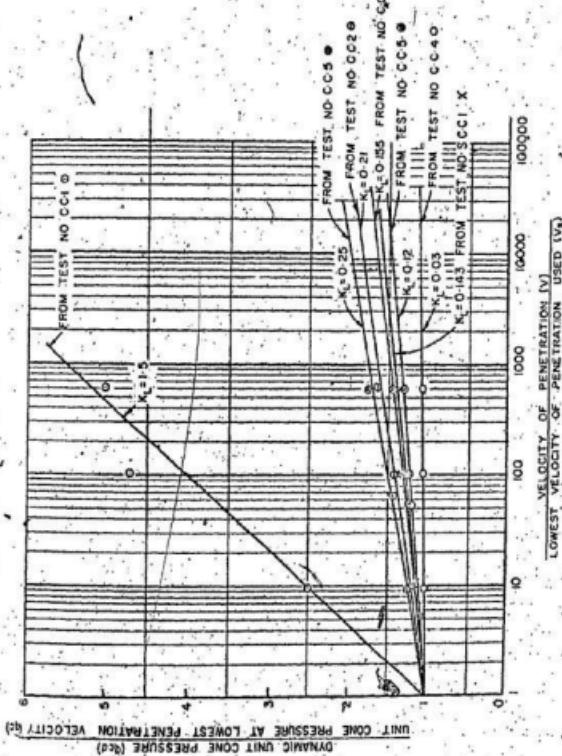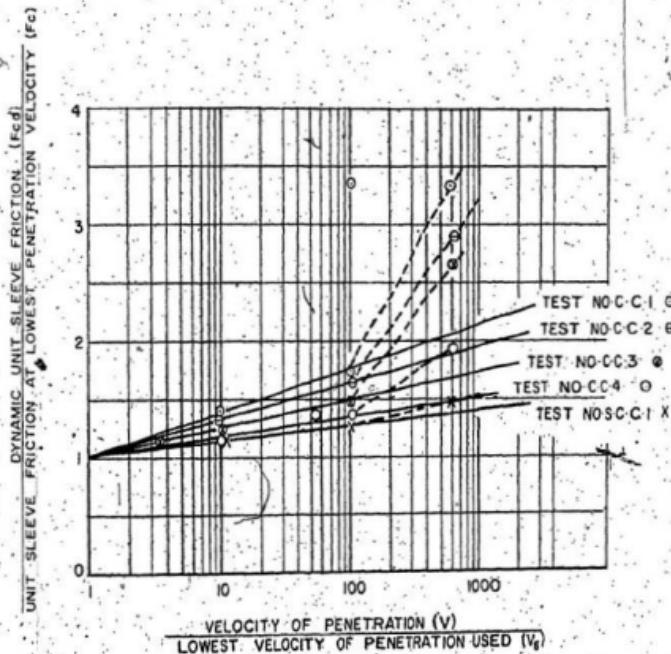
FIG 23 $\frac{F_{cd}}{F_c}$ Vs LOG_{10} $\frac{V}{V_s}$ RELATIONSHIP

$$\log_{10}\left[\frac{\text{penetration velocity (V)}}{\text{lowest penetration velocity used (V}_s)}\right]$$ for different target

strength. Similarly,

$$\frac{\text{Unit dynamic sleeve friction (F}_{cd})}{\text{Unit sleeve friction at lowest penetration velocity (F}_c)}$$

versus

$$\log_{10}\left[\frac{\text{velocity of penetration (V)}}{\text{lowest penetration velocity used (V}_s)}\right],$$ are plotted in Fig. 23.

Figure 22 shows, that except for target strength (τ) = 64 lbs./ft.^{2} the increase in cone resistance can be very well related in logarithmic variation of velocity. The slope of line represents soil viscosity coefficient K_L (for logarithmic variation). Table 1 shows the values of K_L for different target strengths. It is observed that as the strength of the target decreases the slope of the line increases.

TABLE 1

SOIL VISCOSITY COEFFICIENT (K_L)

τ (lbs./ft.^{2})	$K_L = \dfrac{q_{cd} - q_c}{q_c} \Big/ \log_{10} \dfrac{V}{V_s}$
64	1.5
198	0.25
962	0.21
1066	0.155
1354	0.12
1671	0.03

For $\tau = 64$ lbs./ft.^{2}, the increase in cone resistance is
5.5 times for a thousand fold increase in penetration velocity. For
a soil of this strength, to the writer's knowledge, neither qualitative
nor quantitative information is available about its behaviour under
'dynamic' loading. This target was prepared at a water content of 43.5%
which is well above the liquid limit of soil (LL = 37%) and as such
its behaviour would be more like a solvent or suspending medium rather
than a plastic medium. However, to draw any definite conclusion for
such a medium would require further systematic investigation.

The results of an increase in unit sleeve friction resistance
vs. logarithmic variation of velocity do provide a very good correlation
up to a velocity of 0.456 ft./sec. and beyond this velocity a sudden
increase in the sleeve friction was observed in all the cases. This
suggests the existence of some critical velocity and the slope of the
line above the critical velocity is steeper than that of the line below
the critical velocity. In most cases the slopes of both lines are
steeper than that obtained from cone resistance relationship. This
disparity is attributed to the effect of interaction of the penetro-
meter surface and soil particles.

The above findings suggest that an interpretation of results
from 'dynamic' tests to 'static' values requires three sets of soil
viscosity coefficients for a target of a particular strength, which
from a practical point of view is not desirable. In the present
investigations, the soil viscosity coefficient obtained from cone
resistance results has also been used for penetrometer shaft in
comparing the proposed impact penetration theory with experimental

results. Since the soil viscosity coefficient for penetrometer shaft resistance is generally higher than those obtained from cone resistance the use of it to penetrometer shaft resistance would cause a discrepancy. This discrepancy is countered in the theoretical model by the assumption that the unit friction on the shaft is equal to the shearing resistance of soil which for cohesive soil should be equal to the vane shear strength. However, from the direct measurement of the unit sleeve friction for the slowest penetration velocity (0.0044 ft./sec.) the values obtained are significantly lower (10 to 50 percent) than the shearing resistance of the soil.

The preceeding discussions and findings are based on maximum penetration velocity of 2.662 ft./sec. The application of this to the low velocity impact test (impact velocity ranging from 20 ft./sec. to 25 ft./sec.) requires extrapolation of those results. The validity of the extrapolation method was verified from the available impact penetration test results. Typical test results are shown in Figure 24 in which constant velocity penetration test results from Figure 22 and Figure 23 are reproduced for target strength of 1066 lbs./ft.^{2}. The cone resistance ratio calculated from impact penetration test results and the static penetration test for the same target at four different penetration velocities (calculated from accelerometer record as explained in Chapter 4.4) 18.06 ft./sec., 17 ft./sec., 4 ft./sec., and 2.25 ft./sec., and the sleeve friction ratio for the penetration velocity of 18.04 ft./sec. are also shown in Figure 24. The cone resistance for higher penetration velocities are about 10% above the extrapolation line obtained from constant velocity penetration test results. This

MEDIUM-STIFF CLAY

● INTERPOLATED FROM IMPACT TEST RESULTS
AT VELOCITY 19.046 FT/SEC
CONE RATIO 1/787 (TEST NO C.W.13)

▲ AT VELOCITY 17.77 FT/SEC
CONE RATIO 1/787 (TEST NO C.W.11)

■ AT VELOCITY 4 FT/SEC
CONE RATIO 1/58 (TEST NO C.W.11)

▼ AT VELOCITY 2.9 FT/SEC
CONE RATIO 1/1110 (TEST NO C.W.13)

○ FROM CONSTANT VELOCITY PENETRATION TEST RESULTS

FROM LOWER - VEL. RANGE

VELOCITY OF PENETRATION (v)
LOWEST VELOCITY OF PENETRATION (vₒ)

VELOCITY OF PENETRATION (v)
LOWEST VELOCITY OF PENETRATION (vₒ)
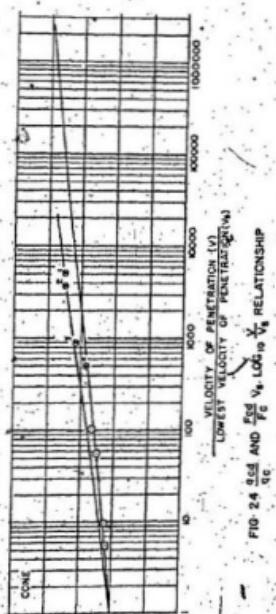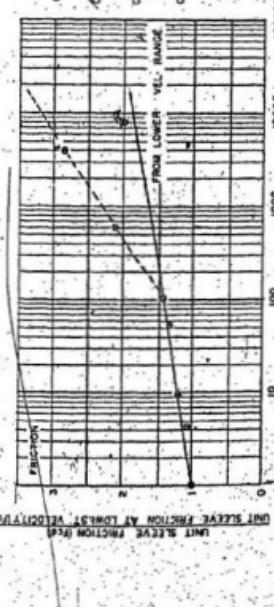
FIG 24 q_c AND f_s V_a LOG₁₀ $\frac{v}{v_c}$ RELATIONSHIP

increase may be attributed to the effect of inertial resistance of the target material (Wang, 1971; Whitman, 1970; Murff and Coyle, 1973A) which is observed in high velocity impact.

Thus, from constant velocity penetration tests the following empirical relationship is established:

$$\frac{q_{cd} - q_c}{q_c} = K_L \log_{10} \frac{V}{V_s} \qquad (18)$$

If it is assumed that Nc_r remains constant during dynamic loading then the above equation can be transformed in the following form:

$$C' = C + K_L C \log_{10} \frac{V}{V_s} \qquad (19)$$

C' = apparent cohesion for 'dynamic' yielding case

C = cohesion for 'static' yielding case.

This is the same relationship assumed in developing the theoretical impact penetration model (Eqn. 4 - Chapter III). The values of soil viscosity coefficient K_L have to be established experimentally and are proposed in Table 1. For soil of intermediate strength the soil viscosity coefficient can be found by linear interpolation between the above limits with good approximation. The validity of Eqn. 19 can further be substantiated from the results of other investigators. The strain rate effect on shear strength of cohesive soils has been studied by various investigators and is briefly described in Chapter III of this thesis. Because of the different nature of the experimental techniques their findings are mostly related to strain rate ratio rather than penetration velocity ratio as in the present case. If the strains for 'static' and 'dynamic' cases are the

same then the ratio of 'dynamic' and 'static' velocities is equal to the ratio of strain rates; thereby Eqn. 19 is written as

$$c' = c + K_L c \log_{10} \frac{\alpha_d}{\alpha_s} \tag{20}$$

where α_d and α_s are strain rates for 'dynamic' and 'static' case respectively. Mitchell (1964) from the rate process theory and Peck (1962) from experimental results proposed similar relationship (Eqn. 20).

For the experimental results shown in Fig. 22, Eqn. 20 demonstrates the increase of 15% and 112% of apparent cohesion at strain rate ratio of 33333 for two extreme cases, soft clay ($\tau = 198$ lbs./ft.^{2}), and stiff clay (1671 lbs./ft.^{2}) respectively. These values are approximately equal to the strain rate sensitivity values suggested by Whitman (1970) for cohesive soils from the tri-axial tests conducted up to maximum strain rate ratio of 33333.

From the experiments, the calculated bearing capacity factor $N_c (= \frac{q_c}{c})$ for penetration velocity of 0.0044 ft./sec. ranges from 10.5 to 11.7 and average mean is 11. These values are well within the range of previously reported values obtained from static penetration tests (Sanglerat, 1972; Ladanyi and Eden, 1969) and are about 10 to 20% higher than the theoretical and empirical values reported by Meyerhof (1961, 1951) and Skempton (1951) respectively for pile foundations. The increase is due to the fact that the measurements, even at this penetration velocity, would cause an increase in cone resistance (for the reasons discussed above) and consequently an apparent increase in N_c value is observed.

Begemann (1965) conducted several static penetration tests and field vane shear tests on clay soils and reported the average N_c equal to 14. For this high N_c value he provided a theoretical justification from Prandtl's classical bearing capacity theory by taking into account the shape factor and assuming that the failure below the tip of the cone is extended above the tip also up to approximately the same distance and thus the area of failure plane is doubled. In fact, comparing the vane shear and static penetration test results Begemann completely ignored one of the important factors i.e., penetration velocity effect on cone resistance, and this results in the values being approximately 40 to 50% higher than that of Meyerhof and Skempton. This fact can be substantiated by examining the present experimental results which indicates that at a penetration velocity of 0.065 ft./sec. (1.98 cm./sec., generally accepted penetration speed of static penetration test is 1.5 cm./sec. to 2 cm./sec.), if the velocity effect on cone resistance is neglected, the average N_c is equal to 13; which is in agreement with Begemann's value. However, it has been demonstrated that the penetration velocity has a significant effect on cone resistance values and as such a correction to this effect must be applied in order to obtain N_c or vice versa for 'static' condition.

5.3.2 Impact Penetration Tests

A series of impact penetration tests were conducted, with the objectives mentioned in Chapter IV, on saturated and partially saturated cohesive targets. The influence of the following selected parameters on penetration mechanism were studied.

(1) Weight of Penetrometer,

(2) Impact velocity,

(3) Nose shape,

(4) Target strength.

In all the tests acceleration/deceleration, cone thrust and local side friction were recorded. Figure 25 is a typical output record for medium stiff clay. Target and penetrometer properties are given with penetration test results where they occur. The salient recorded features of the event, as indicated from accelerometer, cone thrust, and friction sleeve records, include:

(a) From the accelerometer record

(1) Upon impact the penetrometer still accelerates for a while,

(2) then a steady increase in deceleration, and

(3) an abrupt drop in deceleration level with an acceleration pulse or 'dip' towards the end of penetration event.

(b) From cone thrust record

(1) An abrupt rise in cone thrust at the beginning of the event,

(2) then a steady decrease in cone thrust (attributed to penetration velocity effect), and

(3) a sudden drop at the end of the event.

(c) From friction sleeve record

(1) A steady increase in friction at the beginning of the event (due to continuously increasing area of the sleeve),

(2) then a steady friction, and

(3) a gradual decrease in friction with negative friction towards the end of the penetration event.

TEST NO C-9-11
PENETROMETER
6° OD CONE, DIAMETER = 1.406°
WT. OF PENETRATOR = 96.44 LBS/
IMPACT VELOCITY = 19.98 FT/SEC
TARGET
MEDIUM STIFF CLAY
VANE SHEAR STRENGTH/DIA LENGTH
γ = .91 LBS/CU.FT., W = 23.4 %

ACCELEROMETER

CONE

FRICTION SLEEVE

DECELERATION (FT/SEC²)

CONE LOAD (LBS)

FRICTION LOAD (LBS)

PENETRATION TIME IN MILLI SECONDS

FIG 25 TYPICAL PENETRATION TEST RECORDS FOR MEDIUM STIFF CLAY
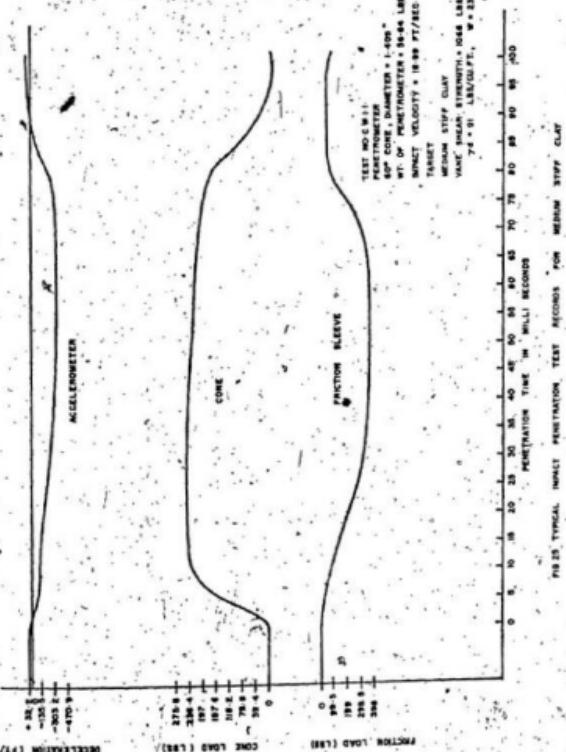
It appears that the 'dip' on the accelerometer record is the result of the rebounding of the penetrometer caused by elastic energy stored in the soil during penetration. The friction record, which at the end of the penetration event shows a substantial negative friction on the sleeve, confirms the occurrence of rebounding phenomena. Although the 'dip' at the end of the event may be important to the understanding of the complete mechanism, its influence on the penetration depth is normally insignificant. Consequently this aspect will not be considered in this analysis.

Figure 26 shows Depth vs. Acceleration/deceleration, velocity, 'dynamic' cone pressure, and 'dynamic' sleeve friction profiles calculated for the test records shown in Figure 25. The 'static' cone pressure profile calculated (from the proposed empirical relationship, Eqn. 18) for the penetration velocity of 0.0044 ft./sec. from dynamic cone pressure profile is also shown in Fig. 26 together with the actual cone pressure profile obtained at this speed from the constant velocity penetration test. The computed values are generally 10 to 12% higher than the actual values for the reasons discussed previously. Similarly, the 'static' sleeve friction profiles can also be obtained from 'dynamic' sleeve friction profiles. In the present analysis 'static' cone pressure is computed for penetration velocity of 0.0044 ft./sec. as being the slowest penetration velocity used in this investigation. However, it can be obtained for any penetration velocity such as 0.06 ft./sec. (1.83 cm./sec.) used in static penetration test. These results clearly demonstrate the ability of the instrument to measure directly the strength characteristics of the target materials.

Weight of Penetrometer

To study the effects of the weight of the penetrometer on penetration mechanism, the impact penetration tests were conducted on two different types of targets having shear strength 1066 lbs./ft.^{2} and 204 lbs./ft.^{2}. The test results are plotted in Figs. 27, 28, 29, 30, 31, and 32. Those results indicate that an increase in the penetrometer weight yields an increase in total penetration, an increase in total time of penetration event and a decrease in measured deceleration. The measured cone thrust and sleeve friction records indicate that an increase in the weight of the penetrometer does not make any significant difference to their magnitudes.

Impact Velocity

The effect of impact velocity on the penetration mechanism was studied by varying the free fall height of the penetrometer. The tests were conducted for impact velocities: 20.01 ft./sec., 18.84 ft./sec., 16.79 ft./sec., 15.26 ft./sec., 12.37 ft./sec., and 0 ft./sec., and the results are shown in Figs. 33, 34, and 35. These results indicate that the increase in penetrometer's impact velocity yields an increase in measured 'peak' deceleration, decrease in total time of penetration event and an increase in total penetration. For approximately up to 60% of the total penetration depth, the rate of gradually increasing deceleration and its magnitude are more or less the same for the tested velocity range. Furthermore, the increase in impact velocity generally yields an increase in cone thrust and sleeve friction values. This is attributed to velocity effects on cone and sleeve friction resistance.

ACCELERATION (FT/SEC²)

PENETRATION VELOCITY (FT/SEC)

UNIT CONE THRUST (LBS/FT²)

UNIT SLEEVE FRICTION (LBS/FT²)

PENETRATION DEPTH (FT)

EXPERIMENTAL VELOCITY PROFILE

ACCELEROMETER RECORD

DYNAMIC CONE PRESSURE

DYNAMIC FRICTION

STATIC CONE PRESSURE PROFILE
CALCULATED FROM THE
RELATIONSHIP
$\frac{q_s}{q_d} = 1 + \frac{mv}{q_d}$, FOR STATIC
VELOCITY OF 0.0044 FT/SEC
(FROM IMPACT TEST)

ACTUAL STATIC CONE PRESSURE PROFILE
OBTAINED BY CONSTANT VELOCITY
PENETRATION TEST AT VELOCITY
OF 0.0044 FT/SEC

FIG-35 TYPICAL IMPACT PENETRATION TEST RESULTS

TEST NO C 811
DEPTH OF PENETRATION = 8.4 FT.
WEIGHT OF PENETROMETER = 86 LBS.
IMPACT VELOCITY = 39.88 FT/SEC
VANE SHEAR STRENGTH = 0.583 LB./FT²
$\gamma = 1.04$ LBS/FT³, $W = 83.4 \%$

FIG 27: PLOT OF PENETRATION DEPTH VS ACCELERATION

TEST NO. C-W-1-1: WEIGHT OF PENETROMETER = 50-64 LBS.
TEST NO. C-W-1-2: WEIGHT OF PENETROMETER = 46-42 LBS.
TEST NO. C-W-1-3: WEIGHT OF PENETROMETER = 35-81 LBS.
KOP CONE = 1-405" DIA. PENETROMETER,
IMPACT VELOCITY = 18-99 FT/SEC
TARGET: MEDIUM STIFF CLAY
γ_t = Wt/ft³
W = 23.9%
γ = 1046 LBS/FT³

111

FIG 28 PLOT OF PENETRATION DEPTH VS VELOCITY

112

UNIT CONE THRUST (LBS/FT²)

UNIT SLEEVE FRICTION (LBS/FT²)

PENETRATION DEPTH (FT)

FOR EXPERIMENTAL DETAILS SEE FIG-27

TEST NO-C.W-I-3

TEST NO-C.W-I-2

TEST NO-C.W-I-1

TEST NO-C.W-I-3

TEST NO-C.W-I-2

FIG-29 PLOT OF PENETRATION DEPTH VS. UNIT CONE THRUST AND UNIT SLEEVE FRICTION

114

TEST NO.C-W-2-1; WEIGHT OF PENETROMETER = 25.97 LBS
TEST NO.C-W-2-2; WEIGHT OF PENETROMETER = 15.9 LBS
60° CONE, 1 = 405" DIA PENETROMETER
IMPACT VELOCITY = 17.49 FT/SEC
TARGET: SOFT CLAY
γ_t = 81.72 LBS/CU FT
w = 54.5 %
τ = 204 LBS/FT².

FIG. 30 PLOT OF PENETRATION DEPTH VS. ACCELERATION

FIG-31 -PLOT OF PENETRATION DEPTH VS. VELOCITY.

PENETRATION VELOCITY (FT/SEC)

PENETRATION DEPTH (FT)

FOR EXPERIMENTAL DETAILS SEE FIG-30

EXPERIMENTAL } TEST NO-C-W-2-2
THEORETICAL } (EQ-11)

EXPERIMENTAL } TEST NO-C-W-2-1
THEORETICAL } (EQ-11)
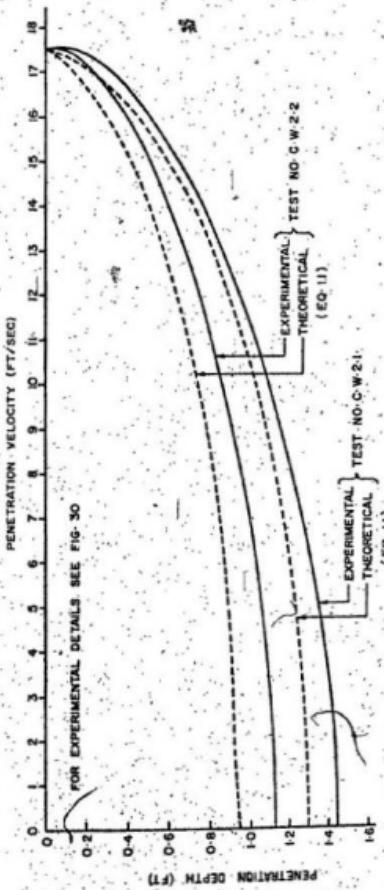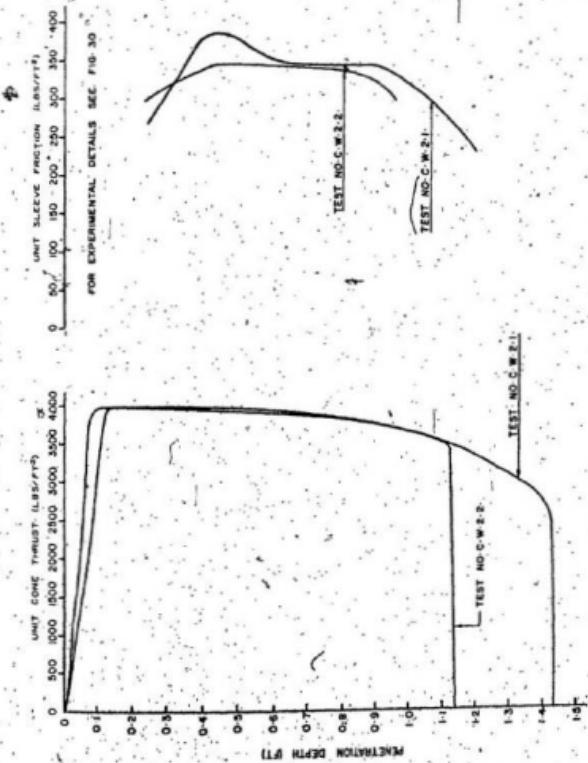
FIG-32 PLOT OF PENETRATION DEPTH VS. UNIT CONE THRUST AND UNIT SLEEVE FRICTION
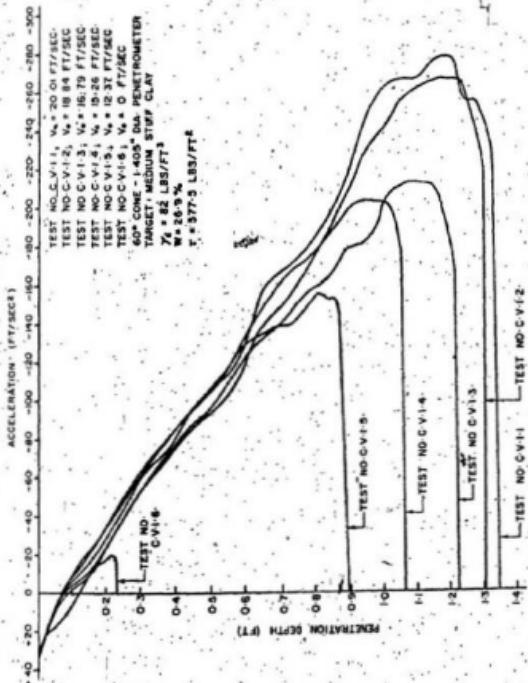
FIG. 33 PLOT OF PENETRATION DEPTH VS. ACCELERATION

118

FIG. 34 PLOT OF PENETRATION DEPTH VS. VELOCITY

TEST NO. C-V-I-6

TEST NO. C-V-I-5 { THEORETICAL, EXPERIMENTAL

TEST NO. C-V-I-4 { THEORETICAL, EXPERIMENTAL

TEST NO. C-V-I-3 { THEORETICAL, EXPERIMENTAL

TEST NO. C-V-I-2 { THEORETICAL, EXPERIMENTAL

TEST NO. C-V-I-1 { THEORETICAL, EXPERIMENTAL
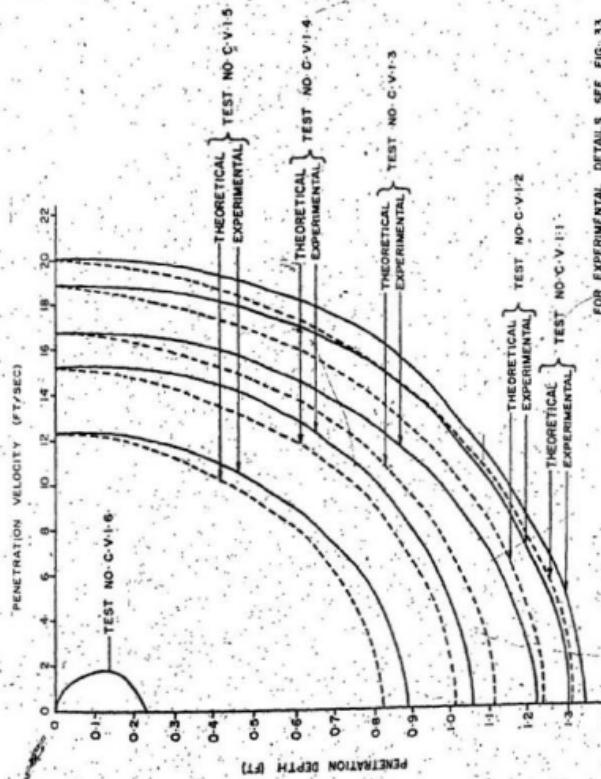
FOR EXPERIMENTAL DETAILS SEE FIG. 33
THEORETICAL CURVES ARE OBTAINED FROM EQ. (III)

PENETRATION VELOCITY (FT/SEC)

PENETRATION DEPTH (FT)
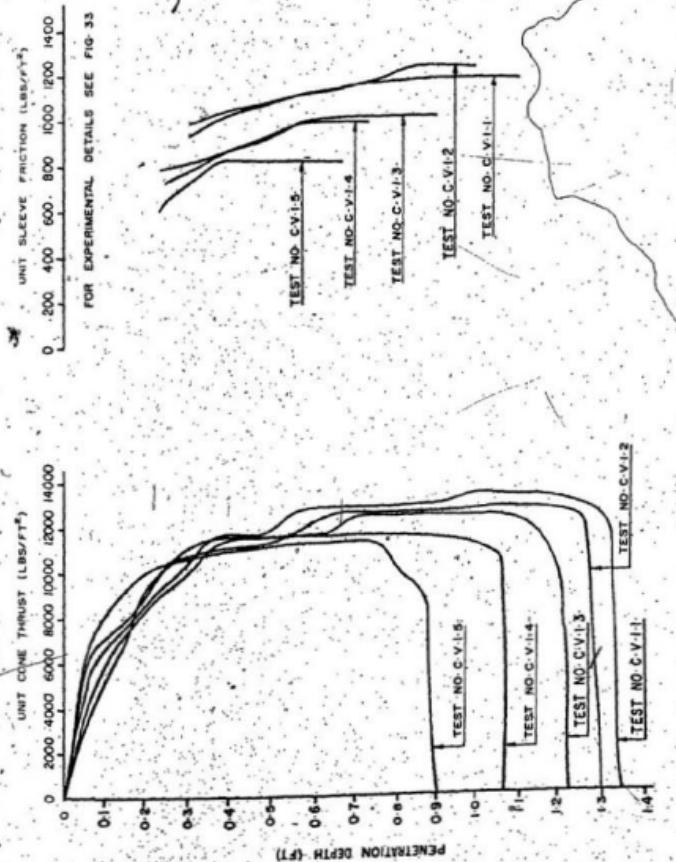
FIG-35 PLOT OF PENETRATION DEPTH VS. UNIT CONE THRUST AND UNIT SLEEVE FRICTION

The effects of impact velocity and the weight of penetrometer on the penetration mechanism have been studied by several investigators and are summarized in sub sections 2.1.2.1, and 2.1.2.2. of this thesis. In contrast to the present investigations of low velocity impact and high frontal loading, their studies are mostly on high velocity impact and low frontal loading and their results are qualitatively in agreement with the above mentioned conclusions.

Nose Shape

The effects of penetrometer nose shapes on the penetration mechanism were studied for four nose shapes: 30°, 60°, 90° and blunt nose (the angles are those formed between the two opposite edges of cone surface) and the results are plotted in Figs. 36, 37, and 38. Those results confirm the findings of previous investigators (Thompson, 1966; Woodward, Clyde, Sherard, and Associates, 1962-67; Young, 1969; and Murff and Coyle, 1972, 1973A) that the increase in nose sharpness yields an increase in the total penetration. The blunt nosed projectile experiences a very high deceleration at impact (several attempts were made in the present investigations to measure the peak deceleration at impact—but it was much higher than that of the rated range of the accelerometer) and then the deceleration trace follows similar to that of other end shapes.

Table 2 shows the average cone thrust and sleeve friction obtained from impact tests for different end shapes.
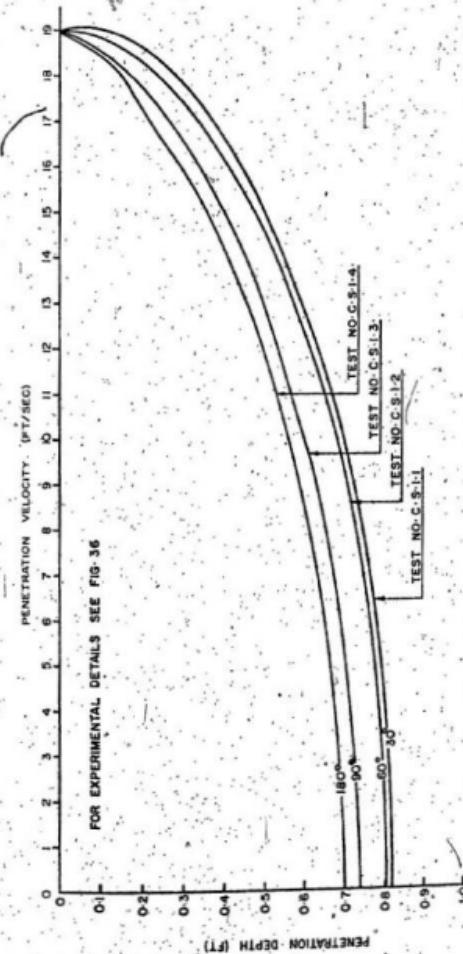
121

TEST NO. C-S1-1, 30° CONE ANGLE
TEST NO. C-S1-2, 30° CONE ANGLE
TEST NO. C-S1-3, 60° CONE ANGLE
TEST NO. C-S1-4, BLUNT NOSE
DIAMETER OF PENETROMETER = 1.405"
WEIGHT OF PENETROMETER = 56.614 LBS
IMPACT VELOCITY = 18.91 FT/SEC
TARGET: MEDIUM STIFF CLAY
$\gamma_t = 99.6$ LBS/CU. FT
W = 22.9 %
C = 1406 LBS/ft²

FIG. 36 PLOT OF PENETRATION DEPTH VS. ACCELERATION

FIG. 37 PLOT OF PENETRATION DEPTH VS. VELOCITY

FOR EXPERIMENTAL DETAILS SEE FIG.36

TEST NO.C.S.1-4

TEST NO.C.S.1-3

TEST NO.C.S.1-1

TEST NO.C.S.1-2

PENETRATION VELOCITY (FT/SEC)

PENETRATION DEPTH (FT)

122
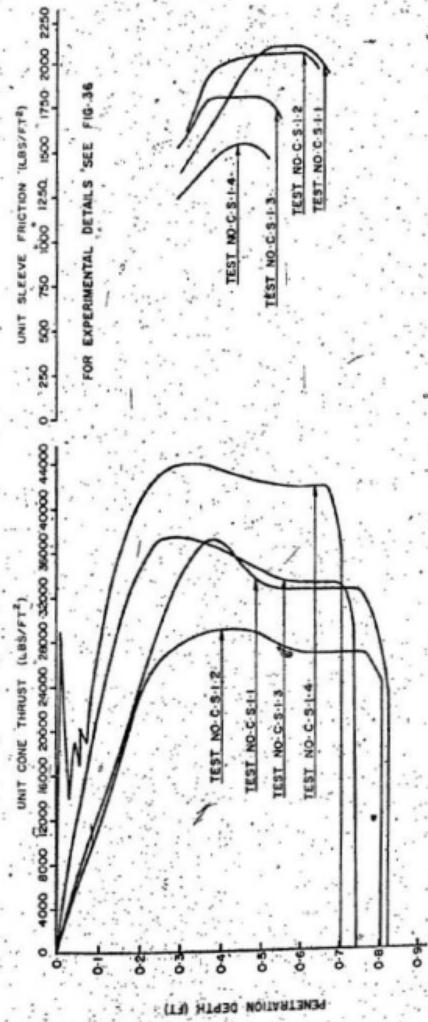
FIG 38 PLOT OF PENETRATION DEPTH VS. UNIT CONE THRUST, AND UNIT-SLEEVE FRICTION

TABLE 2

CONE AND SLEEVE FRICTION RESISTANCES
FOR DIFFERENT NOSE SHAPES

Test No.	End Shape	Cone Thrust (Lbs/ft^2)	Sleeve Friction (lbs/ft^2)	Penetration depth (ft)	Ratio of cone pressure w.r.t. 60° cone	
					Experimental	Meyerhof's theoretical
1	2	3	4	5	6	
C.S.1.1.	30°	32600	2110	0.82	1.2	1.02
C.S.1.2.	60°	27000	2075	0.803	1	1
C.S.1.3.	90°	33200	1825	0.745	1.23	1.04
C.S.1.4.	Blunt end	42000	1550	0.7	1.55	1.2

An examination of Table 2 reveals that the maximum and minimum cone resistances are offered to the blunt shaped and 60° cone respectively. Contrary to the belief of Young (1969) and Woodward Clyde, Sherard and Associates (1962-67) it is seen that the 30° cone offers more resistance than the 60° cone. The cone resistance ratio is given in column (5) of Table 2 for different cone angles with respect to 60° cone. Similarly, the ratio of Meyerhof (1961) bearing capacity factor (N_c) for a different cone angle to 60° cone is given in column (6) of Table 2. The experimentally observed trend is conceivable qualitatively from Meyerhof's theoretical ratios calculated for 'static' condition.

The sleeve friction records indicate that the increase in cone angle yields a decrease in sleeve friction resistance. The sleeve friction resistance for a blunt shape is approximately 35 percent lower than the 30° cone. However, the combined effects of cone and

friction resistances produce little difference and thus a small difference is observed in the total penetration depth. It is noted that, in spite of higher cone and friction resistance for a 30° cone, a 60° cone yields lower penetration depths than a 30° cone. This is because of the geometrical shape viz., 30° cone provides less surface area than a 60° cone for the same height.

Target Strength

Three test results are abstracted in Table 3 to show the effect of target strength on penetration event. As expected, these results indicate that an increase in target strength yields an increase in 'peak' deceleration, a decrease in total penetration and an increase in cone and sleeve friction resistances.

Evaluation of the Proposed Theoretical Model

The foregoing discussions are based on the experimental results in which various previously reported qualitative observations were quantified and rationalised by means of direct measurements of cone thrust and sleeve friction during impact penetration. Another important aspect of this study is to develop a theoretical model applicable to low velocity impact penetration problems. Based on past experience and present investigations, a theoretical model has been developed (see Chapter III) from the fundamental laws of mechanics. In general, the evaluation of the theoretical model reveals the same trends as those observed experimentally. In the following paragraphs the validity of the proposed theoretical model will be evaluated from experimental results. The comparison is limited to the range of variables investigated.

TABLE 3

TEST RESULTS FOR DIFFERENT TARGET STRENGTH

Test No.	Wt. of Penetrometer (lbs.)	Impact Velocity (ft/sec)	Target Strength (τ) (lbs/ft²)	Dry Unit Wt. (lbs/cuft)	Moisture Content %	Peak de-celeration (ft/sec²)	Cone Thrust (lbs/ft²)	Sleeve Friction (lbs/ft²)	Penet-ration Depth(ft.)
C.V.1.2.	56.64	18.84	577.5	82	26.9	268	12800	1250	1.3
C.W.1.1.	56.64	18.89	1066.	91	23.9	357	22000	1990	0.886
C.S.1.2.	56.64	18.89	1410	89.6	22.92	365	27000	2075	0.803

Penetration Velocity Profile

As explained earlier, Eqn. 11 can be used to compute the theoretical velocity profile and maximum penetration depth for known test conditions. Theoretical velocity profiles were computed from Eqn. 11 for most of the tests presented in this thesis and those are shown in Figs. 28, 31, and 34 together with experimentally obtained velocity profiles. The different coefficients occurring in Eqn. 11 depend on target and penetrometer characteristics. The calculated values of those coefficients which have been used as computer input data for the numerical integration of differential Eqn. 11 are shown in Table 4. The theoretical velocity profiles are in agreement with those obtained experimentally. It is noted that in every test the theoretical velocity profiles are slightly higher than the experimental ones for the following reasons:

(1) From beginning to completion of the penetration event the bearing capacity factors used in theoretical calculations are for deep foundation conditions $\left(\frac{D_f}{B} \geq 4 \right)$. Whereas for depths up to $\frac{D_f}{B} \leq 1$ the coefficients for shallow depths should be used and for depths between $1 < \frac{D_f}{B} < 4$ some intermediate values should be used.

(2) In the theoretical derivation, the area of shaft at any penetration depth is calculated assuming a constant perimeter extending from the tip of the cone. Actually it increases gradually from zero at the tip to maximum (equal to perimeter of shaft) at the base of cone.

Accounting for the above mentioned factors in the theoretical model would cause less resistance on the penetrometer than that

assumed in the present analysis and consequently it would provide more penetration depth for the same velocity or vice versa. However, it is felt that those factors would unnecessarily complicate the problem with no significant contribution especially in the case of the deep penetrating penetrometer and, as such, no considerations to this effect are given in the present analysis.

Maximum Penetration *versus* Penetrometer Weight and Impact Velocity

The maximum penetration depth for different penetrometer weights are computed from the theoretical relationship (Eqn. 11) for two different target strengths (τ = 204 lbs./ft.^{2} and 1066 lbs./ft.^{2}). The results are plotted in Fig. 39 for penetrometers up to 100 lbs. Similarly the maximum penetration depth vs. impact velocity relationship is plotted in Fig. 40 up to an impact velocity of 50 ft./sec. for target strength (τ) of 577.5 lbs./ft.^{2}. The experimentally obtained penetration depths for those targets are also shown in those figures.

On the basis of experimental results obtained for experimental velocities ranging from 18 ft./sec. to 115 ft./sec. on kaolin clay, Murff and Coyle (1973A) concluded that maximum penetration depth is almost linear with impact velocity. It is of interest to note that the theoretical curve in Fig. 40 could very well be approximated as a straight line. The present experimental results obtained for impact velocities between 10 ft./sec. to 20 ft./sec. confirm the above relationship.

Table 4 shows the brief summary of experimental and theoretical results. Columns (12), (13), and (14) of that table show the actual penetration depth, theoretically computed penetration depth, and their percentage variation respectively. An examination of column (14) shows
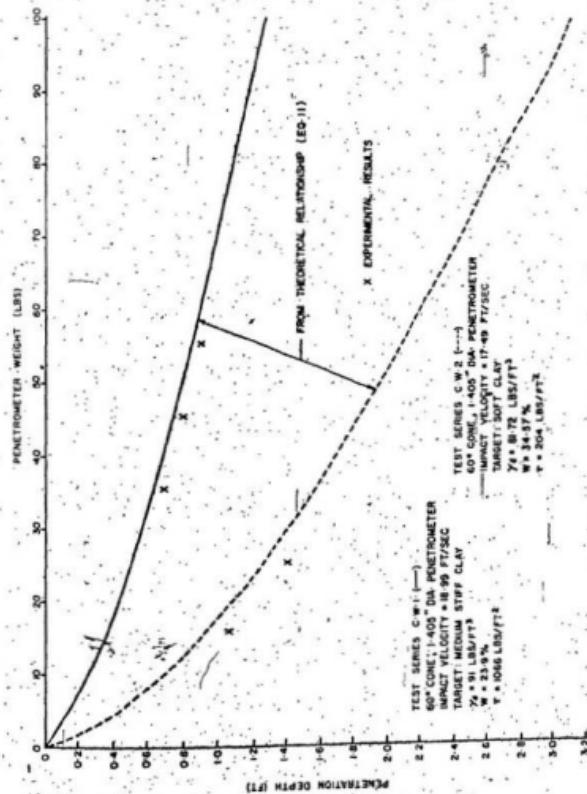
FIG. 39 PENETROMETER WEIGHT VS. PENETRATION DEPTH
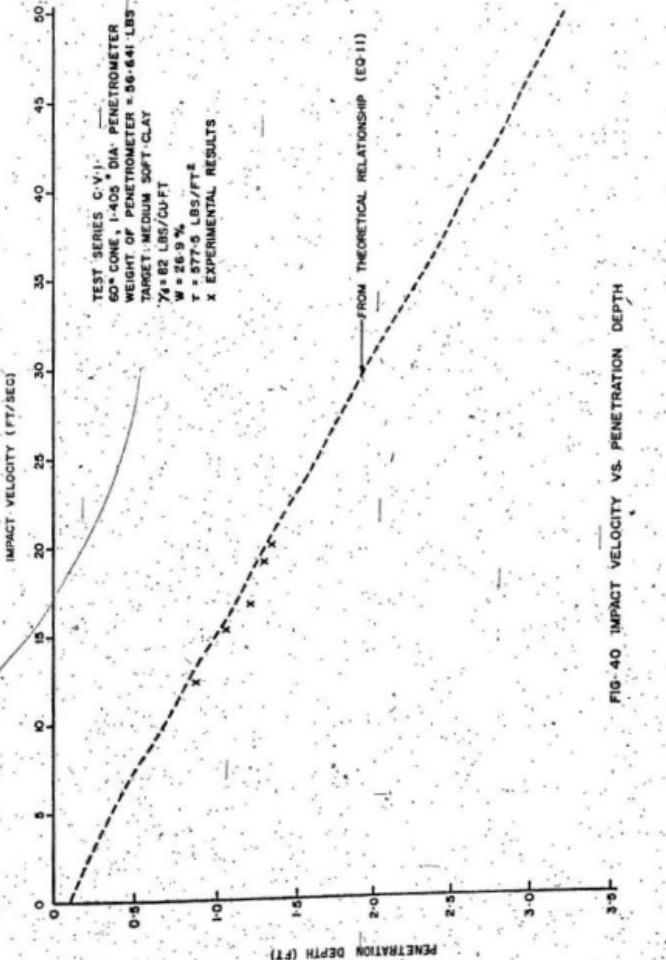
FIG-40 IMPACT VELOCITY VS. PENETRATION DEPTH

TEST SERIES C-V-I.
60° CONE, I•405" DIA PENETROMETER
WEIGHT OF PENETROMETER •56•641 LBS
TARGET: MEDIUM SOFT CLAY
$\gamma_t \cdot 82$ LBS/CU-FT
W = 26-9%
$\tau \cdot 577.5$ LBS/FT²
X EXPERIMENTAL RESULTS

FROM THEORETICAL RELATIONSHIP (EG-II)

IMPACT VELOCITY (FT/SEC)

PENETRATION DEPTH (FT)

130

TABLE 4

DEPTH PREDICTION FOR CLAY TARGET

60° Cone Penetrometer of 1.405 in. diameter

Test No.	Wt. of Penetrometer (lbs.)	Impact Velocity ft/sec	τ (lbs./ft.²)	φ (degrees)	K_L	a	B	γ	M	A	Actual Penetration depth (ft.)	Theoretical Penetration (ft.)	Variation (%)
(1)	(2)	(3)	(4)	(5)	(6)	(7)	(8)	(9)	(10)	(11)	(12)	(13)	(14)
C.W.1.1	56.64	18.99	1066	-	-	0.155 (d)	-47.108 (G)	401.88 (G)	0	1.779	0.043	0.886	0.873	1.4
C.W.1.2	46.42	18.99	1066			0.155 (d)	-57.33 (G)	401.88 (G)	0	1.462	0.043	0.785	0.768	2.1
C.W.1.3	35.81	18.99	1066			0.155 (d)	-67.94 (G)	401.88 (G)	0	1.133	0.043	0.69	0.67	2.9
C.W.2.1	25.97	17.49	204			0.25 (d)	12.616 (L)	84.94 (L)	-0	0.826	9.042	1.44	1.291	10
C.W.2.2	15.9	17.49	204			0.25 (d)	2.546 (L)	84.94 (L)	0	0.514	0.042	1.142	0.952	16.6
C.V.1.1	56.64	20.01	577.5			0.23 (1)	20.029 (c)	222.34 (L)	0	1.778	0.0404	1.35	1.316	2.5

TABLE 4 (CONTINUED)

Test No.	Wt. of Penetrometer (lbs.)	Impact Velocity ft/sec	T (lbs./ft.²)	φ (degree)	K_L	α	B	Y	M	A	Actual Penetration depth (ft.)	Theoretical Penetration (ft.)	Variation (%)
(1)	(2)	(3)	(4)	(5)	(6)	(7)	(8)	(9)	(10)	(11)	(12)	(13)	(14)
C.V.1.2	56.64	18.84	577.5	-	0.23 (I)	20.029 (L)	222.34 (L)	0	1.778	0.0404	1.3	1.24	4.6
C.V.1.3	56.64	16.79	577.5	-	0.23 (I)	20.029 (L)	222.34 (L)	0	1.778	0.0404	1.22	1.115	8.6
C.V.1.4	56.64	15.26	577.5	-	0.23 (I)	20.029 (L)	222.34 (L)	0	1.778	0.0404	1.06	1.011	4.6
C.V.1.5	56.64	12.37	577.5	-	0.23 (I)	20.029 (L)	222.34 (L)	0	1.778	0.0404	0.891	0.823	7.6

(a) = directly obtained from Constant Velocity Penetration test; (G) = General shear failure conditions; (L) = Local shear failure conditions; (I) = Interpolated from Table 1.

that out of ten results presented, the depth prediction for six tests (in 60 percent) are well above the accuracy of 95 percent and up to 90 percent accurate in 9 tests (in 90 percent). Only in one case is it predicted with an accuracy of 83 percent. These results again demonstrate the validity of the proposed theoretical model.

For most of the tests mentioned in Table 4 the velocity profiles and maximum depth of penetration were also computed from Eqn. 14 to evaluate the validity of this relationship. It is interesting to note that Eqns. 11 and 14 give almost identical results for up to the ninety percent penetration depth and beyond this depth the difference was never more than 10 percent (see Appendix A). However, in Eqn. 14 the soil viscosity coefficient (K) is estimated from cone resistances obtained by a constant velocity penetration test at 0.0044 ft./sec. and an impact penetration test assuming a linear relationship (the procedure is explained in subsequent paragraphs).

Estimation of Target Strength

As mentioned in Chapter III, Eqn. 14, in addition to providing the velocity profile and maximum penetration depth, can be used for estimating the conventional shear strength parameters such as C and φ of the target materials for a known impact velocity and maximum penetration depth. Eqn. 16, applicable for pure cohesive soils, is one of the special form of Eqn. 14.

It should be noted that in deriving those relationships it has been assumed that apparent cohesion (C') varies linearly with velocity (Eqn. 12). As such the soil viscosity coefficient (K) is established by assuming a straight line variation between cone pressures obtained

from 'static' and impact penetration tests. An approximate estimation
of K can also be made by extrapolating the logarithmic relationship
obtained from constant velocity penetration tests in Fig. 22. The
error involved in assuming a linear variation is shown in Fig. 41 along
with constant velocity penetration test results for a typical test.
For this target, the relationship obtained by extrapolation of
logarithmic relationship (from Fig. 24) is also plotted on ordinary
scale in Fig. 41. It is seen that the error involved in the two
relationships is almost neutralised for the penetration velocity above
8 ft./sec. while for the penetration velocity below 8 ft./sec. consider-
able error is involved. However, both theoretical and experimental
velocity profiles reveal that for impact velocity of around 20 ft./sec.
almost 85 to 90 percent penetration is generally reached well above the
penetration velocity of 8 ft./sec. The resulting error would not be
very significant. The above reasonings can be substantiated from
previously mentioned facts that "Eqn. 11 and Eqn. 14 give almost
identical results for up to 90 percentage of total penetration . . . ."

A typical calculation for estimating the cohesive strength of
the target material from Test No. C.W.1.1 (detailed in Table 4) is
shown in the following:

Test details

Penetrometer: 60°cone - 1.405 in. diameter, 56.64 lbs. weight.

Impact velocity (V_o) = 18.99 ft./sec.

Maximum penetration depth (Z_m) = 0.886 ft.

Target: Medium stiff clay

Dry density (γ_d) = 91 lbs./ft.^{3}
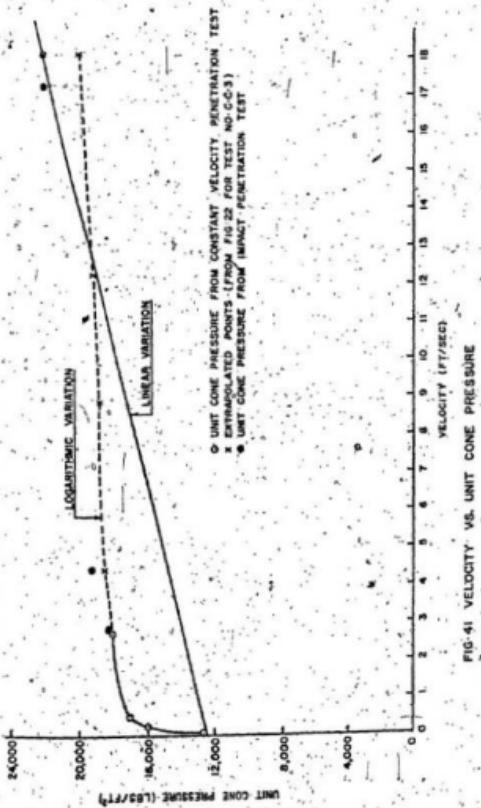
FIG 41 VELOCITY VS. UNIT CONE PRESSURE

○ UNIT CONE PRESSURE FROM CONSTANT VELOCITY PENETRATION TEST
× EXTRAPOLATED POINTS (FROM FIG 22 FOR TEST NO C-C-3)
● UNIT CONE PRESSURE FROM IMPACT PENETRATION TEST

LOGARITHMIC VARIATION

LINEAR VARIATION

UNIT CONE PRESSURE (LBS/FT²)

VELOCITY (FT/SEC)

135

Water content (w) = 23.9%

Bulk density (γ_t) = 112.75 lbs./ft.^{3}

Shear strength (C) = 1066 lbs./ft.^{2}

Unit Cone Pressure at constant velocity of 0.0044 ft./sec. = 12541 lbs./ft.^{2}

Unit Cone Pressure at average penetration velocity of 18 ft./sec. (from impact test) = 22020 lbs./ft.^{2}

Estimation of soil viscosity coefficient K (assuming linear variation): (Note: for explanation of different symbols used in this calculation refer to Chapter III).

Ratio of increase in cone-pressure from 'static' to 'dynamic' =

$$\frac{22020 - 12541}{12541} = 75.58\%$$

If Nc_r is constant for 'static' and 'dynamic' case then cohesive strength would also increase by the same ratio (75.58%).

Vane shear strength (C) = 1066 lbs./ft.^{2}

Apparent cohesion (C') = 1.7558C = 1871.7 lbs./ft.^{2}

Also $C' = C + KV$ or $K = \dfrac{C' - C}{V}$

For impact velocity of 18.99 ft./sec.

Soil viscosity coefficient (K) = 42.42 ~ 40

Bearing capacity factors (estimated from Meyerhof, 1961)

For $\phi = 0$ and semi cone angle $(\alpha) = 30°$

$Nc_r = 10.5$ for rough penetrometer

$Nc_r = 7.5$ for smooth penetrometer

Assuming semi-rough penetrometer; $Nc_r = 9$

$Nq_r = 1$

$N\gamma_r = 0$

$K_o = 1$

$$\alpha = mg - \{\tfrac{2}{3}\,\pi\rho gR^3 + 2\sqrt{3}\,\pi\rho gR^3 + \tfrac{3}{2}\,\pi^2\rho gR^3 + CNc_r\,\pi R^2 + \pi\rho gN_{\gamma_4}R^3\}$$

$$= 55.98 - 0.0967\ C$$

$$\beta = 7.464\ \pi\rho gR^2 + \pi K_o\rho gN_{q_4}R^2 + 2\pi RC$$

$$= 10.25 + 0.367\ C$$

$$\gamma = \pi K_o\rho g R \tan\phi = 0$$

$$A = \frac{7.464}{6.464}\,\pi\rho R = 0.043$$

$$M = m + \sqrt{\tfrac{2}{3}}\,\pi\rho R^3 + 2\sqrt{3}\,\pi\rho R^3 + \tfrac{3}{2}\,\pi^2\rho R^3$$

$$= 1.779$$

$$L = 2\,\pi\,Nc_r\,R^2\,K = 7.736$$

$$N = 4\,\pi\,RK = 29.4$$

Equation 16 can be written in the following form for maximum depth of penetration:

$$M^2 v_o^2 = - (2\alpha M - LMV_o)\,Z_m - \left(A\alpha - BM - \frac{L\alpha}{2V_o} - \frac{NMV_o}{2}\right) Z_m^2$$

$$+ \frac{1}{3}\left(2A\beta + \frac{L A\alpha}{2MV_o} - \frac{L\beta}{2V_o} + \frac{N\alpha}{V_o}\right) Z_m^3$$

$$- \frac{1}{2}\left\{\frac{LA\beta}{6MV_o} - \frac{N(A\alpha - BM)}{4MV_o}\right\} Z_m^4 - \frac{NA\beta}{15MV_o}\,Z_m^5$$

putting the values of the different terms in above expression and solving for $V_o = 18.99$ ft./sec. and

$Z_m = 0.886$ ft. we get $C = 923.5$ lbs./ft.^{2}

Whereas the vane shear strength is 1066 lbs./ft.^{2}

Thus the variation is 13.4%.

The above estimation of C is based on the assumption that unit friction on the shaft is equal to the shearing resistance of the soil which for cohesive soils should be equal to vane shear strength. However, the direct measurement of unit sleeve frictions for the

slowest penetration velocity (0.0044 ft./sec.) is considerably (10 to
50%) lower than the shear strength of soil and this difference is
accounted for in assuming a lower viscosity coefficient. This
simplification may hold good in finding the theoretical velocity
profile and total penetration depth because in that case only total
force on the shaft is considered. However, in estimating the shear
strength this simplification significantly changes the result because
the calculation is based on the assumption that adhesion on the shaft
is equal to shear resistance of soil. Therefore, for calculating the
shear strength it is modified, at a first approximation, by assuming
adhesion on the shaft is equal to 0.8C. The selection of 0.8C is based
on sleeve friction to the vane shear strength ratio obtained in most
of the tests. Thus, the correction of adhesion equal to 0.8C gives

$$\beta = 7.464 \ \pi \rho g R^2 + \pi K_o \rho g N q_c R^2 + 1.6 \ \pi \ RC$$

$$= 10.25 + 0.2936 \ C$$

The other terms remain unchanged.

Proceeding with the modified value of β the cohesive strength of the
target is obtained as:

$$C_{(modified)} = 1050.4 \ lbs./ft.^2; \ percentage \ variation \ 1.5\%.$$

This result, along with the estimated cohesive strength of two
other target strengths, is shown in Table 5. It is noted that by using
modified adhesion value (0.8 C) on shaft the results are very
significantly improved and estimated strengths are within the accuracy
of 94 percent compared to vane shear strengths.

TABLE 5

ESTIMATION OF TARGET STRENGTH

60° Cone Penetrometer of 1.405 in. diameter

Test No.	γ_d (lbs./ft.³)	w (%)	Wt. of Penetrometer (lbs.)	V_0 (ft./sec.)	Nc_r	Nq_r	$N\gamma_r$	K	Zm (ft.)	τ-vane (lbs./ft.²)	C unmodified (lbs./ft.²)	C modified (lbs./ft.²)	Variation (%)
C.W.1.1	91	23.9	56.64	18.99	9 (G)	1	0	40(d)	0.886	1066	923.5	1050.4	1.5
C.V.1.1	82	26.9	56.64	20.01	5.8 (L)	1	0	22.5 (I)	1.35	577.5	552.5	602	4.2
C.W.2.1	81.72	34.5	25.97	17.49	5.8 (L)	1	0	9(d)	1.44	204	176.8	216	5.9

(d) = directly obtained from Constant Velocity and Impact tests.
(I) = Interpolated in proportion to vane shear strength from upper and lower bound values of Table 1.
(G) = General shear failure condition.
(L) = Local shear failure condition.

5.4 Test Results of Series II

The results reported in Series II are mostly on silica sand and include both constant velocity penetration and impact penetration tests.

5.4.1. Constant Velocity Penetration Tests

The constant velocity penetration test results for sandy gravel, loosest sand and densest sand targets are shown in Figs. 42, 43, and 44 respectively. The tests were performed for four different velocities: 0.0044 ft./sec., 0.042 ft./sec., 0.456 ft./sec., and 2.662 ft./sec. Those results indicate that even for a 600 fold increase in penetration velocity there is no appreciable difference in either cone resistance or friction sleeve resistance. This confirms the previously reported results (discussed in Chapter III) that "dynamic effects are minimal for cohesionless soils". Thus the assumption in the theoretical model, that the strain rate effects on angle of internal friction is insignificant during impact penetration, is justified from the present investigation also.

5.4.2. Impact Penetration Tests

The impact penetration test results for a typical saturated sand target has been discussed in this thesis. Those tests were performed at impact velocities of 16.36 ft./sec. and 20.02 ft./sec. The results showing depth vs. acceleration/deceleration, velocity, cone thrust and sleeve friction profiles are plotted in Figs. 45, 46 and 47. The constant velocity penetration test is also shown in Fig. 47.

The weight and impact velocity effects on the penetration

FIG 42 CONSTANT VELOCITY PENETRATION TEST RESULTS

TEST NO 5-C-I
60° CONE, 1.405" DIA PENETRATOR
TARGET: MOIST SANDY GRAVEL
UNIT WEIGHT = 109 LBS/CU FT

UNIT CONE PRESSURE (LBS/FT²)

0.042 FT/SEC
0.456 FT/SEC
0.0044 FT/SEC
2.662 FT/SEC

PENETRATION DEPTH (IN)

UNIT SLEEVE FRICTION (LBS/FT²)

2.662 FT/SEC
0.456 FT/SEC
0.0044 FT/SEC
0.456 FT/SEC

FIG 43 CONSTANT VELOCITY PENETRATION TEST RESULTS

TEST NO. S-C-1
60° CONE, 1·405" DIA PENETRATOR
TARGET: VERY COMPACTED DRY SAND
γ_d = 90·7 LBS/CU·FT

Left graph axes:
PENETRATION DEPTH (IN)
UNIT CONE PRESSURE (LBS/FT²)

Curve labels:
0·0044 FT/SEC
0·456 FT/SEC
0·042 FT/SEC
2·652 FT/SEC

Right graph axes:
UNIT SLEEVE FRICTION (LBS/FT²)

Curve labels:
0·456 FT/SEC
2·652 FT/SEC
0·0044 FT/SEC
0·042 FT/SEC

142

FIG. 44 CONSTANT VELOCITY PENETRATION TEST RESULTS

TEST NO. S-C-2
60° CONE, 1.405" DIA PENETRATOR
TARGET: LOOSE DRY SAND
$\gamma_d = 85.5$ LBS/CU FT

144

TEST NO. 5-V-1.1; Vo = 20.02 FT/SEC
TEST NO. 5-V-1.2; Vo = 18.36 FT/SEC
60% CONC. 1.408" DIA. PENETROMETER
WEIGHT OF PENETROMETER = 56.64 LBS
TARGET: SATURATED SAND
γ_s = 88.57 LBS/CU FT
W = 27.4%
ϕ = 41°

FIG-45 PLOT OF PENETRATION DEPTH -VS- ACCELERATION

FIG 46 PLOT OF PENETRATION DEPTH VS. VELOCITY

FOR EXPERIMENTAL DETAILS SEE FIG-45

EXPERIMENTAL } TEST NO·9·V·I·2
THEORETICAL } (EQ·17)

EXPERIMENTAL } TEST NO 9·V·I·I
THEORETICAL } (EQ·17)

PENETRATION VELOCITY (FT/SEC)

PENETRATION DEPTH (FT)
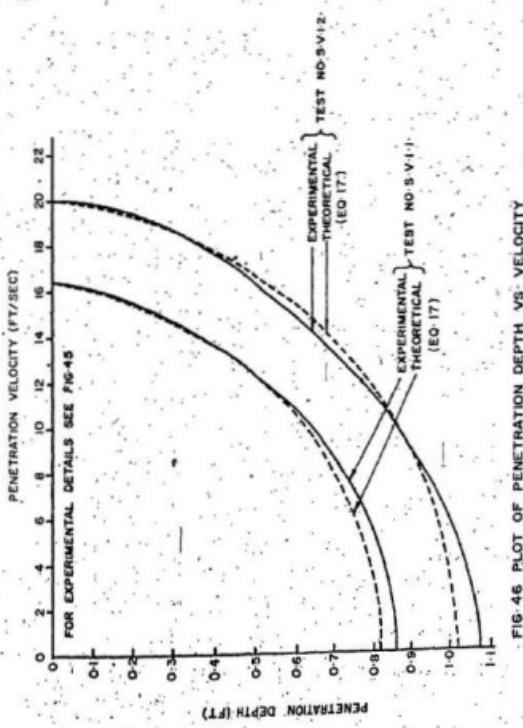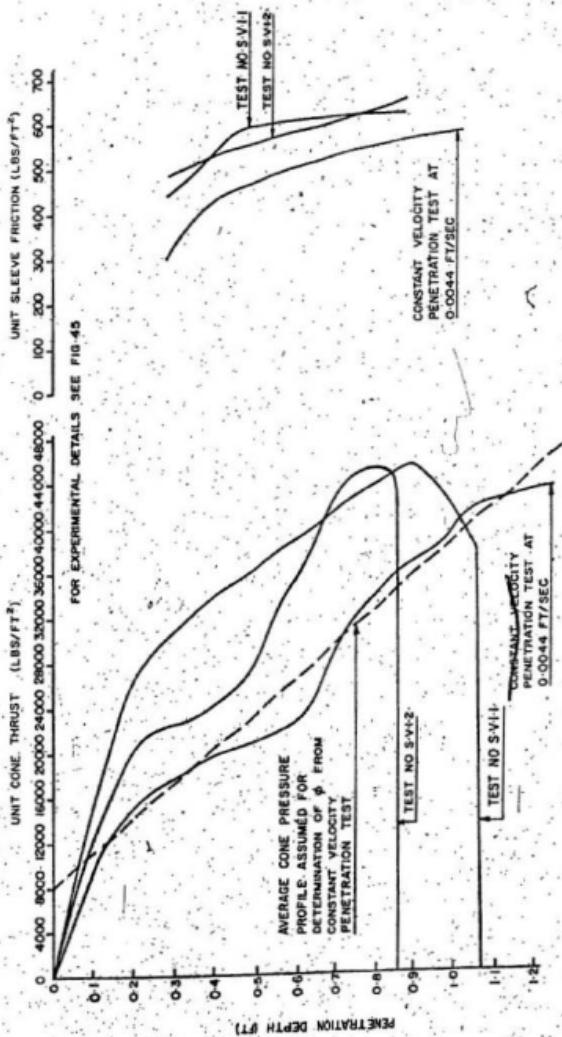
FIG. 47: PLOT OF PENETRATION DEPTH VS UNIT CONE THRUST AND UNIT SLEEVE FRICTION

146

mechanism of sandy targets are, in general, the same as those observed
for clay targets. As expected, the ratio of cone thrust to sleeve
friction is much higher than that obtained for cohesive soils. This
phenomenon shall be discussed in sub-section 5.6 of this chapter.

Evaluation of the Theoretical Model

Velocity Profile and Maximum Penetration Depth

The theoretical evaluation of velocity profile and the
maximum depth of penetration is obtained from Eqn. (17). It is noted
that for the condition K = 0, Eqn. (11) and Eqn. (13) are reduced to
the same linear differential equation. The solution of resulting
equations can be obtained by either the exact method or the pertur-
bation method.

The theoretical and experimental velocity profiles are shown
in Fig. 46. It is seen that for the sand target the proposed theoretical
model is in agreement with the experimental results. The theoretical
depth prediction is well above the accuracy of 95%. For a sand target
also theoretical velocity profiles and depth predictions are lower than
the experimental values for the reasons discussed for clay targets.

Estimation of the Angle of Internal Friction (ϕ)

The following procedure is adopted for estimating the angle of
internal friction (ϕ) from the impact penetration tests and also from
the constant velocity penetration test.

Test details

Penetrometer: 60° Cone - 1.405 in. diameter, 56.64 lbs. weight.

Maximum penetration depth = (a) 1.0744 ft. for V_o = 20.02 ft./sec.

(b) 0.86 ft. for V_o = 16.35 ft./sec.

Constant Velocity of Penetration test = 0.0044 ft./sec.

Target: saturated sand

Dry density (γ_d) = 88.5 lbs./cu. ft.

Water content (w) = 27%

Bulk density (γ_t) = 112.4 lbs./cu.ft.

Cohesive strength (C) = 0

Angle of internal friction ϕ = 41°

Soil viscosity coefficient (K) = 0

(The angle of Internal Friction has been determined by direct shear tests and the results are shown in Fig. 48).

Estimation of ϕ angle from Impact Test

$$\alpha = mg - (\frac{A}{3}\rho g R^3 + 2\sqrt{3}\cdot\pi\rho g R^3 + \frac{3}{2}\pi^2\rho g R^3 + CNc_r\cdot\pi R^2 + \pi\rho g N\gamma_r R^3\cdot]$$

$$= 55.98 - 0.0706 \, N\gamma_r$$

$$\beta = 7.464 \,\pi\rho g R^2 + \pi K_o\rho g Nq_r R^2 + 2\pi RC$$

$$= 9.0178 + 0.6038 \, Nq_r$$

Note: In this calculation K_o is assumed as 0.5. However, in calculating the velocity profile it is estimated from relationship $K_o = 1-\sin\phi$ (Jacky, 1948; Dayal *et al.*, 1971).

$\gamma = \pi K_o\rho g R \tan\phi \approx 0$.

(The friction resistance on the shaft is very little as compared to cone-thrust and as such it is neglected).

FIG.49. DIRECT SHEAR TEST RESULTS

C=0
∅=41°
W=98.5 LBS/CU.FT
W=27 %

C=190 LBS/FT²
∅=30.63 LBS/CU.FT
W=98.5
W=20-25 %

C=400 LBS/FT²
∅=15°
FX=101.62 LBS/CU.FT
W=17 %

SAND 95% , SILT 5%
SAND 50% , CLAY 50%
SAND 50% , CLAY 50%

SAND

41°

15°

15°

15°

NORMAL PRESSURE (P.S.I)

SHEAR STRESS (P.S.I)
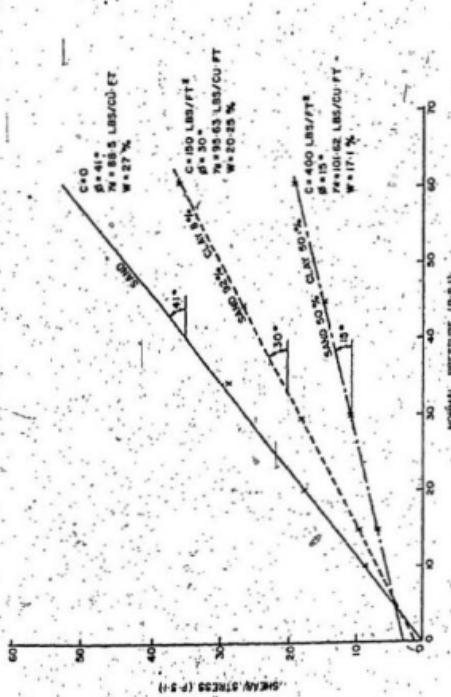
$$\bar{y} = m + \frac{2}{\sqrt{3}} \pi pR^3 + 2\sqrt{3} \pi pR^3 + \frac{3}{2} \pi^2 pR^3$$

$$= 1.779$$

$$A = \frac{7.464}{6.464} \pi pR^2$$

$$= 0.0429$$

The Eqn. 17 can be written in the following form for maximum penetration
depth (neglecting γ):

$$H^2 V_o^{\ 2} = -2 \alpha M Z_m - (A\alpha - BM) Z_m^{\ 2} + \frac{2}{3} AB \cdot Z_m^{\ 3}$$

putting the value of different terms and solving for the conditions

(i) $V_o = 20.02$ ft./sec., $Z_m = 1.0744$ ft.

(ii) $V_o = 16.35$ ft./sec., $Z_m = 0.86$ ft.

gives:

$$N\gamma_r = 1614 \text{ and } Nq_r = 814$$

It is noted that Meyerhof (1961) has not given the values of $N\gamma$ for a
deep circular cone. However, $N\gamma$ is available from Meyerhof (1951) for
deep strip foundation in which the correction for the shape factor
should be applied. The generally recommended shape factor for deep
circular foundation is 0.6.

Thus applying the correction of 0.6 in bearing capacity relationship would
give $N\gamma = 2582$

Estimation of ϕ angle for $N\gamma = 2582$ is 41° (from Meyerhof, 1951)

Estimation of ϕ angle for $Nq_r = 814$ is 40.75° (from Meyerhof, 1961
for rough base and semi cone angle of 30°)

Mean ϕ angle = 40.87°

From direct shear test ϕ angle = 41°

Estimation of ϕ angle from Constant Velocity Penetration test:

The Constant velocity penetration test result for the same target is shown in Fig. 47, with the average cone resistance profile assumed for the estimation of ϕ angle. The ultimate cone pressure at any depth is given as

$$q_c = C \, Nc_r + K_o \, \rho g Z N q_r + 0.6 \, R \rho g N \gamma_r$$

The average cone pressure at Z = 0.5 ft. equals 23400 lbs./ft.^{2}; and

at   Z = 1.0 ft. equals 39200 lbs./ft.^{2}

Solving we get

$N q_r$ = 562 and $N \gamma_r$ = 1926

ϕ angle for $N q_r$ = 562 is 39.5°

ϕ angle for $N \gamma_r$ = 1926 is 40.5°

Mean ϕ angle = 40°

From direct shear test ϕ angle = 41°

At the outset of this investigation, ϕ angle had been estimated from Wang's (1971) impact penetration test data. For example, a 1.5 in. penetrometer weighing 1.056 lbs. was dropped into the dense dry sand target having a unit weight of 110 lbs./cu.ft. Two maximum penetrations were measured and found to be 0.19 ft. and 0.32 ft. at impact velocities of 15 ft./sec. and 25 ft./sec. respectively. The estimated mean ϕ angle from those conditions is 39°, which is in agreement with the ϕ angle obtained as 39.5° from direct shear test.

5.5 Test Results of Series III

The test results reported in Series III are on sand clay mixtures of two different ratios. A description of those mixtures is given in sub-section 5.1 of this thesis. The results include both constant velocity penetration and impact penetration tests.

5.5.1. Constant Velocity Penetration Tests

The constant velocity penetration tests were conducted at four different velocities ranging from 0.0044 ft./sec. to 2.662 ft./sec. for Series IIIA (sand 50% and clay 50%). For Series IIIB (sand 92% and clay 8%) the results could be obtained only at lowest and highest penetration velocities. The results are shown in Figs. 49 and 50. These results indicate that the variation of cone and sleeve friction resistances with respect to penetration depth and penetration velocity for Series IIIA (Test No. S.C.C.1) is similar to that obtained for a cohesive soil whereas for Series IIIB (Test No. S.C.C.2) it resembles that of a sandy soil. It is observed that in test No. S.C.C.1. the 600 fold increase in penetration velocity caused as much as a 40 percent increase in cone resistance whereas in test No. S.C.C.2. the increase of about 10 percent was observed. The ratios $\frac{q_{cd}}{q_c}$ versus $\frac{V}{V_s}$ and $\frac{F_{cd}}{F_c}$ versus $\frac{V}{V_s}$ for test No. S.C.C.1. are plotted in Figs. 22, and 23, respectively with the other results obtained for clay targets.

As concluded earlier, the dynamic effects on ϕ angle is insig- nificant and if this fact is extended for sand-clay mixtures then the increase in strength is mainly contributed from the cohesive strength component. The soil viscosity coefficient (K_L) can be estimated as explained in the following paragraphs.

FIG-49 CONSTANT VELOCITY PENETRATION TEST RESULTS

TEST NO-5-C-C-1
60° CONE, 1 INCH² Dia PENETRATOR
TARGET SAND-CLAY MIXTURE (SERIES III A)
$\gamma_d = 101.62$ LBS/FT³
$W = 17.8\%$
$C = 400$ LBS/FT²
$\phi = 15°$

UNIT SLEEVE FRICTION (LBS/FT²)
0 200 400 600 800 1000

2.482 FT/SEC
0.456 FT/SEC
0.042 FT/SEC
0.0014 FT/SEC

UNIT CONE PRESSURE (LBS/FT²)
0 2000 4000 6000 8000 10000 12000 14000 16000

0.0014 FT/SEC
0.042 FT/SEC
0.456 FT/SEC
2.482 FT/SEC

PENETRATION DEPTH (FT)

153

TEST NO9 C-C 2
60° CONE 140° CONE PENETRATION
TARGET: SAND-CLAY MIXTURE (NUMBER II)
γ_b = 99.93 LB/FT^2
W = 20.25%
C = 450 LB/FT^2
ϕ = 30°

FIG 50 CONSTANT VELOCITY PENETRATION TEST RESULTS

Referring to Eqns. 5 and 6, the ratio of 'dynamic' to 'static'
cone pressure is given by

$$\frac{q_{cd}}{q_c} = 1 + \frac{K_L \log_{10} \frac{V}{V_s}}{1 + \frac{S}{CNc_r}}$$

(21)

where $S = K_o \rho g Z \, Nq_r + \rho g R \, Ny_r$

If $\frac{S}{CNc_r} \ll 1$, then the relationship is similar to that obtained for

cohesive soils (Eqn. 18). Thus K_L can directly be estimated as 0.143
from the cone pressure relationship shown in Fig. 22. It is noted
that the assumption $\frac{S}{CNc_r} \ll 1$ is valid only when the soil has a
comparatively higher cohesive strength and lower angle of internal
friction. For test No. S.C.C.1., the value of K_L calculated from Eqns.
18 and 21 provides a difference of only 5 percent at a penetration
depth of 1.25 ft. However, this value is comparatively quite low to
those reported in Table 1 for cohesive soils of the same strength
range. It is interesting to note that K_L obtained by extrapolation of
the constant velocity penetration test results is in agreement with
those obtained from impact penetration tests for a penetrating velocity
of around 18 ft./sec.

5.5.2. Impact Penetration Tests

The impact penetration tests were conducted for both mixtures
at three different impact velocities ranging from 15.84 ft./sec. to
20.04 ft./sec. Those results are shown in Figs. 51, 52, 53, 54, 55,
and 56. The weight and impact velocity effects on penetration event
of sand-clay mixtures are, in general, the same as those observed for
clay and sand targets. An inspection of cone thrust and sleeve friction

TEST NO. 50-CV-11, V_o=120.0 FT/SEC
TEST NO. 50-CV-12, V_o=128.9 FT/SEC
TEST NO. 50-CV-13, V_o=130.4 FT/SEC
80° CONE, 14-LB TOA- PENETROMETER
WEIGHT OF PENETROMETER =84-84 LBS
TARGET: SAND-CLAY MIXTURE (SERIES III A)
W_S=10.60 LBS/CU-FT
W=17%
C = 400 LBS/FT²
ϕ=15°

ACCELERATION (FT/SEC²)

PENETRATION DEPTH (FT)

TEST NO.50-CV-13
TEST NO.50-CV-12
TEST NO.50-CV-11

FIG.51 PLOT OF PENETRATION DEPTH VS ACCELERATION

FIG-52 PLOT OF PENETRATION DEPTH 'VS' VELOCITY

UNIT SLEEVE FRICTION (LBS/FT²) FIG 51

FOR EXPERIMENTAL DETAILS SEE FIG 51

TEST NO 3 C V I 3

TEST NO 3 C V I 2

TEST NO 3 C V I 1

UNIT CONE THRUST (LBS/FT²)

PENETRATION DEPTH (FT)

STATIC CONE PRESSURE
PROFILE CALCULATED FROM
Ref $\frac{q_u}{q_c} = 0.043$ LOG$_{10}$ $\frac{V}{V_s}$ FOR
STATIC VELOCITY OF
0.0044 FT/SEC

ACTUAL STATIC CONE
PRESSURE PROFILE OBTAINED
BY STATIC PENETRATION TEST AT
VELOCITY OF 0.0044 FT/SEC

TEST NO 3 C V I 1

TEST NO 3 C V I 2

TEST NO 3 C V I 3

FIG 53 PLOT OF PENETRATION DEPTH VS UNIT CONE THRUST AND UNIT SLEEVE FRICTION

FIG 54 PLOT OF PENETRATION DEPTH VS ACCELERATION
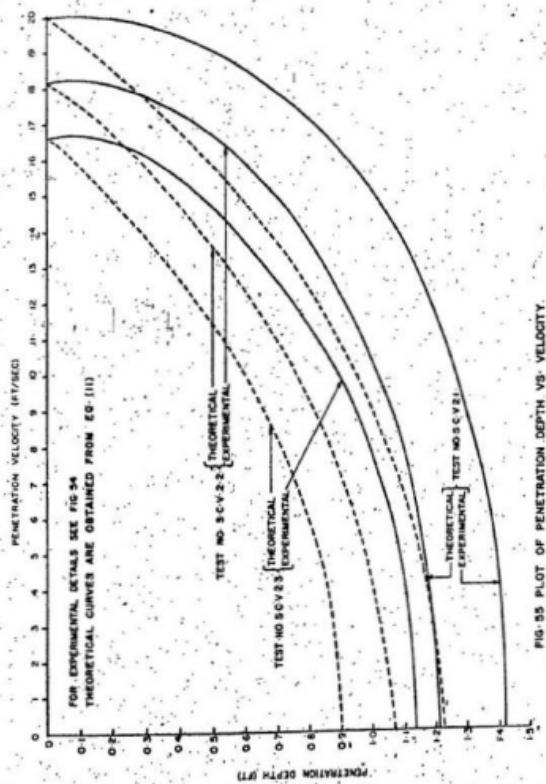
160

FIG 55 PLOT OF PENETRATION DEPTH VS. VELOCITY.

FOR EXPERIMENTAL DETAILS SEE FIG 54
THEORETICAL CURVES ARE OBTAINED FROM EQ (III)

PENETRATION VELOCITY (KFT/SEC)

PENETRATION DEPTH (FT)

TEST NO 9 C.V 2 2 { THEORETICAL
                     { EXPERIMENTAL

TEST NO 9 C.V 8 3 { THEORETICAL
                   { EXPERIMENTAL

TEST NO 9 C.V 8 1 { THEORETICAL
                   { EXPERIMENTAL

FOR EXPERIMENTAL DETAILS SEE FIG 44

UNIT SLEEVE FRICTION (LBS/FT²)

TEST NO 3 C 2 t 3
TEST NO 3 C 2 t 2
TEST NO 3 C 2 t 1

UNIT CONE THRUST (LBS/FT²)×10³

TEST NO 3 C 2 t 3
TEST NO 3 C 2 t 2
TEST NO 3 C 2 t 1

PENETRATION DEPTH (FT)
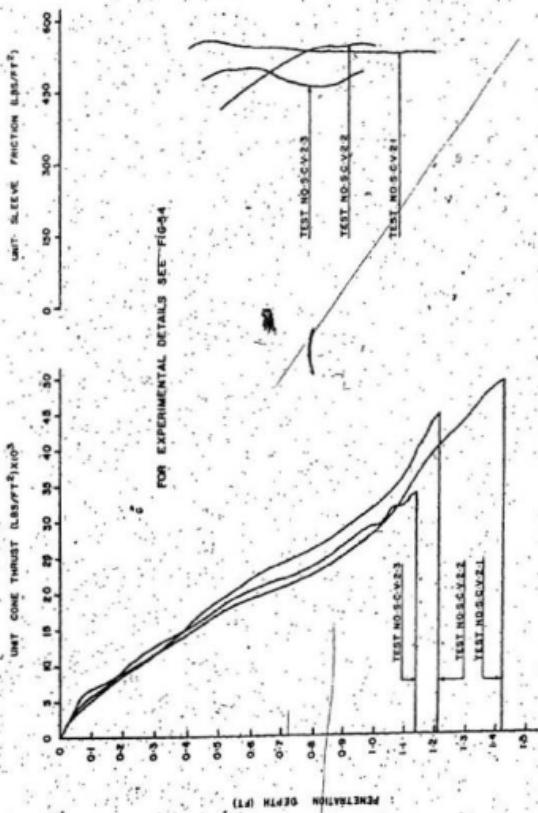
FIG 56 PLOT OF PENETRATION DEPTH V9 UNIT CONE THRUST AND UNIT SLEEVE FRICTION

records reveal that for test series No. S.C.V.1 (clay 50% and sand 50%) the profiles are of a similar shape to that of the clay target and for test series No. S.C.V.2 (clay 8% and sand 92%) the profiles are similar to that of the sand target. Similarly, the ratio of cone thrust to sleeve friction for test series No. S.C.V.1 is approximately four times higher than that of test series No. S.C.V.2. This is because the target S.C.V.1 has a higher percentage of fine soils than target S.C.V.2 and consequently it has a higher cohesion component. This aspect will further be discussed in sub section 5.6 of this chapter.

The unit cone thrust profile obtained by impact penetration tests at three different impact velocities are shown in Fig. 53 for tests S.C.V.1.1., S.C.V.1.2., and S.C.V.1.3. For test No. S.C.V.1.1. the calculated 'static' cone pressure profile from impact penetration test is shown in Fig. 53 together with the cone pressure profile obtained directly from the constant velocity penetration test performed at penetration velocity of 0.0044 ft./sec. The 'static' cone pressure profile is calculated for the penetration velocity of 0.0044 ft./sec from the relationship:

$$\frac{q_{cd} - q_c}{q_c} = 0.143 \, \log_{10} \frac{V}{V_s} , \quad \text{established from constant velocity}$$

penetration tests. Similarly, the 'static' sleeve friction profiles can also be obtained. It is seen that estimated 'static' cone pressure profile from impact test is in agreement with those obtained directly from the constant velocity penetration test. This again shows, that if dynamic effects are known, a very accurate estimation of the cone pressure and sleeve friction for 'static' condition can be made from the proposed

impact penetrometer for sand-clay mixtures also.

Evaluation of Theoretical Model

In the earlier part of this chapter the validity of the proposed theoretical model was evaluated for cohesive and granular target materials. In this sub-section the evaluation of the theoretical model was made on sand-clay mixtures simulating as $c - \phi$ soils. The characteristic shear strength properties of these targets were determined by direct shear test preparing the sample at same moisture content and density. The direct shear test results are shown in Fig. 48.

The theoretical velocity profiles and maximum penetration depth were calculated from general Eqns. 11 or 14. First the theoretical calculations were tried by selecting Meyerhof's bearing capacity factors for deep foundation conditions which gave results approximately 40 percent lower than the test results. This was because the theoretical estimation of cone resistance was very high compared to experimentally obtained cone resistance. Then the calculations were made with bearing capacity factors for shallow foundation condition which gave results 50 to 60 percent higher than experimental results because this provided a lower estimation of cone resistance.

In the process of those calculations it was noted that the value of N_c predominately affected the theoretical results. As explained earlier in sub-section 5.3 the proper selection of bearing capacity factors depends on penetration depth which in impact penetration problem changes from shallow to deep conditions. However, in

previous cases (Series I and II) Nc_r was either not very effective or absent.

Finally, in Series III Nc_r was selected by taking the mean of shallow and deep values for semi-rough conditions. The following are the different bearing capacity factors used in theoretical calculation:

For test series S.C.V.1. (ϕ = 15°)

$$Nc_{r\,(mean)} = 30$$

$$Nq_r = 9$$

$$N\gamma_r = 0.6 \times 6 = 3.6$$

For test series S.C.V.2. (ϕ = 30°)

$$Nc_{r\,(mean)} = 170$$

$$Nq_r = 60$$

$$N\gamma_r = 0.6 \times 150 = 90$$

The computed velocity profiles are shown in Figs. 52 and 53 for test series Nos. S.C.V.1., and S.C.V.2, respectively. The different coefficients used in computation and test details are shown in Table 6. It is seen that the theoretical velocity profiles follow the same shape as those obtained experimentally but are not in very good agreement as in the previous two series. The theoretical and experimental penetration depths are shown in Table 6. The error involved in the theoretical estimation ranges from 7.5 percent to 20 percent.

TABLE 6

DEPTH PREDICTION FOR SAND-CLAY MIXTURES

60° Cone Penetrometer of 1.405 in. diameter

Test No.	Wt. of Penetrometer (lbs.)	Impact Velocity V_o (ft./sec.)	C (lbs./ft.²)	ϕ (degree)	K_L	α	β	γ	M	A	Actual Penetration depth (ft.)	Theoretical penetration depth (ft.)	% Variation
1	2	3	4	5	6	7	8	9	10	11	12	13	14
SCV.1.1	56.64	20.04	400	15	0.143	-73.2	165.1	2.94	1.78	0.0458	1.34	1.236	12.9
SCV.1.2	56.64	18.26	400	15	0.143	-73.2	165.1	2.94	1.78	0.0458	1.21	1.098	9.2
SCV.1.3	56.64	15.84	400	15	0.143	-73.2	165.1	2.94	1.78	0.0458	1.058	0.92	7.5
SCV.2.1	56.64	19.99	150	30	0	-224.5	101.3	6.1	1.78	0.043	1.418	1.23	13.2
SCV.2.2	56.64	18.22	150	30	0	-224.5	101.3	6.1	1.78	0.043	1.21	1.067	12
SCV.2.3	56.64	16.67	150	30	0	-224.5	101.3	6.1	1.78	0.043	1.135	0.902	20.6

165

5.6 Friction Ratio

In the preceding discussions it is seen that the proposed instrument can be used to obtain directly the 'dynamic' strength properties of the target and upon applying the correction for viscous effects the 'static' strength can also be estimated. In addition, the measured cone resistance and sleeve friction during the impact test can be used for an approximate identification of target materials, on the line similar to the friction ratio concept developed for static cone penetration tests. The friction ratio for 'static' case has been defined by Schmertmann (1969) as the dimensionless ratio of unit friction/adhesion along the smooth steel friction jacket to unit bearing capacity of the standard cone point and a definite relationship has been shown (Begemann, 1965) to exist between cone resistance, local side friction and soil type. Mathematically friction ratio (F.R.) for static case is defined as:

$$F.R. = \frac{K_F \ (C + K_0 \rho g Z \tan \phi)}{C \ Nc_r + K_0 \ \rho g Z \ Nq_r + \rho g R N \gamma_r} \tag{22}$$

where K_F is adhesion factor and other terms are defined previously.

The relationship 22 indicates that the friction ratio is inversely proportional to ϕ angle and maximum at $\phi = 0$; equals to:

$$F.R.(static) = \frac{K_F \ C}{C \ Nc_r + K_0 \ \rho g Z \ Nq_r} \tag{23}$$

As the effects of the penetration rate on the friction angle are insignificant for the low velocity range, the friction ratio obtained for granular soils by the impact penetration test should be of the same order as that obtained from the static penetration test.

In the case of cohesive soils, the penetration rate effect gives the following expression for friction ratio under the assumption that soil viscosity coefficient (K_L) is the same for cone and friction sleeve resistances.

$$F.R. (dynamic) = \frac{C \, K_F \, (1 + K_L \, \log_{10} \frac{V}{V_s})}{C \, N_{c_r} \, (1 + K_L \, \log_{10} \frac{V}{V_s}) + K_o \rho g Z \, N q_r} \quad (24)$$

For the laboratory and many field situations(penetration of less than 15 ft.) $K_o \rho g Z \, N q_r$ can be ignored, allowing the expression to be simplified to:

$$F.R. (dynamic) = \frac{K_F}{Nc_r} = F.R. (static)$$

K_F is generally assumed equal to one for static penetration tests (penetration velocity 1.5 cm./sec. to 2 cm./sec.). However, in present investigation it is seen that even for any particular material, neither K_F nor Nc_r is strictly constant. For example, at a penetration rate of 0.0044 ft./sec, Nc_r ($= \frac{q_c}{C}$) varies from 10.5 to 11.7 and K_F ($= \frac{F_c}{C}$) varies from 0.51 to 0.9 for different strength clay targets. As such the friction ratio concept could provide only an approximate estimation to the soil type even in static penetration tests. Furthermore, in 'dynamic' case it has been seen in sub-section 5.3 that the sleeve friction increases gently up to approximately 1 ft./sec. penetration velocity and beyond this velocity a sudden increase in sleeve friction is observed. The slope of these lines are steeper than those obtained from cone resistance relationships. This tendency of sleeve friction suggests that the increase in penetration velocity will cause increase in friction ratio with a

sudden jump at approximately 1 ft./sec. penetration velocity. Table 7 shows the friction ratios at different penetration velocities for different strength clay targets which for most of the tests confirm the above tendency. Similar behaviour is observed for test series, S.C.C.1. (sand 50%, clay 50%). In the case of granular soils, as seen in Table 7, the variation in friction ratio with either penetration velocity or target strength is not very significant. With some simplifying assumptions one can arrive at a range of friction ratio reported herein by using Eqn. 22 or any of the classical bearing capacity theories. These ratios are well within the range suggested by Begemann (1965) and Schmertmann (1969).

Table 8 shows the average friction ratios obtained from impact penetration tests for different target materials which, besides having their own inherent limitations, can be used for an approximate estimation of soil types of the target from impact penetration tests. For cohesive soils, these ratios are generally higher than those obtained from 'static' tests for the reasons discussed above. If a correction to this effect is made, then those friction ratios would fall well within the range of 'static' penetration values. Thus, from friction ratio values also it can be presumed, as a first approximation, that the failure modes during impact penetration are basically of a static nature.

TABLE 7

'STATIC' FRICTION RATIO

Test No.	Soil Type	Friction Ratio (%) Penetration Velocity (Ft./sec.)			
		0.0004	0.042	0.456	2.662
C.C.1.	Clay	6.4	4	4.4	4.2
C.C.2.	Clay	5.4	6	6.3	9.7
C.C.3.	Clay	5.5	5.7	5.8	8.1
C.C.4.	Clay	5.7	6.7	7	10
S.C.C.1	Sand 50% and Clay 50%	4.8	4.8	4.62	5.38
S.C.C.2	Sand 92% and Clay 8%	1.8	—	—	1.72
S.C.1	Densest Sand	(Mean)	1.8		
S.C.2	Loosest Sand	(Mean)	2		
S.G.C.1	Sandy Gravel	(Mean)	0.8		

TABLE 8

'DYNAMIC' FRICTION RATIO

Soil Type	Average Friction Ratio, (%)
Mud (Marine clay)	10
Moist Clay (Series 1)	7.5 to 9
Dry Clay Powder	5
Sand 50%, Clay 50% (Series IIIA)	5.7
Sand 92%, Clay 8% (Series IIIB)	2
Medium to Fine Sand (Series II)	1.78
Gravelly Sand	1.5
Sandy Gravel	0.9

5.7 Layered System

McNeill (1972) in his paper entitled "Rapid Penetration of
Terrestrial Materials--The-State-of-the-Art", emphasized that "at the
present time the analysis of a layered system is not understood. . . ."
In this investigation, tests have been performed on laboratory pre-
pared layered targets. The instrument is equally sensitive for layered
system and two typical examples have been given in Figs. 57 and 58.
The test results shown in Fig. 57 are for a target having 10.5 in.
thick clay powder overlying gravelly sand, whereas, for results shown
in Fig. 58 are for an 8 in. soft clay layer overlying a medium stiff
clay layer. The sudden change in deceleration, cone thrust, and sleeve
friction records in both figures clearly demonstrate the presence of
layered soils. Analysis of the data gave the following results.

(a) From Fig. 57

(1) Depth of top layer = 10.7 in.

(2) Average unit cone thrust for top layer = 5,194 lbs./ft.^{2}

(3) Average unit sleeve friction for top layer = 224 lbs./ft.^{2}

(4) Average unit cone thrust for bottom layer = 28,000 lbs./ft.^{2}

(5) Average unit sleeve friction for bottom layer = 401 lbs./ft.^{2}

The friction ratio for the top layer equals 4.66%; friction ratio
for the bottom layer equals 1.43%.

Also, from Table 8, the soil type gives estimated friction ratio
for the top and bottom layers as 5 and 1.5, respectively.

(b) From Fig. 58

(1) Depth of top layer 8.3 in.

(2) Average unit cone thrust for top layer = 5230 lbs./ft.^{2}

FIG. 57. IMPACT PENETRATION TEST RESULTS FOR LAYERED SYSTEM

60° CONE, 1.405" DIA PENETROMETER
WT OF PENETROMETER = 53.21 LBS
IMPACT VELOCITY = 17.92 FT/SEC
TARGET: LAYERED SYSTEM
2.5" THICK SURFACE LAYER
OVERLYING COMPACTED GRAVELLY SAND

UNIT SLEEVE FRICTION (LBS/FT²)

0   200   400   600   800   1000   1200   1400   1600   1800   2000

PENETRATION VELOCITY (FT/SEC)

0   2   4   6   8   10   12   14   16   18   20

UNIT CONE THRUST (LBS/FT²)×10²

0   2   4   6   8   10   12   14   16   18   20   22   24

ACCELERATION (FT/SEC²)

+50 +25   0   -25   -50   -75   -100 -125 -150 -175 -200 -225 -250 -275 -300 -325

VELOCITY PROFILE

UNIT CONE THRUST

UNIT SLEEVE FRICTION

DECELERATION

PENETRATION DEPTH (FT)

60° CONE, 1.405"DIA PENETROMETER
WEIGHT OF PENETROMETER=56.64 LBS
IMPACT VELOCITY=18.77FT/SEC
TARGET: LAYERED SYSTEM
TOP LAYER: SOFT CLAY
γ_t = 92.2 LBS/CU FT
W = 35.4%
τ = 198 LBS/FT²
BOTTOM LAYER: CLAY
γ_t = 89.5 LBS/CU FT
W = 23%
τ = 1354 LBS/FT²

FIG-88 IMPACT PENETRATION TEST RESULTS FOR LAYERED SYSTEM

(3) Average unit sleeve friction for top layer - 425 lbs./ft.²

(4) Average unit cone thrust for bottom layer - 23700 lbs./ft.²

(5) Average unit sleeve friction for bottom layer - 1800 lbs./ft.²

The friction ratio for top layer equals 8.12%; friction ratio for the bottom layer equals 7.59%; indicating similar materials in both layers.

From Table 8 also materials of both layers are classified as clay soils.

The vane shear strengths for top and bottom layers are 198 lbs./ft.² and 1354 lbs./ft.² respectively, providing an average vane shear strength ratio of 6.8 in the bottom and top layers.

The average 'dynamic' strength ratio calculated from cone thrust records is 4.53. This is less than the 'static' strength ratio because (1) the top layer being a softer than bottom layer is more sensitive to dynamic effects, (2) the penetrating velocity for the top layer is also higher than the bottom layer.

From 'dynamic' cone thrust profiles the 'static' cone resistance profiles are calculated from Eqn. 18 taking the soil viscosity coefficients from Table 1. The calculated average 'static' cone resistances are 2740 lbs./ft.² and 16784 lbs./ft.² respectively; thus providing the average 'static' strength ratio equals 6.12, which is close to the vane shear strength ratio.

CHAPTER VI

FIELD TESTS

The ultimate aim of present work is to develop the capability of the proposed instrument to measure the *in situ* strength properties of 10 to 50 ft. of marine sediment. With this aim, laboratory tests were conducted under fully controlled conditions to study the response of instrument for different test conditions and to understand the penetration mechanism whereby the interpretation of the results could be made from impact penetration tests. Based on the model penetrometer used in the laboratory, the marine impact cone penetrometer was designed and developed for field use and some preliminary tests were conducted on terrestrial soils.

6.1 Marine Impact Penetrometer

Figure 59(d) shows the cross-sectional view of the marine impact penetrometer which, at present, has been developed for 10 to 15 ft. penetration. The penetrometer selected for field tests is again a 1.405 in. diameter cone tipped right circular cylinder and equipped to record acceleration/deceleration, cone thrust, and sleeve friction simultaneously and continuously up to penetrated depth. The feasibility analysis made for the field penetrometer suggests that its three transducers should be of the same rated capacities as those used for the laboratory penetrometer.

It has been proposed to attach the complete instrumentation package including the recorder to the penetrometer to avoid underwater cable problems such as drag, underwater connections, wear and tear, etc.

WIRE TO SHIP

CAST BRONZE WIRE CLAMP

SAFETY PIN

PRESSURE POWERED PIN
(ARMS TRIGGER AT PRESET
DEPTH - OPTIONAL)

TRIGGER RELEASE MECHANISM

TO PILOT WEIGHT

WIRE LENGTH FOR FREE FALL

STABILIZER & ACCELEROMETER
AND RECORDING CASE

EIGHT LEAD-CABLE CONNECTED TO
RECORDER

LEAD WEIGHTS 45 LBS. EACH.
(FOUR STANDARD, UP TO SIX
MAY BE USED)

STEEL COUPLING
(& QUICK MECHANISM FOR CHANGING
CORER & PENETROMETER)

ANNULAR PIPE FOR CABLE CONNECTIONS

PENETRATION ROD (36 M.M. O.D AND 12'
M.M. I.D. FIRST STAGE = 15 FT LENGTH)

STRAIN GAGES
LOAD CELL
FRICTION SLEEVE (150 CM²)
60° CONE WITH 10 SO. CM. BASE

(NOT TO SCALE)

LOWERING   RELEASE   PENETRATION

RELEASE
MECHANISM

WEIGHT
STAND

TRIGGER
LINE

TRIGGER
WEIGHT
(OPEN
BARREL
CORER)

TRIGGERING SYSTEM

*(a)   (b)   (c)   (d)

FIG 59 MARINE IMPACT PENETROMETER

For these reasons a mini-recorder (presently in the assembly stage) of constant band width type has been designed which basically includes signal conditioners, voltage controlled oscillators, mixer amplifiers, and a magnetic tape recorder. The completed assembly, interconnected with transducers and battery to provide power both to recorder and transducers, would finally be housed in a pressurized casing to withstand water pressure and high impact force. This recorder would provide three channel operations with the frequency response of DC-200Hz, accuracy of better than 5 percent, and resolution of 2 μ V at least for two channels and 200 μ V for the remaining channel.

The dropping mechanism of the instrument is similar to that used in the triggered corer for collecting cores. Figure 59 (a, b and c) show the conceptual views of penetrometer and its associated rigging i.e., lowering, release, and penetration. Figure 59(a) shows the position of penetrometer just as it would look a few seconds before it reached the ocean floor. At the very top is the wire which is being paid out from a winch aboard the ship, and connected to the wire is release mechanism which is designed to allow the penetrometer to fall freely for a short distance before it strikes the ocean bottom. The release mechanism is clamped to the winch wire with several tens of feet above the end of the wire. It contains a lever arrangement in which the weight on the trigger line attached to the long arm of the lever counterbalances the weight of the penetrometer on the short arm of the lever. The part of the winch wire below the release mechanism hangs in the loop (shown on the right side of this diagram) and is

attached to the penetrometer.

The trigger weight which hangs down below the penetrometer can be either a small, open barrel corer or simply a dead weight. When the trigger weight hits the bottom, its weight is taken by the soil decreasing the force on the long arm of the lever. As the force on the long arm diminishes, the weight of the penetrometer on the short arm of the lever is no longer supported and the lever rotates, as is shown in Fig. 59(b). When the lever rotates far enough, the penetrometer slips off the short arm of the lever and falls freely towards the bottom of the ocean. After falling from the short arm of the lever the penetrometer is directly connected to the ship by the loop wire. The penetrometer will continue to penetrate the sediment until it is brought to a stop by the soil forces on the penetrometer and, perhaps, by wire forces also when the weight barrel hits the bottom. Figure 59(c) shows the position of penetrometer just before it is pulled out from the ocean bottom. From this system, depending upon the requirements, the pre-selected impact velocity (maximum up to terminal velocity) can be achieved by adjusting the trigger line.

6.2 Preliminary Tests

Originally it was planned to perform *in situ* strength tests of marine sediments in shallow water using the proposed instrument with the existing recording system. To locate a suitable test site several attempts were made with "Benthos" corer and grab sampler in and around the St. John's coast with no positive results. As reported in the navigational chart of this area, most of the ocean bottom is either rocky or covered with 1 to 2 ft. thick sand and pebbles overlying the

flat rock bottom. Few pockets of soft sediment bottom were located during the 'Dawson Cruise' (Allen 1971, 1972) but they were too far off the coast and in deep water, requiring special arrangements of ship timing. As such it was decided to perform the test on land but because of non availability of a suitable site at a feasible location a huge cylindrical target tank was erected.

The target tank is approximately 6 ft. high and 5 ft. in diameter. On the bottom of the tank, first two layers of 6 in. thick plastic foam followed by two layers of 3 in. thick plywood was provided to prevent the tip of penetrometer from hitting the metallic base of the tank. The tank was filled with locally available soil used by brick manufacturers consisting of fine sand and clay with a small fraction of gravel. In preparation of this target no special precautions were taken for its uniformity.

To check the performance of the dropping mechanism, the lever arrangement was hung from a 'Pitman' crane which was lowered slowly so that as soon as the trigger weight hit the ground the penetrometer was automatically released. A high speed movie was also taken to study the complete performance of the event and to check the stability of the penetrometer during free fall and penetration. The test arrangements are shown in different photographs in Fig. 60. The recording system for this test was the same as those used for laboratory tests.

Typical test results obtained from this test at impact velocity of 27.7 ft./sec. are shown in Fig. 61. The impact velocity was calculated from accelerometer records and was also verified by calculating the impact velocity for a free fall height of 12 ft. obtained from

FIELD PENETROMETER   LOWERING   AFTER PENETRATION

FIG 60 PHOTOGRAPHIC VIEWS OF FIELD TEST

FIG. 61 FIELD IMPACT PENETRATION TEST RESULTS

60° CONE, 1.405" DIA PENETROMETER
WT OF PENETROMETER = 260 LBS
IMPACT VELOCITY = 27.7 FT/SEC
DROP HT = 11.97 FT (FROM ACCELEROMETER)
DROP HT FROM TRIGGER LENGTH = 12 FT
SOIL PROPERTY CHANGES
AT 0.5 FT, γ = 206 LBS/FT³
AT 1.25 FT, γ = 590 LBS/FT³
AT 1.5 FT, γ = 370 LBS/FT³

VELOCITY PROFILE

UNIT SLEEVE FRICTION

UNIT CONE THRUST

DECELERATION

HIT FOAM

HIT PLYWOOD

181
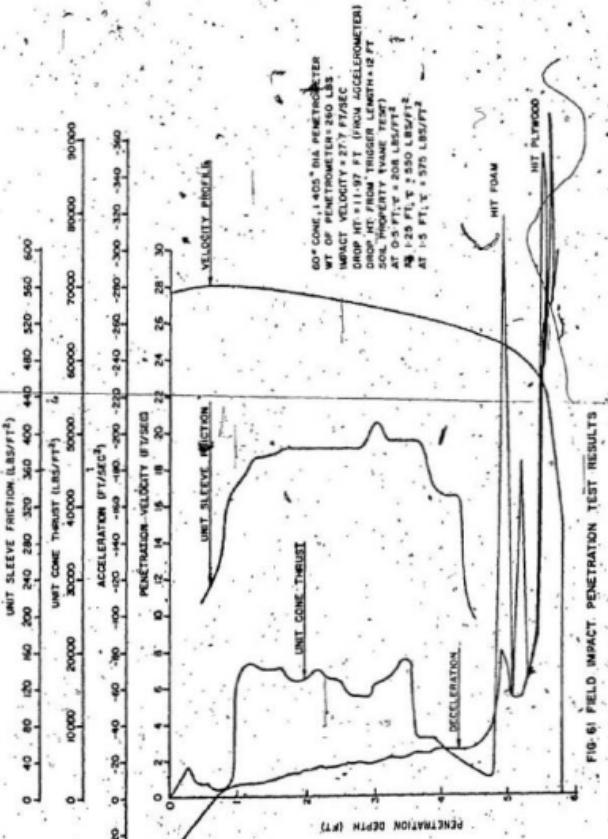
trigger line-length. In underwater use, the impact velocity can be estimated either by accelerometer records or from free fall height for a known hydrodynamical parameters of the penetrometer (Dayal et al., 1973). From these results it is seen that even after penetrating approximately 5 ft. depth the penetrometer is travelling with a velocity of 25 ft./sec. (98 percent of impact velocity) and deceleration of less than one g. It is finally stopped from the high resistive force offered by the hard base at the bottom.

The cone resistance of the top 1 ft. depth is much less than that below this depth and then approximately an uniform resistance is recorded up to 3.5 ft. Beyond 3.5 ft. depth the resistance continuously decreases up to 4.75 ft. depth due to accumulation of the excessive rain water in the bottom of the tank. The final peak of the cone and accelerometer records at approximately 5 ft. depth indicates the presence of a very hard layer (plastic foam and plywood). The sleeve friction profile also shows approximately the same trend. The average friction ratio obtained from this target material is 2.36. The in situ vane shear tests were performed for this target up to a depth of 1.5 ft. and the following results were obtained: at 0.5 ft. depth, τ equals 208 lbs./ft.^{2}; at 1 ft. depth, τ equals 550 lbs./ft.^{2}; at 1.5 ft. depth, τ equals 576 lbs./ft.^{2}.

6.3 Design of Impact Penetrometer for Greater Depth Exploration.

Many of the applications of soil mechanics in marine work require the knowledge of the ocean floor strength from 30 - 50 ft. depth. In this sub section the possibility of using instrumented impact

penetrometer for obtaining the strength profiles up to this depth has been studied. Bryant et al. (1969) and Thigpen (1971) have reported a penetrometer developed by Sandia laboratory for marine use. The penetrometer approximately 5 ft. long and about 3.4 in. diameter, houses an accelerometer and weights 100 lbs. This penetrometer is dropped approximately 6 ft. above the water surface and is not recoverable. The preliminary data indicate that the maximum penetration of 16.4 ft. was achieved in the soft sediment. Korites (1967) and Noorany (1971) have reported the development of a 100 ft. long 4.5 in. diameter piston sampler at Woods Hole Oceanographic Institution which weighs 15 tons. This corer penetrated up to 94 ft. at estimated impact velocity of about 58 ft./sec. and recovered 75 ft. long silty clay core. These samples are indicative of the possible use of the impact cone penetrometer for obtaining in situ strength profiles up to depth of 50 ft. or so.

As can be seen the proposed theoretical model has provided an agreement with experimental results conducted in the laboratory under fully controlled conditions. This model can be used for designing the penetrometer for greater depth exploration work. In general, the design of the impact penetrometer is based on a number of variables for example, impact velocity, weight, diameter, and overall shape of penetrometer, dynamic strength of target, target material and its unit weight, and maximum penetration depth requirements. In addition, the stability of the penetrometer during free fall, and structural and mechanical requirements such as the buckling load on the penetrometer shaft and strength requirements of different components during impact

loading are to be considered in the final design of the penetrometer.
The complete design and development of a greater depth exploratory
penetrometer is itself an independent project requiring the optimization
of the whole system.

The basic data required in the design of complete system are
weight, diameter, and length of the penetrometer. The necessary weight
of the penetrometer has been calculated for different diameter penetro-
meters ranging from 1.5 in. to 4 in. diameter and for maximum pene-
tration depths of 30 ft., 40 ft., and 50 ft., assuming the following
values of different variables. The values of different variables have
been selected from the data available in literature for normal conditions
and from present experience.

Assumed Data

    Soil type: fine soil, cohesive.

    Shear strength (τ) = 400 lbs./ft.^{2}

    Impact velocity (V_o) = 35 ft./sec.

    Soil viscosity coefficient (K) = 20.

    Bulk Unit weight (γ_t) = 100 lbs./cu.ft.

    Nc_r (local condition) = 6

    Nq_r = 1

    Coefficient of earth pressure at rest (K_o) = 1

    $N\gamma_r$ and ϕ = 0 .

The required weight of the penetrometer for different diameters and
penetration depths is calculated from Eqn. (16) by the trial and error
method. The results are shown in graphical form in Fig. 62. As an
example, the design weight of 4 in. diameter penetrometer is 10 tons
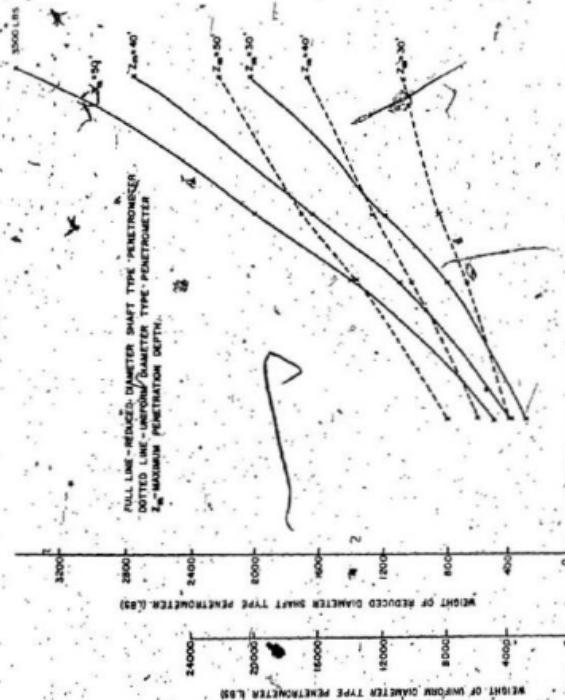
FIG 62. DESIGN WEIGHT OF PENETROMETER FOR DIFFERENT DIAMETER DIFFERENT PENETRATION DEPTH

for maximum penetration depth of 50 ft. which compares favourably with
Woods Hole Oceanographic Institution's piston corer results.

Marine sediments generally consist of fine soils in which the
major part of resistance to the penetrometer is offered from adhesion/
friction on the shaft. If this resistance can be eliminated or
minimized then a considerable reduction in the penetrometer weight
can be made for the same diameter and penetration depth conditions.
For example, by making the diameter of the shaft ½ in. less than the
cone head diameter an all-round clearance of 1/8 in. between the surface
of the shaft and cavity wall could be had; thereby eliminating most
of the resistances offered to the penetrometer shaft. The calculations
to this effect have also been made and the results are shown in Fig. 62.
In those calculations a safety factor of two has been applied to take
into account the bulging and collapsing effects, which may cause some
resistance on the shaft. A comparison of those results indicate that
the reduced diameter shaft type penetrometers require only approximately
16 percent weight of those required for uniform diameter type penetro-
meters. However, before going finally for reduced diameter shaft type
penetrometer for greater depth marine exploration work, some experi-
mental studies should be made in the laboratory under fully controlled
conditions to study the response of this type of penetrometer to
different test conditions, and to observe its stability during the
penetration event.

The available results in Fig. 62 provide a tentative guide line
for optimizing the diameter of the field penetrometer for weight,
penetration depth, and buckling load requirements. Once this is done
other components can conveniently be designed.

CHAPTER VII

CONCLUSIONS AND RECOMMENDATIONS

7.1 Summary and Conclusions

The fundamental objectives of this study were (1) to develop a new instrumentation technique whereby the concept of an impact/projectile penetration test for measuring *in situ* strength properties of marine sediment can be achieved, and (2) to understand the impact penetration mechanism in order to develop a theoretical model applicable to low velocity impact penetration problems. The developed penetrometer has been instrumented with accelerometer, cone thrust, and sleeve friction measuring devices. The experimental results obtained with it demonstrate the achievement of these objectives.

The impact penetration tests performed under fully controlled conditions with this penetrometer in conjunction with constant velocity penetration tests, have provided a rational approach to understanding many of the impact penetration phenomena which in previous investigations were not clear and also were lacking in qualitative and quantitative explanations.

The following conclusions are drawn from the present investigation and are pertinent only to the range of variables investigated in this study.

1. The theoretical model has been generated from momentum considerations by taking into account the various factors influencing the penetration mechanism and adopting Meyerhof's 'static' failure criterion modified for 'dynamic' conditions.

The resulting equation provides a relationship between instantaneous penetration velocity, various static and dynamic soil properties, penetrometer characteristics, and instantaneous depth of penetration. The developed theoretical model is in agreement with the experimental results. This relationship can also be used for estimating the soil properties although only under ideal conditions.

2. The constant velocity penetration tests performed at different velocities reveal that for granular soils, the effects of penetration velocity on the cone and sleeve friction resistances are insignificant. For cohesive soils, the increase in penetration velocity causes an increase in the cone and friction resistances and the ratio of 'dynamic' to 'static' strength can be represented by logarithm of velocity ratio. The constant of this empirical relationship is defined as the soil viscosity coefficient. Furthermore, the ratio of 'dynamic' to 'static' strength is a function of soil strength and consequently the soil viscosity coefficient is also a function of soil strength. The soil viscosity coefficients for tested soils have been established from experimental results for different strength ranges.

3. The resistance on a penetrating penetrometer can be considered in two parts, resistance on the nose and resistance along the side. For granular soils those resistances increase with depth, whereas, for cohesive soils those resistances are more or less constant with depth (beyond the depth of 2D) but increase with

velocity. The total resistance can be considered as having a 'static' component and a 'dynamic' component. The 'static' component consists of resistance on the nose and side resistance developed during 'static' loading. The 'dynamic' component consists of strength mainly due to material strain/penetration rate effects.

4. The two dimensional tests and the friction ratio values obtained from impact penetration tests indicate that failure modes during impact penetration are basically of a static nature.

5. The friction sleeve records indicate the presence of adhesion/friction along the sides of the penetrometer. This clearly demonstrates that cavitation does not occur for the velocity range used in the present investigation, and the side wall resistance is a significant portion of the total resistance in both cohesive and granular soils. Furthermore, the friction ratio concept, developed from static cone penetration tests for assessing soil types, can be extended, albeit with its inherent limitations, to impact penetration tests also. However, for cohesive soils, these ratios are generally higher than those obtained for 'static' conditions because the 'dynamic' to 'static' ratios for friction sleeve resistance are higher than those for the cone at the same penetration velocity.

6. The response of the penetrometer can be related directly to the strength governing parameters of target materials. In cohesive soils, the measured 'dynamic' strength response can be related directly to 'static' strength profiles by applying the

corrections for strain/penetration rate sensitivity.

7. Like the static penetrometer, the proposed impact penetrometer is shown to be sensitive in estimating the depth, strength, and soil type of different layers.

8. The soil resistance offered to different nose shapes during impact penetration are in qualitative agreement with the theoretical values given by Meyerhof (1961) for 'static' conditions.

7:2 Recommendations

In addition to the direct results and conclusions of this study, several interesting new ideas were formulated through the course of this investigation. Such ideas deserve future development and may become the focus of extensive research. Therefore, the following recommendations with regard to future experimental/theoretical studies are suggested.

(a) Experimental Studies

(1) Extensive experiments should be conducted with different sized penetrometers on various types of soils and with different strength characteristics in order to generalise the value of soil viscosity coefficients for cohesive soils of different strength ranges. This would be useful in obtaining the 'static' strength profile directly from impact penetration tests.

(2) The present investigation was limited to low velocity impact penetration tests in which it has been demonstrated that cavitation does not occur. However, the tests should be re-peated at higher impact velocities in order to establish the

limiting velocity upon which cavitation does occur. This
would be useful for future development of the field instrument
and also provide the limiting velocity condition for the
validity of the proposed theoretical model.

(3) At the outset of this study the feasibility analysis for
developing an impact penetrometer for greater depth exploration
has been made. The preliminary calculations show that the
reduced diameter shaft type penetrometer requires only
approximately 16 percent weight of that required for a uniform
diameter type penetrometer. However, before going finally for
a reduced diameter shaft type penetrometer for greater depth
exploration work, some experimental studies should be made in
the laboratory under fully controlled conditions in order to
study the response of this type of penetrometer to different
test conditions, and to observe its stability during impact
penetration.

(4) It has been demonstrated in the present investigation that in
extremely soft cohesive targets ($\tau = 65$ lbs./ft.^{2}) the increase
in 'dynamic' strength is as great as 5 to 6 times the 'static'
strength. No satisfactory explanation has been found for this
phenomenon and it would benefit from further systematic
investigations. This strength range is also reported occasionally
in the literature for the top 1 to 2 ft. depth of ocean floor
sediments. The knowledge of the 'dynamic' characteristics of
such sediment-strength would be useful in estimating the 'static'
properties from the impact penetration test.

(5) *In situ* testing of marine sediment should be conducted with the present instrument in order to observe its performance in underwater use. Furthermore, the knowledge gained from those tests would be useful in the design and development of an impact penetrometer for greater depth exploration work.

(b) Theoretical Studies

(1) In all the tests a 'dip' has been observed at the end of the penetration event. It appears that the 'dip' in the acceleration curve is caused by the energy stored in the soil during the penetration process and that the 'dip' indicates an acceleration in the downward direction, i.e., a force applied to the penetrometer by the soil, which tends to pull the penetrometer downward. This is confirmed from the sleeve friction records which show considerable negative friction at the end of penetration event. This effect is attributed to the results of elastic rebound. A systematic study of this phenomenon may provide some fundamental soil properties such as quasi-static modulus of elasticity and shear modulus.

(2) A blunt nosed projectile/penetrometer is known to experience a greater deceleration spike and force at impact than the projectile/penetrometer with a long, sharp pointed nose. This is attributed to the results of 'soil nose' formation in blunt nosed projectile. An attempt to study this effect may provide a theoretical explanation for the mechanism of the formation of the 'soil nose'.

BIBLIOGRAPHY

Allen, J. H. 1971. Cruise report--C.S.S. Dawson. Memorial University of Newfoundland, St. John's, Newfoundland.

———— 1972. Iceberg Study, Saglek, Labrador including cruise report C.S.S. Dawson. Memorial University of Newfoundland, St. John's, Newfoundland.

Allen, W. A., Mayfield, E. B., and Morrison, H. L. 1957. Dynamics of a projectile penetrating sand. J. App. Phy., 28, No. 3, pp. 868-873.

Andersen, A., Sollie, S., and Richards, A. F. 1965. N.G.I. gas operated sea-floor sampler. Proc. Sixth Int. Conf. Soil Mech. Found. Eng., Montreal, 1, pp. 8-11.

Anon, 1966. Final report on research development and preliminary design for lunar penetrometer system applicable to Apollo program. Publ. No. U-3556 and U-3608, Auronutronic Div. Philco.

Awoshika, A., and Cox, W. R. 1968. An application of similitude to model design of soil projectile system. Univ. of Texas, Austin, Texas, NASA CR-1210.

Begemann, H. K. P. S. 1965. The friction jacket cone as an aid in determining the soil profile. Proc. Sixth Int. Conf. Soil Mech., Found. Eng., Montreal, 1, pp. 17-20.

Bellman, R. E. 1966. Perturbation methods in science and engineering. Holt, Rinehart and Winston, New York.

Bryant, W., Richards, A. F., and Keller, G. H. 1969. Shear strength of sediments measured in place near the Mississippi Delta compared to measurements obtained from cored material. 19th Annual Meeting Gulf Coast Assoc. Geol. Soc., pp. 267 (abstract only).

Calhoon, M. L. 1956. Effect of sample disturbances on the shear strength of clay. Trans. ASCE, 121, pp. 925-939.

Carden, H. D. 1967. Experimental study of the application of the penetrometer technique to the lunar surveying staff concept. Langley Research Center, Langley Station, Hampton, Virginia, NASA TND -3937.

Carnahan, B., Luther, H. A., and Wilkes, J. O. 1969. Applied numerical methods. John Wiley & Sons, Inc. New York.

Casagrande, A., and Shannon, W. L. 1949. Strength of soils under dynamic loads. Trans., ASCE, 114, pp. 755-772.

Casagrande, A., and Wilson, S. D. 1951. The effect of rate of loading on the strength of clays and shales at constant water content. Geotechnique, 2, pp. 251-263.

Caudle, W. N., Pope, A. V., McNeill, R. L., and Morgason, B. R. 1967. The feasibility of rapid soil investigation using high speed earth penetrating projectiles. Proc. Int. Symp. Wave Propag. Dyn. Prop. Earth Mater., ASCE, Albuquerque, N.M. pp. 945-955.

Chisholm, P. B., Peleze, R. M., and Pugh, F. L. 1962. An earth trajectory model for subsurface ballistic and thrusted vehicles. Air Force Special Weapons Center, Kirtland Airforce Base, Albuquerque, N.M. TDR AFSWC-TDR-62-106.

Chou, Y. T. 1972. Penetration in clay by the viscoplasticity method. Proc. Conf. on Rapid Penetration Terr. Mater., Texas A & M Univ., Texas, pp. 431-452.

Clark, L. V., and McCarty, J. L. 1963. The effect of vacuum on the penetration characteristics of projectile into fine particles. Langley Research Center, Langley Station, Hampton, Virginia, NASA TND-1519.

Colp, J. L. 1965. An experimental investigation of the continuous penetration of a blunt body into a simulated cohesionless soil. Sandia Corp., SC-RR-65-260. Albuquerque, N.M.

Cunny, R. W., and Sloan, R. C. 1962. Discussion on static and dynamic behaviour of small footing. J. Soil Mech. Found. Div., ASCE, 88, No. SM4, Part I, pp. 200-206.

Dayal, U., Gairola, S. S., and Raju, V. S. 1971. Coefficient of earth pressure at rest of granular soils. J. Indian Nat. Soc. Soil. Mech. and Found. Eng., 9, No. 4, pp. 371-386.

Dayal, U., Allen, J. H., and Jones, J. M. 1973. Marine impact cone penetrometer, Proc. Conf. Int. Ocean 73, Dusseldorf, West Germany, pp. 912-923.

Doyle, E. H., McClelland, B., and Ferguson, G. H. 1971. Wire line vane probe for deep penetration measurements of ocean sediment strength. Offshore Techno. Conf., 1, OTC 1327, pp. 21-27.

Dunlop, W. A. 1972. Influence of soil properties on penetration resistance. Proc. Conf. Rapid Penetration Terr. Mater., Texas A & M Univ., Texas. pp. 515-526.

Euler, L. 1745. Neue grundsaetye der artillerie. Euler's Opera Omina, 14, Series II. Teubner, Berlin (Reprinted in 1922).

Evans, I. 1950. The measurements of surface bearing capacity of soils in the study of earth crossing machinery. Geotechnique, 2. pp. 46-57.

Fenske, C. W. 1957. Deep vane tests in Gulf of Mexico. Symp. Vane Shear Testing of Soils, ASTM Spec. Publ. 193, pp. 16-25.

Goldsmith, W. 1960. Impact. Edward Arnold Publishers, London.

Grasshoff, H. 1953. Investigations of values of dynamic penetration resistance to model piles in sand and clay, obtained from tests. Third Int. Conf. Soil Mech. Found. Eng., Switzerland. pp. 47-50.

Hakala, W. W. 1965. Resistance of granular medium to normal impact of a rigid projectile. Ph.D. Thesis, Virginia Polytechnic Institute, Blacksburg, Va.

Hamilton, E. L. 1963. Sediment sound velocity measurements made in situ from Bathyscaph Trieste. J. Geophysical Research, 68, pp. 5991-98.

Hamilton, E. L. 1965. Sound speed and related physical properties of sediments from experimental Mohle (Guadalupe site). Geophysics, 30, pp. 257-661.

Hampton, D., and Yoder, E. J. 1958. The effect of rate of strain on soil strength. Proc. 44th Ann. Road School, Purdu Univ. Indiana. pp. 116-129.

Hanks, B. R., and McCarty, J. D. 1966. Investigation of the use of penetrometers to determine the capability of dust materials to support bearing load. Langley Research Center, Langley Station, Hampton, Virginia. NASA TND-3200.

Harrison, W., and Richardson, A. M. 1967. Plate load test on sandy marine sediments, Lower Chesapeak Bay. Marine Geotechnique, Ed. by A. F. Richards, Univ. of Illinois Press, pp. 274-290.

Hechtl, H. 1964. Impact tests on soils and their significance for trafficability. Ph.D. Thesis, Princeton Univ.

Hirst, T. J., Richards, A. F., and Inderbitzen, A. L. 1971. A static cone penetrometer for ocean sediments. Symp. Underwater Soil Sampling, Testing and Construction Control, ASTM Spec. Tech. Pub. 501. pp. 69-80.

Hvorslev, M. J. 1949. Subsurface exploration and sampling of soils. U.S. Army Eng., W. E. S., Vicksburg, Miss.

Inderbitzen, A. L., Simpson, F., and Gosa, J. 1971. Comparison of *in situ* and laboratory vane shear measurements. Marine Tech. Soc. J., 5, No. 4, pp. 22-34.

Iversen, H. W., and Balent, R. 1951. A correlating modulus for fluid resistance in accelerated motion. J. Applied Phys. 22, No. 3, pp. 324-328.

Jackson, J. G. Jr., and Hadala, P. F. 1964. Dynamic bearing capacity of soils, Report 3, the application of similitude of small-scale footing tests. U.S. Army Engr., W.E.S., Vicksburg, Miss. Tech. Report No. 3-599, Report 3.

Jacky, J. 1948. The coefficient of earth pressure at rest. J. Soc. Hungarian Architects and Eng., Budapest, pp. 355-358.

Jerbo, A. 1967. Geotechnical and strength aspects of Bothnian clay sediments. Marine Geotechnique. Ed. by A. F. Richards, University of Illinois Press.

Keller, G. H. 1965. Deep sea nuclear sediment density probe. Deep Sea Research, 12.

Korites, B. J. 1969. A numerical technique for estimating the response of a gravity corer penetrating a marine sediment. J. of Terramechanics, 6, No. 4, pp. 35-61.

Kretschmer, T. R., and Lee, H. J. 1969. *In situ* determination of sea floor bearing capacity. Proc. Conf. Civ. Eng. Oceans, II, ASCE, Miami Beach, Florida, pp. 679-702.

Ladanyi, B., and Eden, W. J. 1969. Use of deep penetration test in sensitive clays. Proc. Seventh Int. Conf. Soil Mech. Found. Eng., Mexico, 1, pp. 225-236.

Lai, J. Y., Richards, A. F., and Keller, G. H. 1968. In place measurements of excess pore pressure in Gulf of Mexico clay. (Abstract). Am. Geophy. Union Trans., 49, pp. 221.

Lang, H. A. 1956. Lunar Instrument Carrier-landing factors. Rand, R.M. - 1725, ASTIA Doc. No. AD-112403.

LeCrossette, D. H. 1965. The scientific experiments on surveyor. Instru. Soc. Am., 2, No. 3.

Lee, H. J. 1973. Engineering properties of some North Pacific and Bearing sea soils. Tech. Note N-1283, Naval Civil Eng. Lab., Port Heuneme, California.

Lewis, L., Nacci, V., and Gallagher, J. 1969. *In situ* investigation of ocean sediments. Proc. Conf. Civ. Eng. Ocean-II, ASCE, Miami Beach, Florida, pp. 641-653.

Maurer, W. C., and Rinehart, J. S. 1960. Impact crater formation in rock. J. Applied Phys. 31, No. 7, pp. 1247-1252.

McCarty, J. L., and Carden, H. D. 1962. Impact characteristics of various materials obtained by an accelerometer—time history technique applicable to evaluating remote targets. Langley Research Center, Langley Station, Hampton, V., NASA TND-3200.

_____ 1968. Response characteristics of impacting penetrometers appropriate to Lunar and Planetary mission. Langley Research Center, Langley Station, Hampton, Vi, NASA TND-4454.

McClelland, B. 1956. Engineering properties of soils on the continental shelf of the Gulf of Mexico. Proc. Eighth Texas Conf. Soil Mech. Found. Eng., Univ. of Texas.

McNary, J. F., and Frohlich, H. 1970. An in situ sediment vane shear testing device. Marine Geo., 8, No. 5, pp. 367-370.

McNeill, R. L. 1972. Rapid penetration of terrestrial materials—The state of the art. Proc. Conf. on Rapid Penetration Terr. Mater., Texas A & M Univ., Texas, pp. 11-126.

Meigh, A. C., and Skipp, B. O. 1960. Gamma-ray and Neutron methods of measuring soil density and moisture. Geotechnique, 10, pp. 110-126.

Menard, L. 1960. Mesures in situ des proprietes physiques des sols. Locole Nat. de Ponte et Chauss, de Paris, Men. et Doc., No. 14.

Meyerhof, G. G. 1951. The ultimate bearing capacity of foundations. Geotechnique, 2, No. 4, London, pp. 301-322.

_____ 1961. The ultimate bearing capacity of wedge shaped foundations. Proc. Fifth Int. Conf. Soil Mech. Found. Eng., Paris, 2, pp. 105-109.

Migliore, H. J., and Lee, H. J. 1971. Seafloor penetration tests: presentation and analysis of results. Technical Note N-1178, Naval Civil Eng. Research Lab., Port Hueneme, California.

Mitchell, J. K. 1964. Shearing resistance of soils as a rate process. J. Soil Mech. Found. Div., ASCE, 90, No. SM1, pp. 29-62.

Mitchell, J. K., Quigley, D. W., and Smith, S. S. 1969. Impact records as a source of lunar surface material property data. Final Report, 1, NASA contract NASR O5-003-189, Space Science Lab., Series 10, Issue 28.

Moore, H. J. 1967. The use of ejected blocks and secondary impact craters as penetrometer on the lunar surface. Appendix A of Preliminary Geological Evaluation and Apollo Landing Analysis of Area Photographed by Lunar Orbiter III—NASA Report.

Murff, J. D., and Coyle, H. M. 1972. A laboratory investigation of low velocity penetration. Proc. Conf. on Rapid Penetration Terr. Mater., Texas A & M Univ., College Station, Texas, pp. 319-359.

_____. 1973a. Low velocity penetration of Kaoline clay. J. Soil Mech. Found Div., ASCE, 99, No. SM5, 375-389.

_____. 1973b. Prediction method for projectile penetration. Tech. Note, J. Soil Mech. Found. Div., ASCE, 99, No. SM11, pp. 1033-1037.

Noorany, I. 1971. Underwater soil sampling and testing--A-state-of-the-art review. Symp. Underwater Soil Sampling, Testing, and Const. Control, ASTM, Spec. Tech. Pub. 501, pp. 3-41.

Noorany, I., and Seed, H. B. 1965. In situ strength of soft clay. J. Soil Mech. Found. Div., ASCE, 99, No. SM2, pp. 49-80.

Orzze, O., and Broms, B. 1970. Strength and deformation properties as determined by a free falling weight. Proc. Swed. Geotechnical Inst., No. 23.

Palmore, J. I. 1961. Lunar impact probe. ARS. J., pp. 1066-1073.

Peck, G. M. 1962. Bearing theories related to model tests on a remoulded clay. M. Eng. Thesis, McGill Univ., Montreal.

Poncelet, J. V. 1829. Course de mechanique industrielle. Paris.

Prandll, L. 1920. Über die Härte plastischer Körper. (On the hardness of plastic bodies). Nachr. Kgl. Ges. Wiss. Göttingen, Math-Phys. Kl.

Preiss, K. 1968. In situ measurements of marine sediment by Gamma-radiation. Deep Sea Research, 15, pp. 637-641.

Preslan, W. L. 1969. Accelerometer-monitored coring. Proc. Conf. Civ. Eng. Oceans-II, ASCE, Miami Beach, Florida, pp. 655-678.

Reeves, G. N. 1969. A finite element study of the penetration of a soil half-space by a rigid projectile. Ph.D. Thesis, Texas A & M Univ., College Station, Texas.

Resal, H. 1895. Sur la penetration d'un projectile dans les semi pluides et les solicles. Cr. 120, pp. 397-401.

Reichmuth, D. R. 1967. Soil projectile interaction during impact. Ph.D. Thesis, Univ. of Texas, Austin, Texas.

Richards, A. F. 1962. Investigation of deep sea sediment cores II: Mass physical properties. U.S. Navy Hydrographic Office Tech. Report 106.

Richards, A. F. 1964. Local sediment shear strength and water content variability on the continental slope off New England. Paper in Marine Geology Shepard Commemorative Volume, Ed. by R. L. Miller. The MacMillan Company, New York, pp. 479-487.

_____ 1967. Marine Geotechnique. Univ. of Illinois Press.

Richards, A. F., and Keller, G. H. 1961. A plastic barrel sediment corer. Deep Sea Research, 8, pp. 306-312.

Richards, A. F., and Parker, H. W. 1967. Surface coring for shear strength measurements. Proc. Conf. on Civil Eng. in the Oceans-I, ASCE, San Francisco, California, pp. 445-488.

Richards, A. F., McDonald, V. J., Olson, R. E., and Keller, G. H. 1971. In-place measurement of deep sea soil shear strength. Symp. Underwater Soil Sampling, Testing, and Const. Control, ASTM Special Pub. 501, pp. 55-68.

Rinehart, J. S. 1960. Stresses associated with lunar landings. Contribution No. 11, Mining Res. Lab., Colorado School of Mines.

Robertson, H. P. 1941. Terminal ballistics. Comm. Passive Protection Against Bombing. Natl. Res. Council, Washington, D.C.

Robins, B. 1742. New principles of gunnery, London Press, London.

Ruiter, J. D. 1971. Electric penetrometer for site investigations. J. Soil Mech. Found. Div., ASCE, 97, No. SM2, pp. 457-472.

Sandia Laboratory. 1968. Introduction to terradynamics. Sandia Lab. Rep. SC-M-68-239, Albuquerque, N.M.

Sanglerat, G. 1972. The penetrometer and soil exploration. Elsevier Publishing Company, Amsterdam.

Schmertmann, J. H. 1969. Dutch friction-cone penetrometer exploration of research area at field 5, Eglin AFB, Florida. Conducted for U.S. Army Eng. WES, Vicksburg, Miss., Contract No. DACA 39-69-C-0035.

Schimming, B. B., Haas, H. J., and Saxe, H. C. 1966. Study of dynamic and static failure envelopes. J. Soil Mech. Found. Div., ASCE, 92, No. SM2, pp. 105-124.

Schmid, W. E. 1972. The determination of soil properties in situ by an impact penetrometer. Princeton Soil Eng. Res. Series No. 3.

_____ 1969. Penetration of object into the ocean bottom. Civil Eng. in the Ocean-II, ASCE, Miami Beach, Florida, pp. 167-208.

Scott, R. F. 1962. Problem of the penetration of a projectile into soil, a soil like medium or compressible rock (pumice). Four unpublished Report, California Inst. of Tech., California.

_____ 1966. Self propelled soil penetrometer. Patent applied for California Inst. Res. Found., California.

_____ 1967A. In place soil mechanics measurement. Marine Geotechnique, Ed. by A. F. Richards, Univ. of Illinois Press. pp. 264-271.

_____ 1967B. In place measurement of the ocean floor soils by accelerometer. Proc. Conf. on Civil Eng. in the Oceans-1, ASCE, San Francisco, California, pp. 419-444.

Selig, E. T. 1961. A technique for observing structural soil interaction. Armour Res. Found. of Illinois Inst. of Tech.

Selig, E. T., and McKee, K. E. 1961. Static and dynamic behaviour of small footings. J. Soil Mech. Found. Div., ASCE, 87, No. SM6, pp. 29-47.

Shenkman, S., and McKee, K. E. 1961. Bearing capacities of dynamically loaded footings. Symp. on Soil Dynamics, 64th Annual Meeting of the ASTM, Special Tech. Pub. No. 305, pp. 78-90.

Shipley, E. N. 1967. Surveyor and LM Penetration in a model lunar soil. Bellcomm Inc., Technical Memorandum TM-67-1014-1.

Skempton, A. W. 1959. Cast in situ bored piles in clay. Geotechnique, 4, 153-173.

_____ 1951. The bearing capacity of clays. Building Res. Congress, London, Div. 1, pp. 180-189.

Smith, R. J. 1969. Technique for predicting sea floor penetration. U.S. Naval Post Graduate School, Monterey, California.

Taylor, D. W. 1948. Fundamentals of soil mechanics. John Wiley and Sons, New York.

Taylor, R. J., and Demars, K. R. 1970. Naval in place sea floor test equipment. Naval Civil Eng. Lab., Port Hueneme, California, Tech. Note N-1135.

Terzaghi, K., and Peck, R. B. 1948. Soil mechanics in engineering practice. John Wiley and Sons, New York.

Thigpen, L. 1971. Water entry technology—A review (U). Sandia Lab., Albuquerque, N.M., SC-DR-71-0196.

Thompson, L. J. 1966. Dynamic penetration of selected projectile into particulate media, Sandia Lab. Rep. SC-R-R-66-376, Albuquerque, N.M.

U.S. Navy Hydrographic Office. 1955. Instruction manual for oceanographic observations. Second Ed. U.S. Navy Hydrographic Office Pub. No. .607, Washington, D.C.

Vey, E., and Nelson, R. D. 1965. Studies of lunar soil mechanics. I.I.T. Res. Inst. Project No. M272, Phase III Final Rep., Contract NASR-65(0Z).

_____ 1967. Environmental effects on properties of ocean sediments. Proc. Conf. on Civil Eng. in the Oceans-I, ASCE, San Francisco, California, pp. 531-568.

Wang, L. W. 1971. Low velocity projectile penetration. J. Soil Mech. Found. Div., ASCE, 97, No. SM12. pp. 1635-1653.

Whitman, R. V. 1957. The behaviour of soils under transient loadings. Proc. Fourth Int. Conf. Soil Mech. Found. Eng., London, England.

_____ 1970. The response of soils to dynamic loadings. Final Report, U.S. Army Eng., WES, Vicksburg, Miss. Contract No. DA-22-079-Eng-224.

Whitman, R. V., and Healy, K. A. 1962. Shearing resistance of sands during rapid loadings. Rep. 62-113, M.I.T., Cambridge, Mass.

Wilkes, P. R. 1972. Marine sediment penetrometer development at Sandia laboratories. Proc. Conf. on Rapid Penetration Terr. Mater., Texas A & M Univ., Texas, pp. 477-514.

Womack, D. P., and Cox, W. R. 1967. Measurements of dynamic characteristics of soils with penetrometers. Report NASA CR-849, Univ. of Texas, Austin, Texas.

Wu, T. H. 1966. Soil mechanics. Allyn and Bacon, Inc., Boston, U.S.A.

Young, C. W. 1969. Depth prediction for earth-penetrating projectiles. J. Soil Mech. Found. Div., ASCE, 95, No. SM3, pp. 803-817.

APPENDICES

APPENDIX A

PERTURBATION SOLUTION OF THE NON-LINEAR DIFFERENTIAL EQUATION

Equation (13) may be written in dimensionless form by substituting the following dimensionless parameters for various terms occurring in the equation.

Mass $(M_2) = \dfrac{M}{\rho R^3}$ Time $(T_1) = T\sqrt{\dfrac{g}{R}}$

Velocity $(V_1) = \dfrac{V}{\sqrt{Rg}}$ Cohesion $(B) = \dfrac{C}{\rho Rg}$

Depth $(Z_1) = \dfrac{Z}{R}$ Soil Viscosity Coefficient $(K_1) = \dfrac{K}{\rho \sqrt{Rg}}$

Substituting above values the following non-dimensional form is obtained for Equation (13):

$$\frac{dV_1^2}{dZ_1} + \frac{2A_1 V_1^2}{M_2 + A_1 Z_1} = \frac{2(\alpha_1 - \beta_1 Z_1 - \gamma_1 Z_1^2)}{M_2 + A_1 Z_1} + \frac{K_1(\ell + nZ_1) V_1}{M_2 + A_1 Z_1} \tag{A1}$$

where $\ell = -2Nc_r$

$n = -4\pi$

$\alpha_1 = \frac{m}{\rho R^3} \left\{ \frac{2}{3}\pi + 2\sqrt{3}\,\pi + \frac{3}{2}\,\pi^2 + \pi B N c_r + \pi N \gamma_r \right\} = \frac{\alpha}{\rho g R^3}$

$\beta_1 = 7.464\,\pi + \pi\,K_0\,Nq_r + 2\pi B = \frac{\beta}{\rho g R^2}$

$\gamma_1 = \pi\,K_0\,\tan\phi = \frac{\gamma}{\rho g R}$

$$M_2 = \frac{m}{\rho R^3} + \frac{2}{3} \pi + 2\sqrt{3} \pi + \frac{3}{2} \pi^2 = \frac{M}{\rho R^3}$$

$$A_1 = \frac{7.464}{6.464} \pi = \frac{A}{\rho R^2}$$

Substituting $V_1^2 = U$ in Eqn. (A1), we get

$$\frac{dU}{dZ_1} + \frac{2A_1 U}{M_2 + A_1 Z_1} = \frac{2(\alpha_1 - \beta_1 Z_1 - \gamma_1 Z_1^2)}{M_2 + A_1 Z_1} + \frac{K_1 (\ell + nZ_1)}{M_2 + A_1 Z_1} \sqrt{U} \,, \qquad (A2)$$

K_1 being a small quantity. The above equation is solved by the Perturbation Method (Bellman, 1965):

The solution U of Eqn. (A2) may be represented as

$$U = U_o + K_1 \, U_1 + K_1^2 \, U_2^2 \ldots \ldots \qquad (A3)$$

Considering only functions U_o and U_1, and making the necessary changes, Eqn. (A2) may be re-arranged as:

$$\frac{dU_o}{dZ_1} + \frac{2A_1 U_o}{M_2 + A_1 Z_1} + K_1 \left[\frac{dU_1}{dZ_1} + \frac{2A_1}{M_2 + A_1 Z_1} U_1 \right]$$

$$= \frac{2(\alpha_1 - \beta_1 Z_1 - \gamma_1 Z_1^2)}{M_2 + A_1 Z_1} + \frac{K_1 (\ell + nZ_1)}{M_2 + A_1 Z_1} \, U_o^{\frac{1}{2}} \qquad (A4)$$

In order that this equation may be satisfied for all values of K_1, the coefficients of equal powers of K_1 on the two sides of the equation must be equal.

$$\frac{dU_o}{dZ_1} + \frac{2A_1 U_o}{M_2 + A_1 Z_1} = \frac{2(\alpha_1 - \beta_1 Z_1 - \gamma_1 Z_1^2)}{M_2 + A_1 Z_1} \qquad (A5)$$

$$\frac{dU_1}{dZ_1} + \frac{2A_1 U_1}{M_2 + A_1 Z_1} = \frac{1 + n Z_1}{M_2 + A_1 Z_1} \sqrt{U_0} \tag{A6}$$

The solution of Eqn. (A5) is obtained from the general solution given by Bellman (1966) for the boundary condition;

$U_0 = V_i^2$ at $Z_1 = 0$, where $V_i = $ Constant $= \frac{V_0}{R g}$ and

$V_0 = $ Impact Velocity.

$$U_0 = V_i^2 \left\{ \exp \left(- \int_0^{Z_1} \frac{2A_1}{M_2 + A_1 Z_1} dZ_1 \right) \right\}$$

$$+ \exp \left(- \int_0^{Z_1} \frac{2A_1}{M_2 + A_1 Z_1} dZ_1 \right) \int_0^{Z_1} \left[\exp \left\{ 2 \int_0^S \left(\frac{2A_1}{M_2 + A_1 Z_1} dZ_1 \right) \right\} 2 \left(\frac{\alpha_1 - \beta_1 Z_1 - \gamma_1 Z_1^2}{M_2 + A_1 Z_1} \right) \right] dZ_1 \tag{A7}$$

Simplyifying Eqn. (A7) we get

$$U_0 = \frac{1}{(M_2 + A_1 Z_1)^2} \left[2\alpha_1 M_2 Z_1 + (A_1 \alpha_1 - \beta_1 M_2) Z_1^2 - \frac{2}{3} (\gamma_1 M_2 + A_1 \beta_1) Z_1^3 \right.$$

$$\left. - \frac{A_1 \gamma_1 Z_1^4}{2} + M_2^2 V_i^2 \right] \tag{A8}$$

or

$$U_0 = \frac{M_2^2 V_i^2 (1 + P)}{(M_2 + A_1 Z_1)^2} \tag{A9}$$

where

$$P = \frac{1}{M_2^2 V_i^2} \left\{ 2\alpha_1 M_2 Z_1 + (A_1 \alpha_1 - \beta_1 M_2) Z_1^2 - \frac{2}{3} (\gamma_1 M_2 + A_1 \beta_1) Z_1^3 - \frac{A_1 \gamma_1 Z_1^4}{2} \right\} \tag{A10}$$

Similarly, the following solution is obtained for Eqn. (A6) for the

boundary condition, $U_1 = 0$ at $Z_1 = 0$

$$U_1 = \frac{M_2 V_i}{(M_2 + A_1 Z_1)^2} \left[-(\ell + nZ_1) \int_0^{Z_1} \sqrt{(1+P)} \, dZ_1 - n \int_0^{Z_1} \int_0^{Z_1} \sqrt{(1+P)} \, ds \, dZ_1 \right]$$ (A11)

Eqn. (A9) can be represented as

$$V_1^2 = U_o = \frac{M_2^2 V_i^2 (1 + P)}{(M_2 + A_1 Z_1)^2}$$

Upon impacting at a velocity V_i the penetrometer starts decelerating which causes a gradual reduction in penetration velocity and finally, at the completion of the penetration event the penetrometer is brought to a stop ($V_1 = 0$) by the resistive force offered to the motion. For the two physical conditions; at $Z_1 = 0$, $V_1 = V_i$ and at $Z_1 = Z_n$, (maximum penetration depth), $V_1 = 0$, the values of P are obtained as 0 and -1, respectively. In certain situations (when the penetrometer is very heavy and the target material is soft) P may become more than zero for a while, indicating an increase in penetration velocity for a very short distance after impact. However for all practical applications P will never be more than one (as can be seen in Table A1). Table A1 shows the values of P at different penetration depths for various test conditions; P varies from + 0.0067 to -1. This indicates that $|P| < 1$ at depths of penetration considered.

Since $|P| < 1$, substituting $1 + \frac{P}{2}$ (neglecting higher order terms) for $\sqrt{1+P}$ the approximate solution is obtained for Eqn. (A11) as:

$$U_1 = \frac{1}{(M_2 + A_1 Z_1)^2} \left[\beta M_2 V_1^2 Z_1 + \frac{\ell \alpha_1 Z_1^2}{2 V_1} + \frac{\ell (A_1 \alpha_1 - \beta_1 M_2)}{6 M_2 V_1} Z_1^3 \right.$$

$$- \frac{\ell(\gamma_1 M_2' + A_1 \beta_1)}{12 M_2 V_1} Z_1^4 - \frac{A_1 \ell \gamma_1 Z_1^5}{20 M_2 V_1} + \frac{n M_2 V_1}{2} Z_1^2 + \frac{n \alpha_1}{3 V_1} Z_1^3$$

$$\left. + \frac{n(A_1 \alpha_1 - \beta_1 M_2)}{8 M_2 V_1} Z_1^4 - \frac{n(\gamma_1 M_2 + A_1 \beta_1)}{15 M_2 V_1} Z_1^5 - \frac{n A_1 \gamma_1 Z_1^6}{24 M_2 V_1} \right] \qquad (A12)$$

Substituting for U_o and U_1 from Eqns. (A8) and (A12), respectively in

$$V_1^2 = U = U_o + K_1 U_1 \text{, the final solution is written as:}$$

$$V_1^2 = \frac{1}{(M_2 + A_1 Z_1)^2} \left[\left\{ 2\alpha_1 M_2 - L_1 M_2 V_1 \right\} Z_1 + \left\{ A_1 \alpha_1 - \beta_1 M_2 - \frac{L_1 \alpha_1}{2 V_1} - \frac{N_1 M_2 V_1}{2} \right\} Z_1^2 \right.$$

$$- \frac{1}{3} \left\{ 2\gamma_1 M_2 + 2 A_1 \beta_1 + \frac{L_1 A_1 \alpha_1}{2 M_2 V_1} - \frac{L_1 \beta_1}{2 V_1} - \frac{N_1 \alpha_1}{V_1} \right\} Z_1^3$$

$$- \frac{1}{2} \left\{ A_1 \gamma_1 - \frac{L_1}{6} \frac{(\gamma_1 M_2 + A_1 \beta_1)}{M_2 V_1} + \frac{N_1 (A_1 \alpha_1 - \beta_1 M_2)}{4 M_2 V_1} \right\} Z_1^4$$

$$+ \left\{ \frac{L_1 A_1 \gamma_1}{20 M_2 V_1} + \frac{N_1 (\gamma_1 M_2 + A_1 \beta_1)}{15 M_2 V_1} \right\} Z_1^5 + \frac{N_1 A_1 \gamma_1 Z_1^6}{24 M_2 V_1} + M_2 V_1^2 \right] \qquad (A13)$$

where $L_1 = -\ell K_1 = 2\pi N c_r K_1$

$N_1 = -n K_1 = 4\pi K_1$

Eqn. (A13) provides an approximate solution for Eqn. (A1) in non-dimensional form. To make it simplified and readily applicable to

practical problems Eqn. (Ai3) can again be transformed in following dimensional form:

$$V^2 = \frac{1}{(M+AZ)^2} \left[\left\{ 2\alpha M - LMV_0 \right\} Z + \left\{ A\alpha - BM - \frac{L\alpha}{2V_0} - \frac{NMV_0}{2} \right\} Z^2 \right.$$

$$- \frac{1}{3} \left\{ 2\gamma M + 2AB + \frac{LA\alpha}{2MV_0} - \frac{LB}{2V_0} + \frac{N\alpha}{V_0} \right\} Z^3$$

$$- \frac{1}{2} \left\{ A\gamma - \frac{L}{6} \frac{(\gamma M + AB)}{MV_0} + \frac{N(A\alpha - BM)}{4MV_0} \right\} Z^4$$

$$\left. + \left\{ \frac{LA\gamma}{20MV_0} + \frac{N(\gamma M + AB)}{15MV_0} \right\} Z^5 + \frac{NA\gamma}{24MV_0} Z^6 + M^2 V_0^2 \right] \qquad (A14)$$

Where $L = 2\pi N c_s R^2 K$

$N = 4\pi R K$

$V_0 = $ Impact Velocity

This is Eqn. (14) in the text (Chapter III) where all the terms are defined.

Eqn. (A14) is an approximate solution of Eqn. (13) and the validity of it for present applications can be established by comparing the results with numerical solution of Eqn. (13). The numerical solution of Eqn. (13) is obtained by the Runge-Kutta integration method as explained in Chapter III. The maximum depths of penetration calculated by approximate method (Eqn. A14) and numerically for Eqn. (13) are shown in Table A2 for various tests mentioned in Table 4 (Chapter V) together with depths obtained from Eqn. (11), Eqn. (17), and experimentally.

The results obtained from Eqn. (17) which is based on the assumption that soil viscosity coefficient (K) is zero provide the variation of 20 to 60 percent; thereby showing the importance of soil viscosity effects on impact penetration mechanism for cohesive soils.

As can be seen in Column (7) of Table A2 the maximum variation in results obtained by numerical and approximate methods for Eqn. (13) is 6.5 percent only which justifies the validity of the use of the Perturbation method and various assumptions made in formulating Eqn. (A14) for present usage. Column (9) shows the percentage variation in predicted depths obtained from Eqn. (A14) which for most of the tests are within 90 percent accuracy and are of the same order as those obtained from Eqn. (11). The maximum variation in results obtained by using Perturbation method and numerical method is 6.5 percent for test C.W.1.1. For this test the velocity profiles calculated by Perturbation method and numerically are shown in Fig. A1 together with those obtained from logarithmic relationship (Eqn. 11). The velocity profiles obtained experimentally and from Eqn. 17 (assuming K equals to zero) for the test C.W.1.1. are also plotted in Fig. A1. As can be seen in Fig. A1 the velocity profiles obtained by using either Eqns. (11 and 13) or Eqn. (A14) provides approximately same results for up to 85 to 90 percent of total penetration depth. However as expected, out of the three relationships discussed above the logarithmic relationship gives the best agreement with experimental one.

TABLE A1

VARIATION OF P WITH DEPTHS FOR VARIOUS TESTS

z (ft.)					Test No.					
	C.W.1.1	C.W.1.12	C.W.1.3	C.W.2.1	C.W.2.2	C.V.1.1	C.V.1.2	C.V.1.3	C.V.1.4	C.V.1.5
0.1	-0.0209	-0.0293	-0.0430	+0.0067	-0.0022	+0.0025	+0.0028	+0.0035	+0.0043	+0.0065
0.2	-0.0545	-0.0739	-0.1056	+0.0065	-0.0133	-0.0012	-0.0014	-0.0018	-0.0021	-0.0032
0.3	-0.1008	-0.1339	-0.1880	-0.0003	-0.0396	-0.0113	-0.0127	-0.0160	-0.0194	-0.0295
0.4	-0.1599	-0.2093	-0.2902	-0.0164	-0.0752	-0.0276	-0.0312	-0.0393	-0.0475	-0.0724
0.5	-0.2317	-0.3002	-0.4123	-0.0349	-0.1222	-0.0503	-0.0568	-0.0715	-0.0866	-0.1318
0.6	-0.3164	-0.4069	-0.5145	-0.0626	-0.1809	-0.0794	-0.0896	-0.1128	-0.1366	-0.2079
0.7	-0.4141	-0.5929	-0.7166	-0.0975	-0.2513	-0.1149	-0.1296	-0.1632	-0.1976	-0.3008
0.8	-0.5247	-0.6674	-0.899	-0.1395	-0.3340	-0.1569	-0.1769	-0.2228	-0.2697	-0.4105
0.9	-0.6484	-0.8202	-1.1004	-0.1879	-0.4264	-0.2052	-0.2315	-0.2915	-0.3529	-0.5371
1.0	-0.7851	-0.9913		-0.2454	-0.5359	-0.2601	-0.2934	-0.3694	-0.4473	-0.6807
1.1	-0.935	-1.1775		-0.3092	-0.6555	-0.3215	-0.3627	-0.4566	-0.5528	-0.8413
1.2	-1.0982			-0.3807	-0.7872	-0.3894	-0.4393	-0.5531	-0.6696	-1.0191
1.3				-0.4594	+0.9333	-0.4639	-0.5234	-0.6589	-0.7977	
1.4				-0.5453	1.247	-0.5450	-0.6149	-0.7741	-0.9372	
1.5				-0.6400		-0.6328	-0.7139	-0.8987	-1.0881	
1.6				-0.7417		-0.7272	-0.8203	-1.0328		
1.7				-0.851		-0.8283	-0.9344			

TABLE A1 (CONTINUED)

Z (ft.)					Test No.					
	C.W.1.1	C.W.1.2	C.W.1.3	C.W.2.1	C.W.2.2	C.V.1.1	C.V.1.2	C.V.1.3	C.V.1.4	C.V.1.5
1.8				-0.9685		-0.9361	-1.056			
1.9				-1.0940		-1.0506				
Z_P	1.141	1.001	0.843	1.827	1.35	1.857	1.755	1.576	1.443	1.189
Z_E	0.886	0.785	0.69	1.44	1.142	1.35	1.3	1.22	1.06	0.891

Z_E = Actual Penetration Depth.

Z_P = Depth at which $P = 1$ (theoretical maximum penetration depth for condition $X = 0$).

TABLE A2

DEPTHS OF PENETRATION OBTAINED BY VARIOUS FORMULAE

All depths are in ft., the test details and values of coefficients are given in Table IV.

Test No.	Numerical Integration		From Eqn.(14)	From Eqn.(17) (K = 0)	Experi-mentally	% variation of (4) w.r.t.(3)	% variation of (4) w.r.t.(2)	% variation of (4) w.r.t.(6)	% variation of (5) w.r.t.(6)
	From Eqn.(11)	From Eqn.(13)							
(1)	(2)	(3)	(4)	(5)	(6)	(7)	(8)	(9)	(10)
C.W.1.1.	0.873	0.895	0.837	1.141	0.886	6.5	4.1	5.5	59.6
C.W.1.2.	0.768	0.785	0.738	1.001	0.785	6.0	3.9	6.0	27.5
C.W.1.3.	0.67	0.658	0.616	0.843	0.69	6.4	8.0	10.7	22.2
C.W.2.1.	1.291	1.36	1.38	1.827	1.44	1.5	6.9	4.1	26.9
C.W.2.2.	0.952	0.95	1.01	1.35	1.142	6.3	6.0	11.5	18.2
C.V.1.1.	1.316	1.357	1.368	1.857	1.35	0.8	3.9	1.3	37.5
C.V.1.2.	1.24	1.285	1.308	1.755	1.3	1.8	5.4	0.6	35.0
C.V.1.3.	1.115	1.155	1.195	1.576	1.22	3.4	7.2	2.0	29.2
C.V.1.4.	1.011	1.058	1.112	1.443	1.06	5.1	9.9	4.9	36.1
C.V.1.5.	0.823	0.882	0.913	1.189	0.891	3.5	10	2.4	33.4
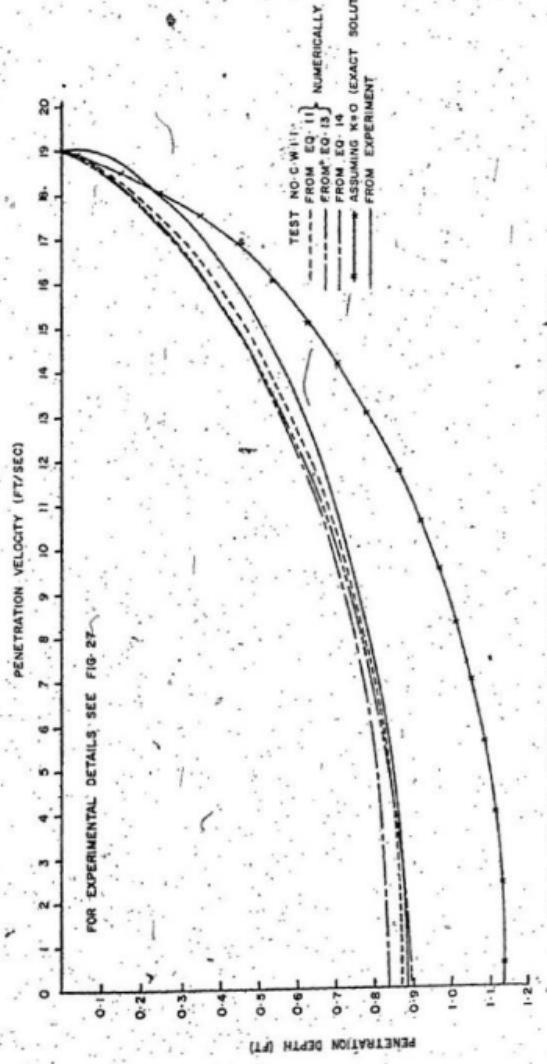
FIG A1 TYPICAL RESULTS FOR MAXIMUM VARIATION IN PERTURBATION METHOD

FOR EXPERIMENTAL DETAILS SEE FIG-27

TEST NO-C-W.III.
FROM EQ-11 } NUMERICALLY
FROM EQ-13-J
FROM EQ-14
ASSUMING K=O (EXACT SOLUTION)
FROM EXPERIMENT

PENETRATION VELOCITY (FT/SEC)

PENETRATION DEPTH (FT)

212

APPENDIX B

DESIGN OF CONE AND FRICTION SLEEVE LOAD CELLS

The purpose of this appendix is to explain the procedures adopted in designing and developing the cone and the friction sleeve load cells. As mentioned in Chapter 4.1, the cone and friction sleeve have the same dimensions as those of the 'Fugro' penetrometer.

Diameter of cone and friction sleeve = 1.405 in. (35.6 mm.)

Base area of cone = 1.55 in.^{2} (10 cm.^{2})

Surface area of sleeve = 23.25 in.^{2} (150 cm.^{2})

Length of sleeve = 5.268 in.

Mechanical Design

(a) Cone-Strain Tube

For design load of 2000 lbs.

Assumed:

(i) Internal diameter of tube = 0.7 in.

(ii) Outer diameter of tube = 0.8 in.

∴ Wall thickness = 0.05 in.

Sectional area of tube = $\frac{\pi}{4}$ (0.8^2 - 0.7^2) = 0.1179 in.^{2}

Stress (for maximum load of 2000 lbs.) = $\frac{2000}{0.1179}$ = 16,964 lbs./in.^{2}

Assuming E (Modulus of elasticity) of material = 29 X 10^6 p.s.i.

Strain = $\frac{16964}{29 \times 10^6}$ = 585 µ strain

Assuming yield stress of steel = 35,000 p.s.i.

Safety Factor = $\frac{35,000}{16964}$ = 2.06

This dimension would be adequate if the steel is not heat treated. If the steel is heat treated to a nominal yield stress of 100,000 p.s.i. then safety factor would be:

$$S.F. = \frac{100,000}{16,964} = 5.89$$

and as such the wall area should be reduced to obtain a better sensitivity. However the metal selected for the present penetrometer is non heat treated steel, the assumed dimensions would be adequate.

(b) Sleeve Strain Tube:

Design load = 1000 lbs.

Assumed:

(i) Internal diameter of tube = 1.0 in.

(ii) Outer diameter of tube = 1.05 in.

∴ Wall thickness = 0.025 in.

Sectional area of tube = 0.0806 in.^{2}

Stress (for maximum load of 1000 lbs.) = $\frac{1000}{0.0806}$ = 12,407 p.s.i.

Strain = $\frac{12407}{29 \times 10^6}$ = 428 μ strain

Safety factor (for non heat treated steel) = $\frac{35000}{12407}$ = 2.82

Thus the assumed dimensions would be adequate.

The internal mechanical arrangements of the cone body, sleeve strain tube and friction sleeve are shown in Fig. B1, Fig. B2, and Fig. B3 respectively. The cross-sectional view of the complete assembly is shown in Fig. 7.
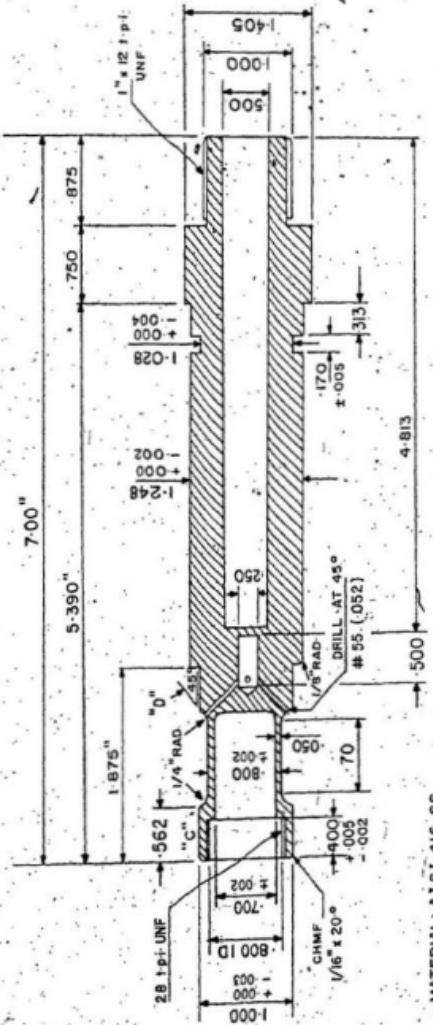
FIG B1 · CONE BODY

MATERIAL: AISI 416 SS

SURFACE C IS POLISHED AND FREE FROM LONGITUDINAL SCRATCHES.

SURFACE D IS LIGHT PUSH FIT AND STUCK TO I.D OF SLEEVE STRAIN TUBE.

215

FIG· B2· SLEEVE STRAIN TUBE

1·443"

1·050 +·000 -·001

1·000 +·001 -·000

1·000 +·001 -·000

·025

SURFACE B IS MACHINED SMOOTH AND HAND PUSH FIT IN RECESS R OF FRICTION SLEEVE I.D· AND TIGHT PUSH FIT TO SURFACE D OF CONE BODY .'

FIG· B3· FRICTION SLEEVE

5·268

·170 ±·005

1·405

1·220 +·003 -·000

1·002 +·002 -·000

R

1·050 +·001 -·001

"A"

1·250 +·004 -·000

1/16" x 20° CHMF

·100

·100

·130

·078

·500

MATERIAL : AISI 416 SS
SURFACE A IS POLISHED AND FREE FROM LONGITUDINAL SCRATCHES
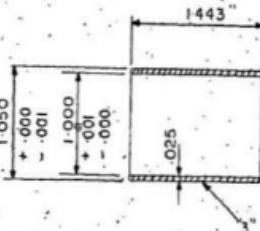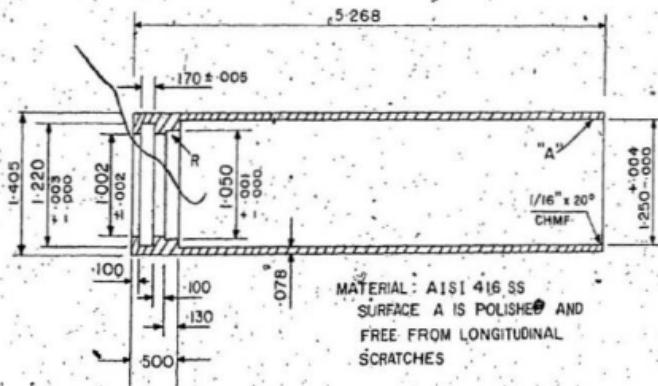
## Electrical Design

The strain gages are used for measuring the cone and sleeve friction loads. Each load cell contains four pairs of strain gages arranged in such a manner that automatic compensation is made for bending effects and only axial stress is measured. The four strain gages are arranged in the axial direction and the remaining four in circumferential direction, at equidistance, on the periphery of the tube. The wiring diagram and the strain gage arrangement is shown in Fig. B4.

Estimation of Bridge Output:

Assumed: Poissons Ratio (μ) = 0.3

Selected: Gage Resistance (R) = 120 Ω

Gage Factor $(G.F.)$ = 2.1

$$GF = \frac{\Delta R}{R} / \epsilon$$

or $\Delta R = GF \cdot R \cdot \epsilon$

Dissipation for $\frac{1}{8}$ in.^{2} gage $(W) \sim 15$ W/in.$^2 \equiv 234$ mW/gage

$$V_{gage} = \sqrt{RW} = \sqrt{120 \times 0.234} = 5.3V$$

Gage Current = $\frac{20}{4 \times 120}$ = 41.7 mA

Assuming nominal strain in the cone and sleeve tube is 500 $\mu\epsilon$, and current (I) is nominally constant (with constant current supply),

$$\Delta R = 2.1 \times 500 \times 10^{-6} \times 120 = 0.126 \ \Omega$$

$$\therefore \ \% \text{ resistance change} = \frac{0.126}{120} = 0.105\%$$
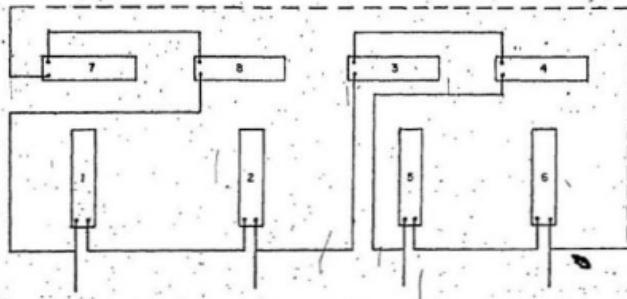
1,2,5 & 6 = AXIAL STRAIN GAGES
3,4,7 & 8 = CIRCUMFERENTIAL STRAIN GAGES
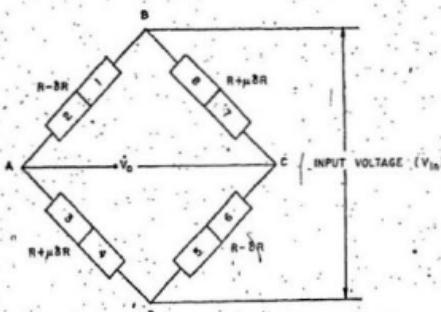
FIG B4: WIRING DIAGRAM OF STRAIN GAGE ARRANGEMENT

$$\Delta V_{AB} = IR - I(R - \delta R) = I\delta R = I.GF.\epsilon.R.$$

Bridge Output Voltage $= I \delta R \approx Vo$

$$I = \frac{V_{in}}{4.R}$$

or $\quad Vo = V_{in} \left(\frac{\delta R}{4R} \right) = V_{in} \left(\frac{GF.\epsilon}{4} \right).$

Sensitivity (S) $= \frac{Vo}{V_{in}} = \frac{GF.\epsilon}{4}$

For 500 μs nominal strain at full scale load

$$S = \frac{2.1 \times 500 \times 10^{-3}}{4} = 0.262 \text{ mV/V}$$

Calibration: Cone and friction load cells were calibrated on 'Instron' testing machine. For the calibration of load cells special jigs were designed and fabricated so that only axial load was applied during compression of the tube. The cells were loaded up to design loads at 50 lbs. increments. A very good linearity was obtained in output voltage and applied loads. Following are the mechanical sensitivity of load cells calibrated at 8 VDC excitation:

Cone Load Cell: 1 mV = .378 lbs.

Friction sleeve load cell: 1 mV = 237.5 lbs.

APPENDIX C

PROCEDURE FOR DOUBLE INTEGRATION OF

ACCELEROMETER RECORDS

The purpose of this appendix is to describe the double integration procedure used to compute time histories of velocity and displacement for the system from the measured acceleration history.

The motion of the system is rectilinear along a vertical axis. The system was assumed to behave as a rigid body, thereby permitting the use of the equations for rectilinear motion of a particle to describe its motion. From elementary kinematics, instantaneous velocity and acceleration are defined as:

$$V(t) = \lim_{\Delta t \to 0} \frac{\Delta Z}{\Delta t} = \frac{dZ}{dt} \tag{C1}$$

$$a(t) = \lim_{\Delta t \to 0} \frac{\Delta V}{\Delta t} = \frac{d^2 Z}{dt^2} \tag{C2}$$

where

t = time

$Z(t)$ = displacement at time t

$V(t)$ = velocity at time t

$a(t)$ = acceleration at time t

From these definitions, the following integral equations are derived for the case where the initial velocity is V_o (impact velocity) and initial displacement is zero.

$$V(t) = \int_0^t a(t) \, dt + V_0 \tag{C3}$$

$$Z(t) = \int_0^t \left\{ \int_0^t a(t) \, dt + V_0 \right\} dt + Z_0 \tag{C4}$$

If the acceleration function is such that a mathematical solution of the foregoing differential equations of motion is not possible, an approximate solution can be obtained by numerically integrating the area under the measured acceleration-time history.

The first step in the numerical integration procedure is to establish a zero time and a zero acceleration base line on the accelerometer trace. The zero time is established from the fact that, as soon as the penetrometer hits the target the accelerometer trace start decreasing from a constant line trace representing 1g for free fall condition. The zero base line is established above the constant free fall trace from a known sensitivity of the accelerometer. This can also be verified from the accelerometer trace while the penetrometer is at the rest position either before dropping or after completing the penetration. The acceleration below the base line was assigned positive values with a maximum of 1g at the time of impact and values above the base line were assigned negative acceleration (deceleration). Acceleration values a_0', a_1', a_2', ... , a_i', ... , a_n', are then scaled from the chart record at corresponding times t_0, t_1, t_2, ... , t_i ..... , t_n. For the tests in this study, 2.5-msec time intervals are used. Assuming the area under the acceleration curve to be composed of a series of trapezoidal increments, t_{i-1}, a_{i-1}', a_i', t_i, a summation equation for the velocity at any time t_i can be written as

$$V'_i = \sum_{i=1}^{i} \left(\frac{a'_i + a'_{i-1}}{2} \right)(t_i - t_{i-1}) + V_o \qquad (C5)$$

Again assuming trapezoidal increments, the area under the velocity curve can be summed to compute displacement using the equation

$$Z_i = \sum_{i=1}^{i} \left(\frac{V'_i + V'_{i-1}}{2} \right)(t_i - t_{i-1}) + Z_o \qquad (C6)$$

Velocity, and displacement histories were computed from Eqns. C5 and C6 respectively for all the impact tests.

The actual penetration depths were also measured after each test. The computed and actual penetration depths were generally in agreement and the maximum variations of 2.6% were noticed. The variations may be accounted for the following reasons:

(i)   The actual measurement was done with an accuracy of 0.125 in.

(ii) In some cases the location of the original surface after
      penetration was difficult because of irregular upheaval of
      the surface.

(iii) Error in acceleration trace data reduction.